2011-01-01

Joint Geophysical Data Analysis For Geothermal Energy Exploration

Antony Munika Wamalwa
University of Texas at El Paso, amwamalwa@gmail.com

JOINT GEOPHYSICAL DATA ANALYSIS FOR GEOTHERMAL ENERGY EXPLORATION

ANTONY MUNIKA WAMALWA

Department of Geological Sciences

APPROVED:

_____
Laura Serpa, Ph.D., Chair

_____
Elizabeth Anthony, Ph.D.

_____
Diane Doser, Ph.D.

_____
Aaron Velasco, Ph.D.

_____
Kevin Mickus, Ph.D.

_____
Benjamin C. Flores, Ph.D.
Acting Dean of the Graduate School

JOINT GEOPHYSICAL DATA ANALYSIS FOR GEOTHERMAL ENERGY EXPLORATION

by

ANTONY MUNIKA WAMALWA, M.S., B.S.

DISSERTATION

Presented to the Faculty of the Graduate School of

The University of Texas at El Paso

in Partial Fulfillment

of the Requirements

for the Degree of

DOCTOR OF PHILOSOPHY

Department of Geological Sciences

THE UNIVERSITY OF TEXAS AT EL PASO

December 2011

Acknowledgements

Many people helped in making this study a success. Although I may not mention all of them here dues to limited space, I would like to extend my gratitude to Dr. Laura Serpa for the opportunity she gave me to study geophysics and some fruitful discussion we had over the period. I would also like to thank Dr. Kevin Mickus for his insightful discussions and data processing and interpretation, Dr. Diane Doser, Dr. Elizabeth Anthony, Dr. Aaron Velasco, Dr. Terry Pavlis, and Dr. Peter Omenda for the helpful reviews. I would also like to thank Andrew Sabin and Wei-Chuang Huang of the United Stated geothermal Program at Coso, California for availing the MT data for Coso geothermal field study. Much thanks to Dr. Silas Simiyu and the Geothermal Development Company (GDC) for giving the data collected over the geothermal fields in Kenya. Thanks to Charles Muturia of DGC and Karen Christopherson of Chinook Geoconsulting, Inc. for the helpful discussions on data collection and processing.

I would like to thank Kenny, Sarahi, and Christian Gross for the support they awarded me during my entire stay in El Paso. It behooves me to recognize and be thankful for the contribution of Mellisa Jimenez for kindness and support whenever in want and how she played a role of a dear sister that made me feel at home while in El Paso. To friends and colleagues at the geology department who form a long list, I thank you all.

I greatly appreciate the patience and support of my dear parents Jared and Mary Wamalwa who also gave me the chance to get education. I would like to appreciate the patience and encouragement from Jamillah Wanyonyi and George Munika and all my family members. This work was supported by NSF grants EAR0749382 awarded to Dr. Laura Serpa, and a UTEP Student Research Grant Awarded to Antony Wamalwa.

This Dissertation was submitted to the Supervising Committee on the 16th of November 2011

Abstract

Geophysical data modelling often yields non-unique results and hence the interpretation of the resulting models in terms of underlying geological units and structures is not a straightforward problem. However, if multiple datasets are available for a region of study, an integrated interpretation of models for each of the geophysical data may results to a more realistic geological description. This study not only demonstrates the strength of resistivity analysis for geothermal fields but also the gains from interpreting resistivity data together with other geophysical data such as gravity and seismic data. Various geothermal fields have been examined in this study which includes Silali and Menengai geothermal fields in Kenya and Coso geothermal field in California, USA.

Table of Contents

Acknowledgements iv

Abstract v

Table of Contents vi

SECTION 1 1

Resistivity Investigation of the Geothermal Potential at the Silali Volcano, Northern Kenya Rift, Using Electromagnetic Data. 1

1.1 Abstract 1

1.2 Introduction 2

1.3 Previous studies 4

1.2.1 The Silali volcano 5

1.3 Magnetotelluric (MT) and Transient Electromagnetic (TEM) field survey 8

1.3.1 Data acquisition and processing 9

1.3.2 MT distortion analysis 10

1.4 Data interpretation 11

1.4.1 2D modeling of MT data 14

1.5 Conclusions 20

1.6 Acknowledgements 23

1.7 References 24

SECTION 2 27

Joint Geophysical Analysis of the Coso Geothermal Field, south-eastern California 27

2.1 Abstract 27

2.2 Introduction 28

2.3 Coso Geothermal Field 29

2.4 Previous geophysical studies 32

2.4.1 Seismic 32

2.4.2 Gravity 33
2.4.3 Resistivity 35
2.5 Magnetotelluric method and data analysis 36
2.6 Gravity data analysis 42
2.7 Conclusions 48
2.8 Acknowledgements 50
2.9 References 51
SECTION 3 55
Geophysical Characterization of the Menengai Volcano, Central Kenya Rift from the Analysis of Magnetotelluric and Gravity Data 55
3.1 Abstract 55
3.2 Introduction 56
3.3 Previous geophysical studies in the Kenya Rift 57
3.3.1 Menengai Volcano 60
3.4 Geophysical data analysis 61
3.4.1 Gravity 61
3.4.2 Gravity data interpretation 68
3.4.3 Magnetotellurics 69
3.4.4 Data collection and processing 70
3.4.5 Data interpretation 72
2.4.6 Two-dimensional modeling 75
3.5 Integrated analysis 80
3.6 Conclusions 83
3.7 Acknowledgements 84
3.8 References 85
SECTION 4 91
APPENDIX 91

4.1 Cover Letters.....91
SECTION 5.....92
VITA.....92

SECTION 1

Resistivity Investigation of the Geothermal Potential at the Silali Volcano, Northern Kenya Rift, Using Electromagnetic Data.

(Paper submitted to Journal)

WAMALWA, Antony M.[1,2], *and SERPA, Laura F.*[1]
1. Department of Geological Sciences, University of Texas at El Paso, 500 W. University, El Paso, TX 79968,
2. Geothermal Development Company, P.O. Box 100746, 00101, Nairobi, Kenya

1.1 Abstract

The Silali volcano is one among a number of volcanoes found along the axis of the Kenya rift system that has experienced immense volcanism and faulting. We investigate the resistivity distributions within the Silali volcano region in order to define the magmatic, geothermal, and structural features of this active volcano. The data reveal a NE trending fault west of the volcano in the Kapedo region, a magma chamber beneath the caldera, and a potential fluid circulation zone within the caldera region. The depth to the magma chamber is estimated to be about 6 km from the surface. A low resistivity zone (less than 20 ohm.m) at shallow depths (1-2 km) is interpreted to be a low temperature clay (smectite) alteration zone resulting from fluid circulation as heat is transferred to shallower depth. The resistivity increases abruptly beneath the inferred alteration zone and we postulate that resistivity change is due to a change in clay mineralization to a chlorite-dominated system. This change is temperature dependent and occurs at approximately 240^0C. The inferred temperature boundary is consistent with an active volcanic system with an approximately 800^0C magma body at a depth of 6 km.

1.2 Introduction

An increase in resistivity with temperature has been observed in most high temperature geothermal systems *(e.g Anarson et al., 2010; Lichoro 2009; Ooskoi et al 2005; Cumming and Mackie, 2010, Flovenz et al., 2005)* and it is often interpreted as a change in clay mineralization from smectite to chlorite due to increasing temperatures with depth. The reduced resistivity in the smectite dominated region is attributed to the electrical double layer of the smectite molecule where surface conduction results from free mobile ions. This process is suppressed by the strong bonding in the chloride molecule and hence restricted ion mobility and high resistivity characterize the chlorite rich zone *(Flovenz et al., 2005; Cumming et al., 2000; Wright et al., 1985).*

In many geothermal sites around the world; i.e. Krafla in Iceland, Olkaria in Kenya, and Coso in the United States; smectite and zeolite minerals form between 70^0C and 220^0C while chlorite and illite minerals form at temperatures above 240^0C(e.g. *Newman et al., 2008; Cumming and Mackie, 2010; Arnason et al., 2010; Perelin et al., 1996).* Hence, resistivity methods can be used to map this transition because the smectite-zeolite region has low resistivity and the chlorite-illite region has high resistivity boundaries A map of this subsurface temperature boundary *(Flovenz et al., 2005; Lichoro, 2009; Newman et al., 2008; Onacha, 2006; Oskooi et al., 2005)* could provide a basis for discriminating between other material or structures such as fracture zones or magma that have a resistivity that differs from the clays within a given temperature region.

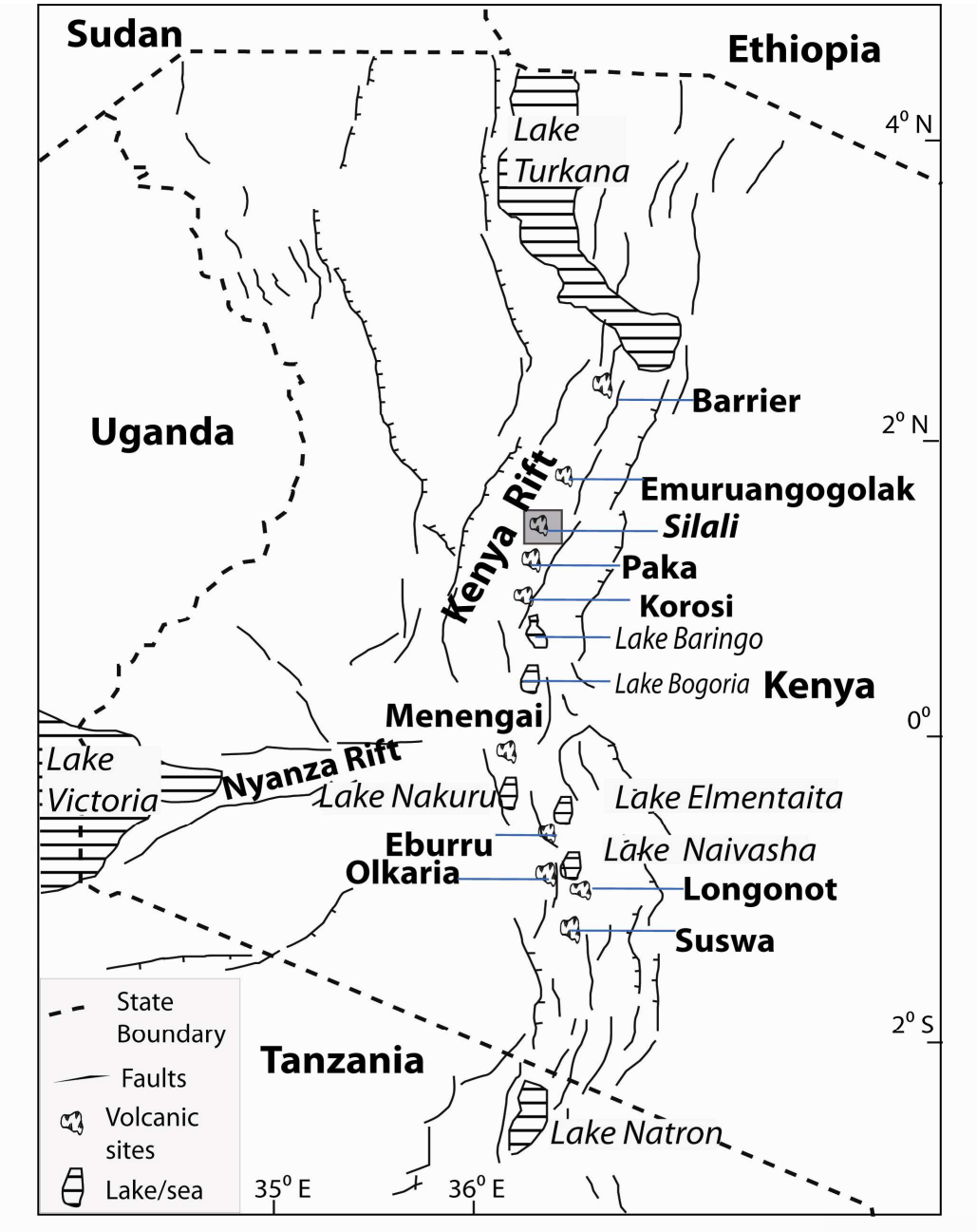

Figure 1: Map showing the Kenya rift and the volcanic centres and lakes. Silali (Shaded box) is the volcanic centre in focus for this study.

In this study we examine the Silali volcano located in the northern part of the Kenya rift system (Figure 1). Magnetotelluric (MT) data are used to image the resistivity structure around the Silali volcano and the associated geothermal prospect. A shallow low resistivity zone is imaged and correlated with the region of intense fracturing around the Silali caldera

where we infer there is high porosity and enhanced fluid circulation. This low resistivity region is an indication of the temperature dependent change in clay mineralogy due to hydrothermal circulation. We also identified zones of high permeability that may comprise the plumbing for the geothermal system. At volcanoes where there has been recent eruption activity, like Silali, magma remnants at depth also can be imaged using resistivity analysis. Hence we imaged apparent magmatic material that remained in the subsurface beneath the volcano as part of this study.

1.3 Previous studies

The East African Rift System (EARS) in Kenya (Figure 1) was initiated in the Miocene and continues to be active today. As part of the rifting, the region experienced crustal thinning, up-warping of the asthenosphere, and volcanism *(Simiyu and Keller, 1997, 2001; Smith 1994; Smith, 1994; Keller et al., 1994; Hay and Wendlandt, 1995).* The northern section of the Kenya rift has experienced more crustal thinning and less uplift than the central rift region *(Simiyu and Keller 1997; Mariita and Keller 2007).* Several young volcanoes, including Suswa, Longonot, Olkaria, Eburru, Menengai, Silali, and Barrier (Figure 1), are located along the rift valley floor and these volcanic centres are the target of geothermal exploration in Kenya *(Simiyu, 2010; Omenda et al., 2000).*

The Kenya rift has been extensively studied as the basis for understanding the processes of continental plate breakup *(e.g. Keller et al., 1994; Simiyu and Keller, 1997; Simiyu and Keller, 2001; Khan et al., 1999; Prodehl et al., 1997; Swain 1976; Mariita and Keller, 2007).* However, detailed studies that focus on the various volcanic centres along the rift are limited. Studies *(Simiyu 1991; Omenda, 1997; Onacha, 2006)* of the Olkaria and Eburu volcanic complexes, and the Menengai, and Longonot volcanoes have resulted in the development of a geothermal plant at the Olkaria volcanic field to generate electricity. Due to the rugged

terrain that limits accessibility, the Silali volcano had not been studied. However, the growing need for geothermal energy development in Kenya has given incentive to the first detailed geophysical data collection around the caldera region which we present in this paper.

Previous studies (*Fairhead, 1976; Swain, 1976; Swain et al., 1994; Simiyu and Keller, 1997; Marrita and Keller, 2007)* have indicated that the location of the volcanic centres along the rift, including the Silali volcano, coincides with a 50 km wide gravity maxima with an amplitude about 20 mGals which is typical for most geothermal fields around the world *(Monstero et al., 2005).* This high gravity anomaly was interpreted as the result of a shallow magma chamber and dykes along the rift axis. The gravity data distribution however is sparse (about 5km spacing) and hence could not adequately image detailed structures around the volcano.

The on-going exploration for geothermal resources along the Kenya Rift provides subsurface information through both geophysical data interpretation and the subsequent drilling to produce geothermal energy. The interpretation of the geophysical data often is tested only a short time after it is gathered because of the rapid development of geothermal prospects in Kenya at this time. Thus, we anticipate this interpretation of the geophysical data from Silali volcano presented here will be tested by drilling within the next 2-10 years.

1.2.1 The Silali volcano

The Silali volcano *(Figures 1 and 2)* is the largest of the Quaternary shield volcanoes, measuring 30km by 25km, in the northern section of the Kenya Rift *(Dinkley et al., 1993; Smith et al., 1995).* This volcano stands 800 m above the rift floor and was formed by alternating episodes of faulting, subsidence and infilling associated with pyroclastic deposition and basaltic volcanism that created a 7.5km by 5km caldera at its summit. These processes were accompanied by fracturing and decompression of a magma chamber and

regional extension and injection of dykes beneath the volcano *(Smith et al., 1995; Williams et al., 1984).*

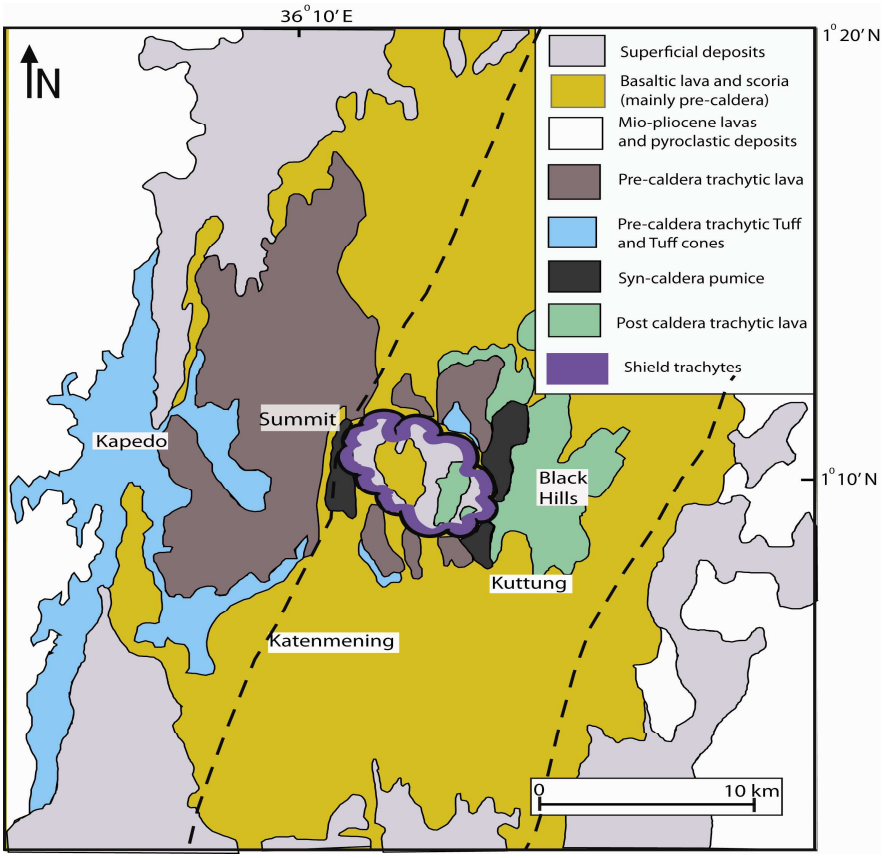

Figure 2: A simplified geological map of the Silali region. The Silali caldera is defined by the shield trachyte. The dashed lines are the boundaries of intensely faulted region. *Modified from William et al, (1984).*

The geology of the Silali region can be divided into groups based on the times of emplacement as: the post caldera group, the pre-caldera group, the western flank group, and the caldera wall group. The post caldera group consists of the intra-caldera and extra-caldera sub-groups that are mainly basalts and trachytes. The Katenmening lava and the Kapedo tuffs are distinctive markers for the pre-caldera group and the caldera wall group, respectively *(Smith et al, 1995; Williams et al., 1984).* The western flank of the caldera is covered by the Arzett tuff and the Summit and Discoid trachytes *(Macdonald et al., 1995).* Fault surfaces have exposed the different sequences. For example, east of the volcano, basalts overlie or are

faulted against west-dipping Miocene trachytes and basalts, while on the west, basalts are exposed near Kapedo and overlie trachytes and pyroclastic deposits *(Smith et al., 1995).* The numerous faults around the Silali volcano have a generalized north to northeast trend, with a zone of intense faulting, approximately 10 km wide, which defines a series of en echelon grabens *(Figures 2 and 3).* The eastern part of the caldera is more fractured than the western part, and fissures within the intensely faulted region may have favoured the flow of material, like lava, to the surface *(Smith et al., 1995).*

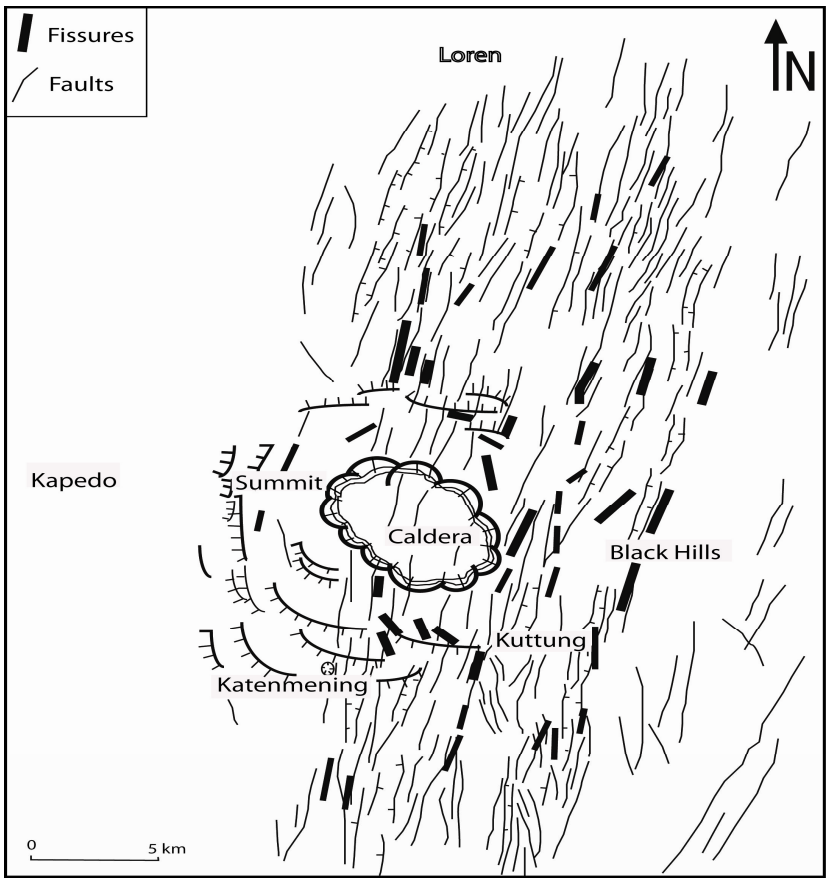

Figure 3: Tectonics of the Silali region with thin lines signifying the numerous faults while the bold dark lines are fissures. Modified from Smith et al., (1995).

1.3 Magnetotelluric (MT) and Transient Electromagnetic (TEM) field survey

The MT and the TEM methods are electromagnetic techniques used to determine subsurface resistivity distribution where rocks have been fractured, sheared, weathered, hydrothermally altered, or have fluids. For the MT method, naturally-occurring, time-varying electric (**E**x and **E**y) and magnetic (**H**x, **H**y, and **H**z) fields are recorded at the surface of the earth *(Vozoff, 1991; Nabighian, 1991).* The MT method has an advantage over other electromagnetic techniques because it allows investigation from a few tens of meters to several hundred kilometres depth.

The TEM method requires an energy source and a steady current sent through an insulated wire loop that has been laid on the surface of the earth *(Nabighian and Macnae, 1991).* The earth is energized when the current at the transmitter is abruptly switched off. As a result, currents are induced in the ground according to Faraday's law. These currents spread within the Earth and decay with time thus creating a secondary vertical decaying magnetic field that generates a voltage change. A detector at the centre of the loop records the voltage which is converted to apparent resistivity for interpretation *(Meju, 1996).*

Several stations were deployed simultaneously to allow for cross remote-referencing for the computation of MT impedances. The electric and magnetic fields were converted to frequency domain and the 2 x 2 impedance tensors, Z, were estimated using the remote-referencing method proposed by Chave and Thompson, (1989). The electric field of high and low frequency electromagnetic waves correspond to shallow and deep penetration of the earth, respectively.

1.3.1 Data acquisition and processing

The MT and TEM data used in this study were collected during the months of March to August, 2010. Two hundred and fifteen MT and one hundred TEM stations were acquired in Silali by the Geothermal Development Company (GDC). The MT data were collected using Phoenix MTU-5A equipment in a period range of 0.001-1000 sec. Telluric lines were 100 m long, except where they were restricted by rugged terrain. A station grid with 1km spacing was used within the caldera and the grid spacing was increased to 2-3km outside the caldera. The magnetic coils and the potential electrodes were oriented in orthogonal east and north directions. Eight to ten stations were deployed simultaneously which is useful for remote and cross referencing. Each MT sounding was pre-processed for cross-power estimates that were then analysed to estimate the impedance, resistivity and phase *(Chave et al., 1989; Rodi and Mackie, 2001).* The TEM data were collected using a Zonge GDP 32 transmitter and receiver.

The data collection in the Silali region was done with the following objectives:

(1) Image the magmatic material that remained in the shallow crust of Silali after some was emptied in the formation of the caldera.

(2) Map zones of high fracture permeability that form the plumbing system of thermal fluids in the region by identifying hydrothermal alteration zones.

(3) Define a possible geothermal reservoir from imaged alteration zones and also infer temperature distributions from resistivity anomalies.

(4) Delineate lithology, thickness of volcanic flows and depth to the Precambrian basement.

1.3.2 MT distortion analysis

Magnetotelluric soundings are often distorted by small-scale heterogeneities at the recording site. The effect is noticeable from the shift of the apparent resistivity at all frequencies and can be corrected by using the complimentary TEM data *(Meju, 1996)*. The TEM method does not use electrodes that are in contact with the ground and hence the data are not affected by these shifts *(Pellerin and Hohmann, 1990; Cumming and Mackie, 2010)*.

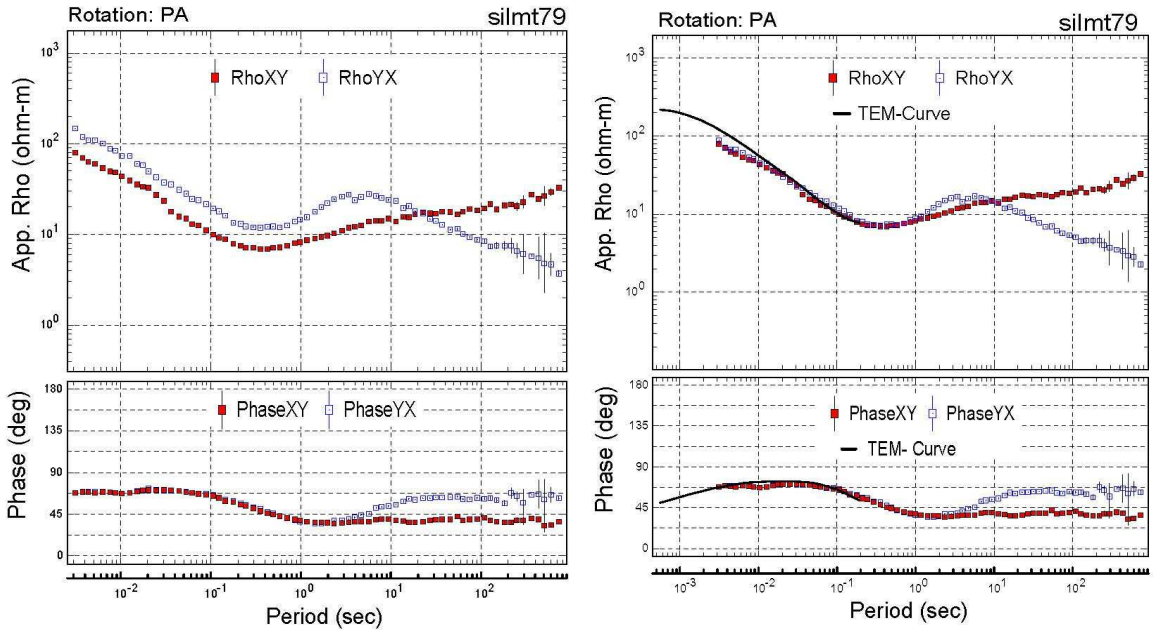

Figure 4: A plot of TEM and MT data at station 79 rotated to principal axes. The first plot is the MT plot before static shift correction and the second plot that includes the TEM plot is corrected for shift of MT apparent resistivity. Resistivity XY (red) is in the north-south direction while YX (blue) is the east-west orientation.

These preliminary models could then be used to build 2D and 3D models of the subsurface. The XY and the YX apparent resistivity and phase correspond to the north-south and east-west directions. These plots appear to coincide at short periods but diverge at long periods which indicate the lateral change in resistivity at long periods. The onset of this separation indicated a change in geology or presence of geological structures with depth. The short

period indicate that the geology is more 1D in nature while longer periods where the plots split imply 2D or 3D geology *(Volpi et al., 2003, Onacha, 2006; Oskooi et al 2005).*

1.4 Data interpretation

Initial data analyses were conducted in order to gain information on the general resistivity distribution of the study region. First, skew and polar diagrams were analysed where most of the data showed 1D characteristic at short periods and 2D and or 3D geology at medium or long periods. One-dimensional Occam (minimum structure) inversions were conducted for each MT sounding after static shifts were corrected *(Figure 5).* This technique is simple but provides useful information before completing more detailed analyses on the data such as a 2D or 3D inversion. In some cases, the results of 1D inversion show a good correlation to the 3D inversion and in particular for short periods *(e.g. Arnason et al., 2010; Cumming et al., 2000).*

The 1D models show that highly resistivity rocks overlie less resistive rocks near the surface of the earth for most soundings (Figure 5). The shallow low resistivity zone beneath the first layer is underlain by a more resistive block and resistivity then gradually decreases with depth. The 1D models were used to generate resistivity maps to analyse the lateral resistivity distribution (Figure 6). The results (both the profile and maps) indicate that resistivity in the region varies both laterally and with depth.

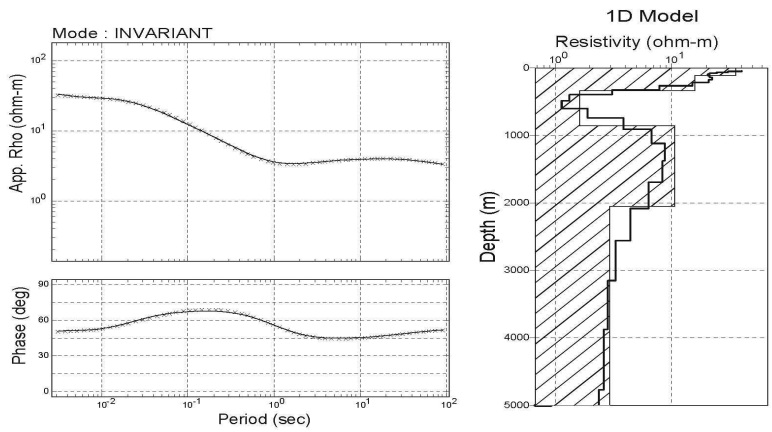

Figure 5; One-dimensional Occam (unshaded with bold lines) and layered (shaded) resistivity inversion models of MT data at station silmt172.

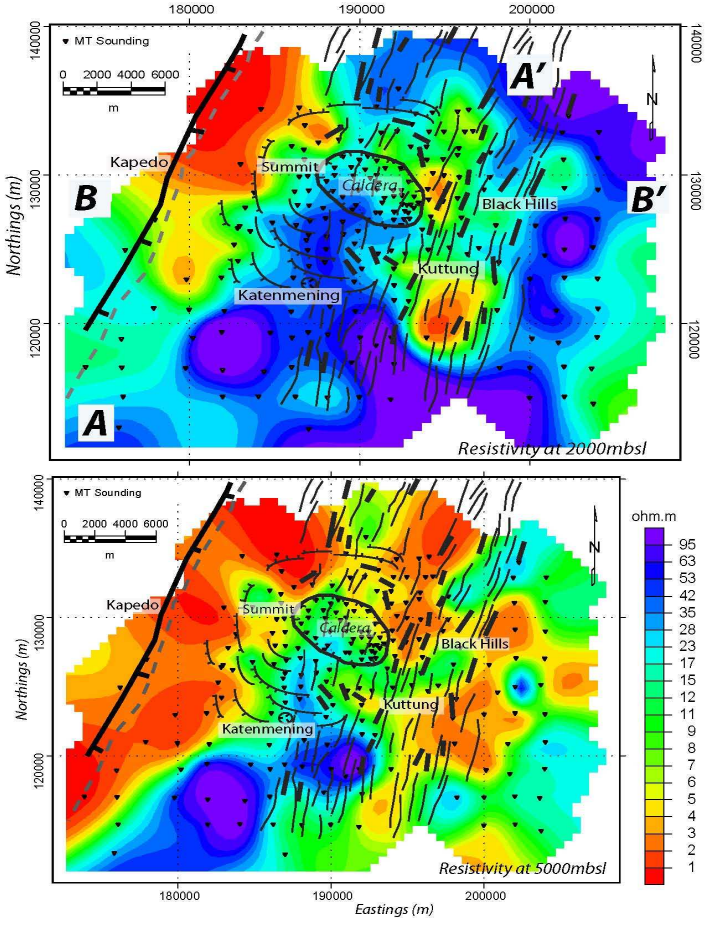

Figure 6: Resistivity distribution map at 5000m (bottom) and 2000 (top) below sea level (mbsl) derived from 1D model of MT data. The thin lines are faults, bold thick short line are fissures. A fault going thru Kapedo is shown by the dark line with the Suguta River (dashed line) parallel to it. Points labelled B,B', and AA' are the ends of 2D profiles.

The resistivity at 2000 m below sea level reveals a northeast trending resistivity boundary and at 5000 m below sea level (Figure 7) the boundary is more evident west of the caldera at Katenmening, and southeast of Kapedo signifying a geologic boundary exists along this path with a high resistivity region on the east side and low resistivity region on the west side of the boundary. The high resistivity region starts at the western edge of the caldera and extends eastward past the Black Hills. The high resistivity infer to be pre-Miocene and Miocene volcanic flows that overly Precambrian basement rocks composed primarily of gneisses, schist and migmatite *(Smith, 1994).* Hautot et al., (2000) modelled magnetotelluric data collected over the Baringo region just 40 km south of Silali and imaged a deeper low resistivity layer embedded in a high resistivity region which they interpreted to be a layer of sediments that separates the underlying Precambrian rock and the overlying basaltic lava. Our data did not show this layer of conductive sediments that underlay the volcanic flows. The conductivity at depth imaged in this study mainly due to intense faulting and fracturing allowing fluid circulation, mineralization, or temperature or a combination of more than one of these factors.

In contrast, the western side of our study area that includes the Kapedo region is characterized by low resistivity and few mapped faults. However, few major faults with a northeast strike runs through the Kapedo region but young pyroclastic deposits, tuffs and alluvium in the region might have covered other small faults. The extent of this low resistivity region westwards is not well constrained because there is no data farther to the west past the Kapedo region. We interpret this low resistivity zone as fault(s). The resistivity boundary that runs through the Kapedo region correlates well with a mapped faults running through Kapedo and a channel of the Suguta River. It is likely that the flow of the Suguta River is controlled by these fault(s) as inferred by our data in the Kapedo region.

1.4.1 2D modeling of MT data

We also modelled the MT data with a 2D regularized inversion algorithm *(Rodi and Mackie, 2001)* that jointly minimizes data misfit and deviations of the final model from the initial model. Data were rotated so that one axis was perpendicular and the other parallel to the geo-electric strike. In this way, the data are polarized into two modes, the TE mode where the electric field is parallel to the geo-electric strike and the TM mode where the electric field is perpendicular to the geo-electric strike. This process helps to enhance anomalies and minimize errors.

Our results, presented here, are from 2D inversions of joint TE and TM modes data. In all of our inversions, the RMS errors were 5% or less after 60 iterations which was considered reasonable. There was a relatively good match between the observed and the calculated TM and TE data (Figure 7) although in some cases the fit was hampered by noisy data. In order to check the convergence of our models, three different arbitrary resistivity half space models were used as the initial model. The final result showed insignificant variation in the resistivity structure therefore we concluded that the results were independent of the selected initial model.

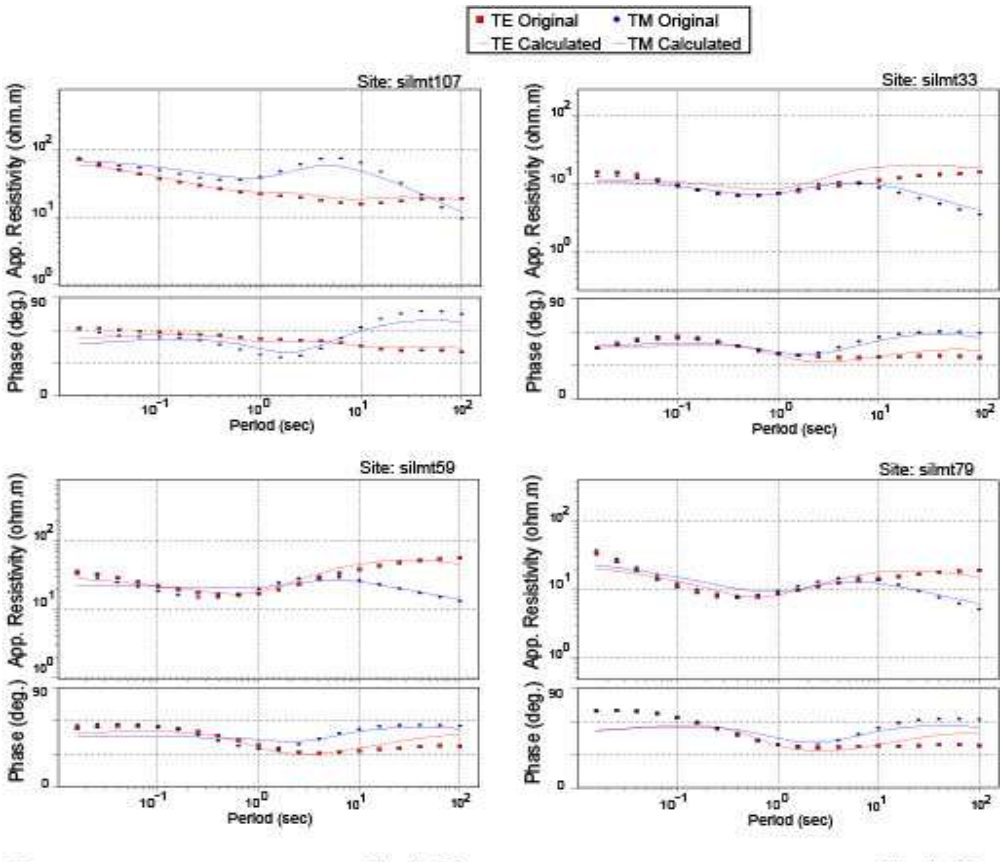

Figure 7: Plots of the calculated and original TE and TM data after 2D inversion were run. Most of the stations showed a good fit. Some of the models gave better fits than others depending on the quality of data and complexity of geology and geologic structures.

Our results (Figure 8 and 9) show that resistivity varies both laterally and with depth in the Silali region that can be attributed to temperature change, lithology change, presence of fluids, fluid phase change (liquid to vapour), and mineralogy. Very shallow (top 500 m) high resistivity (i.e the Summit region) interpreted as dry, unsaturated sediments and pyroclastic flows or unfractured basalts. Deeper (below -1000m) high resistivity (> 100 ohm-m) is inferred to be mainly due to unaltered volcanic flows such as the basalt and trachyte layer that dominate this region or the Precambrian basement rock. The shallow (above -2000m) low resistivity (< 20 ohm-m) zone that spreads laterally and covering almost the entire study area is perceived to be a product of thermal alteration to clays with low permeability, and water

saturated sediments and fracture systems that may imply high porosity and permeability, while the deeper low resistivity (LRZ2) is inferred to be the magma volume (Figure 8 and 9).

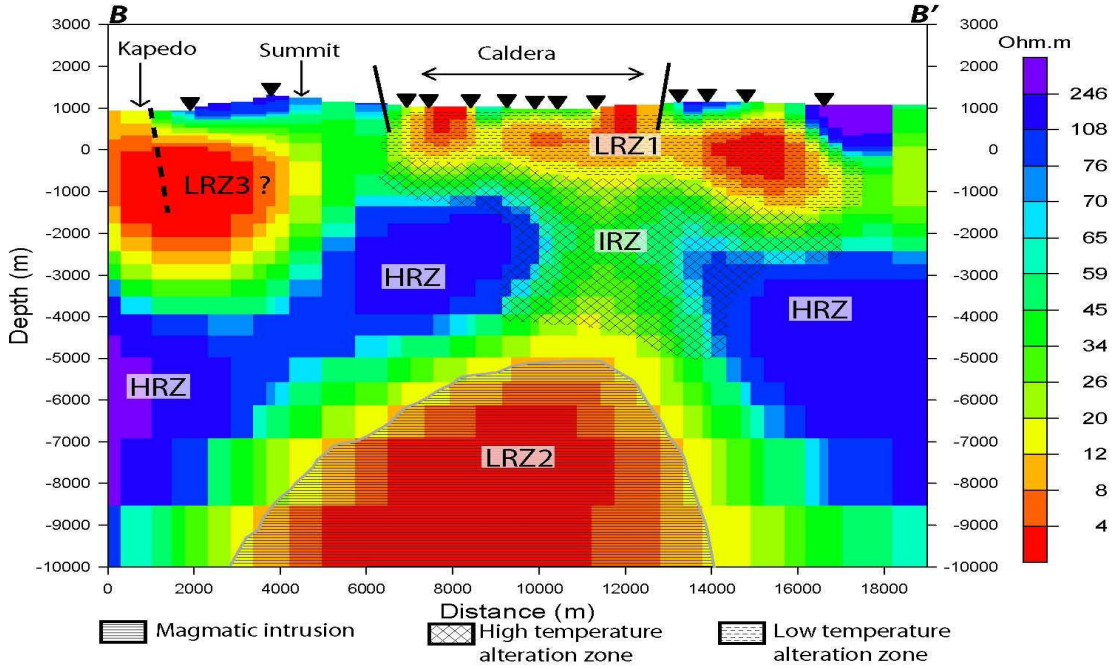

Figure 8: Two-dimensional resistivity inversion model of both TM and TE on a line that connects point B to the west and point B' to the east. The profile cuts through the Silali caldera, the Summit and the Kapedo areas. The inverted triangles are the MT data stations. HRZ = High Resistivity Zone, LRZ = Low Resistivity Zone and IRZ = Intermediate Resistivity Zone. The Solid lines are the caldera wall faults while the dashed line is an inferred fault.

The 2D resistivity models reveal four major regions: 1) a shallow low resistivity zone (LRZ1) with resistivity less than 20 ohm-m, 2) a high resistivity zone (HRZ) with resistivity greater than 100 ohm-m, 3) a deep low resistivity zone (LRZ2) with resistivity less than 12 ohm-m, and 4) an intermediate resistivity zone (IRZ) of resistivity ranging from 12 to 70 ohm-m appears to connect the LRZ1 and the LRZ2.

The shallow low resistivity zone, LRZ1, is suggested here to be a low temperature (~70^0C) hydrothermally altered zone or clays. This shallow low resistivity zone extends covers almost the entire of the caldera floor and also extends eastwards from the caldera covering the

mapped zone of intense faulting and fracturing. The high fracturing allowed thermal fluids circulation transferring heat from deep to shallow depth and later rocks forming low temperature clay and minerals such as smectite and the zeolite which favour the flow of electrical currents and hence reduce the bulk resistivity of rocks in this region. The region of intermediate resistivity (IRZ) that underlies LRZ1 is inferred to be of higher temperature as compares to LRZ1 as temperature increase with depth. We postulate that this increase in resistivity is related to increase in temperature and also mineralogy. We suggest that the high temperature hydrothermal which form at temperature above 240^0C such as chlorite and illite to be present in the IRZ zone. These minerals are good resistors to the flow of electrical current as compared to the smectite and zeolite minerals and hence the increase in resistivity. At this high temperatures most of the water is in gaseous state which could also contribute the high resistivity we envisage this zone (IRZ) to the hydrothermal reservoir that could be drilled for steam.

The deeper low resistivity region, LRZ2, beneath the caldera (Figure 8 and 9) is inferred to be magmatic material or intrusion at a depth of about 5000m below sea level (bsl). This interpretation is consistent with the interpretation of similar anomalies found in Krafla, Iceland and Olkaria Kenya where deep, low resistivity regions have been confirmed to be molten rocks *(Onacha 2006; Lochoro, 2009; Simiyu and Keller 2000).* Since the resistivity variations in this here is believed to be related to temperature variation, we anticipate that the low resistivity zone (LRZ1) to be within a temperature range of 70^0C - 220^0C, while the underlying IRZ to have temperature range of 240^0C to 350^0C at about 3000-4000 m below sea level where an estimated depth to the brittle-ductile transition zone and a temperature about 800^0C at the LRZ2 (magma body) *(e.g. Oskooi et at., 2005; Flovenz et al., 2005).*

The high resistivity zone (HRZ) is interpreted as unaltered basalts and Precambrian basement rocks. This high resistivity could be attributed to low porosity and permeability. The low resistivity zone (LRZ3) is inferred to be a fault and a shallow aquifer around the Kapedo region. Hot springs seeps are found around the Kapedo region and also water wells drilled in Kapedo confirms the presence of a shallow aquifer or fractured zone with water flow. However the constraint in this region is not good due to insufficient data.

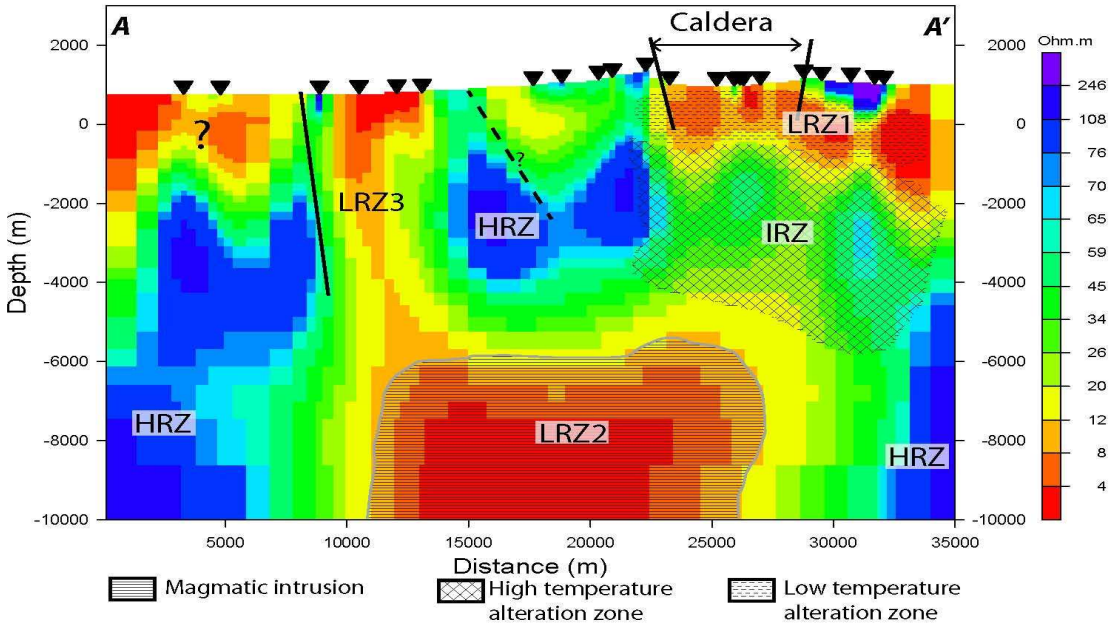

Figure 9: Two-dimensional resistivity inversion model of both TM and TE on a line that joins point A to the southwest and point A' to the northeast. The profile cuts through the Silali caldera. The inverted triangles are the MT data stations. HRZ = High Resistivity Zone, LRZ = Low Resistivity Zone and IRZ = Intermediate Resistivity Zone. The solid lines are known faults while the dashed line is an inferred fault from our data.

In high temperature geothermal field, fluid circulations within fractures transfer heat to shallow depth and later the rocks which they interact. Well log information (e.g. lithology and temperature) and surface resistivity measurement have shown a good correlation that have aided in the interpretation of resistivity signature up to drillable depths where

temperature and resistivity have been observed to increase with depth to the geothermal reservoir *(Newman et al., 2008; Anarson et al, 2010).* With proofs from the numerous resistivity studies, it is believed that the increase in resistivity with depth to the base of the reservoir in high temperature geothermal fields is controlled by a change mineralogy and temperature where low temperature electrical conductive minerals like smectite and zeolite at shallow depth while high temperature electrically resistive mineral like chlorite and illite at greater depths in the reservoir region *(Pellerin et al., 1996; Anarson et al., 2000; Flovens et al., 2005; Oskooi et al., 2005; Newman et el 2008).* These minerals have strong electronic bonding and hence suppress electrical current in regions where they are found *(Flovenz et al., 2005; Cumming et al., 2000 Wright et al., 1985).* The lower low resistivity in geothermal is often interpreted to be magma material an interpretation that has been supported by micro-earthquake studies where events do not occur in this region due to the ductile property of the *rocks (e.g. Onacha, 2006).*

Regional gravity studies covering the Silali area by Swain, (1994) and later Mariita and Keller, (2007) indicated the presence of a high density body at the Silali volcano which they interpreted as a magmatic intrusion whose depth resolution was poor due to data sparseness and in this study we have imaged the depth of the magma chamber to be about 6 km deep. On the other hand, Hautot et al (2000) imaged a deeper conductive body (between 4 to 8 km depth) which they interpreted to be a layer of sediments between the basement rocks and the overlying volcanic piles in the Baringo region just south of Silali that previous studies could not identify. In fact, our data, even at 10km below sea level could neither show such a layer nor indicate the boundary between the Precambrian rocks and the overlying volcanic pile. In addition, investigations such as that of the Kenya Rift International Seismic Project (KRISP) experiment *(e.g. Keller et al., 1994)* have indicated that the depth to the Precambrian decreases from the central region (depth of about 5 km) northwards with the depth of the

basement around Baringo about 3 km. Hence the depth to the Precambrian basement in the Silali region which is about 50km north of Baringo is expected to be about 3 km or even less but could be identified from out data.

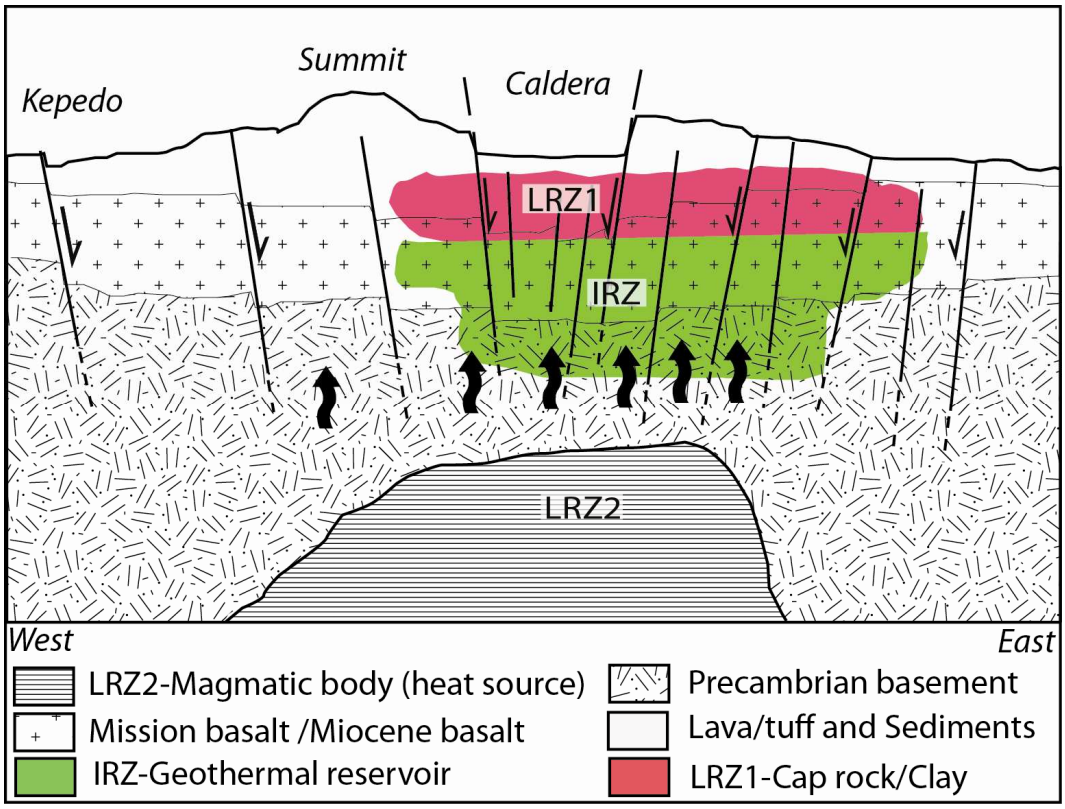

Figure 10: This is a generalized resistivity interpretation of the Silali region of an east-west slice through the caldera. The contact between the Precambrian basement and the overlying basalt is not known. The dark thick black wavy lines with arrows indicate heat transfer in this system.

1.5 Conclusions

This study has identified resistivity anomalies that are interpreted to be from permeable fracture zones, hydrothermally altered zones, and a magmatic body in the shallow crust of the Silali region. Volcanic flows cover much of the study region and are resistive to electrical currents unless altered by fluids or fractures. The boundary between the volcaniclastics and the Precambrian basement could not be identified in these data. A northeast-striking fault is

imaged in our data and correlates with the Suguta River channel west of the caldera which runs through Kapedo. A magmatic body is inferred to be located about 6 km below the surface of the volcano. We infer the magma body was shallow before the caldera formed and much of the shallow magma was emptied during and after the caldera formation. The volcanic process enhanced fracturing and formed conduits for fluid movement.

The shallow boundary between an upper, low resistive layer (LRZ1) and the underlying intermediate resistivity zone (IRZ) at depths of less than 2000 m appears to mark the change in clay mineralogy from an upper layer of smectite alteration to a lower chlorite dominated region. The boundary between these two zones indicates the region where the temperature has reached approximately 240^0C at some time during the history of the volcano. We can use this boundary to speculate on the events associated with the caldera formation and subsequent history of the volcano.

In particular, if this temperature boundary were the product of uniform conductive heating from a deep heat source, it might be expected that the 240^0C temperature isotherm was relatively flat when the alteration occurred. Alternatively, if the heat source were shallow then the 240^0C isotherm should roughly mimic the shape of the heat source in the subsurface at the time of the clay alteration. In addition, if the boundary were formed prior to the caldera eruption, we might expect it to now dip toward the region of caldera collapse because it would have collapsed as the magma escaped. However, the inferred 240^0C isotherm dips away from the caldera in our data. We suggest this indicates the isotherm is young and its shape is related to the modern day fluid migration from a relatively shallow heat source because it approximately mimics the shape of the inferred magmatic intrusion at a depth of 6000 m.

The likely mechanism for heat transfer at Silali is fluid migration based on the distribution of the shallow low resistivity zone. We suggest that a hydrothermal reservoir lies below the shallow conductors (LRZ1). Hot springs and fumaroles found in this region are surface indicators of a significant hydrothermal resource. We consider the above interpretation reasonable although speculative. We recommend additional studies and drilling to support our arguments. However, if this model is supported by drilling, then it will provide an additional tool for identifying likely sites for geothermal development based on a model of the subsurface temperature distribution and fluid migration.

1.6 Acknowledgements

We would like to thank Dr. Silas Simiyu and the Geothermal Development Company for allowing us to use their data for this study and also providing the software for data processing. We also thank the Dr. Peter Omenda for the insightful reviews of this work. Many thanks for Karen Christopherson of Chinook Geoconsulting, Inc and Charles Muturia of GDC for the discussion on data collections and processing. This work was supported by NSF grants EAR0749382 awarded to Dr. Laura Serpa.

1.7 References

Arnason, K., 1989. Central loop transient electromagnetic sounding over a horizontally layered earth. (No. OS-89032/JHD-06) Reykjavik: Orkustofnun.

Arnason, K., Eysteinsson, H., Hersir, G. P., 2010. Joint 1D inversion of TEM and MT data and 3D inversion of MT data in the Hengill area, SW Iceland. Geothermics, 39, 13-34.

Berktold, A., 1983. Electromagnetic studies in geothermal regions. J. Geophys. Surv 6. 173-200

Constable, S., Parker, P., Constable, C., 1987. Occam's inversion: a practical algorithm for generating smooth models from electromagnetic sounding data. Geophysics, 52. pp. 289–300.

Chave, A.D., Thompson, D.J., Ander, M.E., 1989. On the robust estimation of cross power spectra, coherence, and transfer function, J. Geophys. Res., 92, 633-648.

Cumming, W., 2009a, Geothermal resource conceptual models using surfece exploration data. Proceedings 34th workshop on Geothermal Reservoir Engineering, Starnford University, Starnford, CA.

Cumming, W., Mackie, R., (2010). Resistivity imaging of geothermal resource using 1D, 2D, and 3D MT inversion and TDEM static shift correction illustrated by a Glass mountain case history. Proceeding World Geothermal Congress, 2010.

Cumming, W., Nordquest, G., astra, D., (2000). Geophysical exploration for geothermal resources: an application for combined MT –TEM. In: Society of exploration Geophysics Annual Meeting Teaching program expanded Abstracts, 6-11 August, Canary, Canada, pp. 1071-1074.

Dinkley, P.N., Smith, M., Allen, D.J., Darling, W.G., 1993. The geothermal activity and geology of the northen sector of the Kenya rift valley. British geological ssurvel research, Report SC/93/1,185pp.

Fairhead, J.D., 1976. The structure of the lithosphere beneath the Eastern rift, East Africa, deduced form gravity studies. Tectonophysics 30, 269-298

Flovenz, O., Spangenberg, E., Kulenkampff, J., Anarson, K., Karlsdottir, R., and Huenge, E., 2005. The role of electrical conduction in geothermal exploration. Paper presented at the World Geothermal Congress, Antalya, Turkey.

Hay, D.E., Wendlandt, R.F. and Keller, G.R., 1995. The region of Kenya rift plateau-type flood phonolites: integrated petrologic and geophysical constrain on the evolution of the upper mantle beneath the Kenya rift, J. Geophys. Res., 100, 5435-5444.

Ingham, M., 2004. High resolution electrical imaging of fault zones. Phy. of the earth and planetary interior. 150. p. 93-105.

Keller, G.R., Mechie, J., Braile, L.W., Mooney, W.D and Prodehl, C., 1994a. Seismic structure of the uppermost mantle beneath the Kenya rift, in Crustal and upper Mantle

structures of the Kenya Rift, eds Prodehl, C., Keller, G.R. and Khan, M.Z., Tectonophysics, 236, 201-210.

Keller, G.R., Mechie, J., Braile, L.W., Mooney, W.D and Prodehl, C., 1994b, The East African rift system in light of KRISP 90, in Crustal and upper Mantle structures of the Kenya Rift, eds Prodehl, C., Keller, G.R. and Khan, M.Z., Tectonophysics, 236, 453-464.

Lichoro, M.C., 2009. Joint 1-D inversion of TEM and MT data from Olkaria Domes geothermal area, Kenya, UTP-GTP, Iceland, Report 16, 45pp.

Macdonald, R., Davis, G.R., Upton, B.G.J., Dunkley, P.N., Smith, M. Leat, P.T., 1995. Petrogenesis of the Silali volcano, Gregory rift, Kenya. J. Geol. Soc. London. London, 152, 703-720.

Macdonald, R., Scallet, B., 2006.The Central Kenya peralkaline province: Insight into the evolution of peralkaline salic magma. Lithos 91, 59-73, doi:10.1016/j.lithos.2006.03.009

Mariita, N. O., Keller, G. R., 2007. An integrated geophysical study of the northern Kenya rift. J. Afr Earth Sc. 48, 80-94.

Meju, M. A., (1996). Joint inversion of TEM and MT data soundings: some effective practical considerations. Geophysics 61, 56-65.

Monastero, F.C., Katzenstein, A.M., Miller, J.S., Unruh, J.R., Adams, M.C. and Richards-Dinder, K., 2005. The Coso geothermal field: A nascent metamorphic core complex., Geol. Soc of America Bulletin, 117, 1534-1553.

Nabighian, M.N., 1991. Electromagnetic Method in Apllied Geophysics, Soc of Explor. Geophys, Tusla, Okla.

Newman, G. A., Hoversten, M.,Gasperikova, E., Wannamaker, P. E., (2008). Three-Dimensional magnetotelluric characterization of the Coso geothermal field. Geothermics 37, 369-399.

Omenda, P.A., 1997. The Geochemical Evolution of Quaternary Volcanism in the South-Central Portion of the southern Kenya rift. PhD. Dissertation, University of Texas at El Paso, 218pp.

Omenda, P.A., Opondo, K., Lagat, J., Mungania, J., Mariita, O., Onacha, S., Wetangula, G., Ouma, P., 2000. Ranking of geothermal prospect in the Kenya rift. Kenya Electricity Generating Company Limited, Internal report, pp 121.

Onacha, S.A., 2006. Hydrothermal fault zone mapping using seismic and electric measurements. PHD thesis, Duke University, pp. 249

Oskooi, B., Pedersen, L.B., Smirnov, M., Arnason, K., Eysteinsoon, H. and Manzella, A., 2005. The deep geothermal structure of the Mid-Atlantic Ridge deduced from MT data in SW Iceland. J. Physics of the Erath and Planetary Interiors, 150, 183-195.

Pellerin, L., and Hohmann, G. W., 1990. Transient electromagnetic inversion: a remedy for magnetotelluric static shift. Geophysics 55, 1241-1250.

Pellerin, L., Johnston, J. M., Hohmann, G. W., 1996. A numerical evaluation of electromagnetic methods in geothermal exploration. Geophysics 61, 121-130.

Rodi, W., Mackie, R.L., 2001. Nonlinear conjugate gradient algorithm for 2D magnetotelluric inversion. Geophysics 66, 174-187.

Simiyu, S. M., 2010. Status of Geothermal Exploration in Kenya and Future plans for Its Development. In: Proceedings of the world geothermal congress, Bali, Indonesia. 11pp

Simiyu, S. M., Keller, G. R., 2001. An integrated geophysical analysis of the upper crust of the Southern Kenya rift. Geophys. J. Int. 147, 543-561.

Simiyu, S. M., Keller, G. R., 1997. An integrated analysis of the lithospheric structure across the east African plateau based on gravity analysis and recent seismic studies. Tectonophysics Vol. 278.

Smith, M., 1994. Stratigraphic and structure constraints on the mechanism of active rifting in the Gregory rift Kenya. In: C. Prodehl, G. R. Keller and M. A. Khan (Editors), Crustal and Upper mantle structure of the Kenya rift. Tectonophysics, 236, 3-22.

Smith, M., Dunkley, P.N., Deino, A., Williams, L.A.J., McCall, G.J.H., 1995. Geochronology, stratigraphy and structural evolution of Silali volcano, Gregory Rift, Kenya., J. Geol. Soc. Lon, London. 152, 297-310.

Spichak, V., Manzella, A., 2009. Electromagnetic sounding of geothermal zones. J. Appl. Geophys. 68, 459-478.

Volpi, G., Manzella, A., Fiordelisi, A., 2003. Investigation of the geothermal structures by magnetotelluric (MT): an example from the Mt. Aminata area, Italy. Geothermics, 32. 131-145.

Vozoff, K., 1991. The magnetotelluric method, in Electromagnetic method in Applied Geophysics, edited by M.M Nabighian, pp. 641-711, Soc. Of Explor. Geopgys., Tusla, Okla.

Wannamaker, P. E., 1999. Affordable magnetotellurics; interpretation in natural environments. In; Orastaglio, M., Spies, B. (Eds.), Three-Dimension Electromagnetic. Geophysical Development Series, Vol. 7. Soc. Expl. Geophys., Tulsa, p. 724.

Willams, L.A.J., 1978. Character of Quaternary volcanism in the Gregory Rift Valley, in Geological Background to Fossil maned. Bishop, W.W., J. Geol. Soc. London, London. , pp. 55-69,

Williams, L.A.J., Macdonald, R., Chapman, G.R., 1984. Late Quaternary caldera volcanoes of the Kenya rift valley. J. Geophys. Res. 89, 8553-8570.

Wright, P. M., Ward, S. H., Ross, H. P., West, R. C., 1985. State-of-the-art geophysical exploration for geothermal resources. Geophys. 55. 2666-2699.

SECTION 2

Joint Geophysical Analysis of the Coso Geothermal Field, south-eastern California

(Paper submitted to Journal)

WAMALWA, Antony M.[1,3], MICKUS, Kevin L.[2], and SERPA, Laura F.[1], DIANE, Doser I.[1]
1. Department of Geological Sciences, University of Texas at El Paso, 500 W. University, El Paso, TX 79968,
2. Geosciences, Missouri State University, 901 S National Ave, Springfield, MO 65804-0087
3. Geothermal Development Company, P.O. Box 100746, 00101, Nairobi, Kenya

2.1 Abstract

In this paper we derive and interpret 3-D density models from gravity data and 2-D resistivity models from MT data collected in the vicinity of the Coso geothermal field. Our data show zones of both low resistivity and low density at about 6 km depth in the Devils Kitchen and the Coso Hot Springs areas. We interpret these zones to indicate the presence of cooling magmatic material that provides the heat for the geothermal system in these regions. A zone marked by high resistivity and low density is indicated to lie directly above the interpreted magma body extending to within 1 km depth below the surface in the reservoir region where it is capped by a low resistivity clay zone. In addition, density models show the high density bodies correlate with volcanic peaks or mountains which may imply a region of dense mafic intrusions or dikes.

2.2 Introduction

The Coso Geothermal field in southeastern California has been the topic of numerous geophysical investigations (e.g., Duffield et al 1980; Feng and Lees, 1980; Feng and Lees, 1998; Wu and Lees, 1999; Adams et al., 2000; Lees and Wu, 2000; Vlahivic et al., 2002; Wannamaker et al., 2004; Hauksson and Unruh, 2007; Newman et al., 2008; Unruh et al., 2008) conducted to determine the depth to and the nature of the heat source, and to image the plumbing system for geothermal fluids. Recently studies have suggested that the Coso geothermal field could be overlying an emerging metamorphic core complex (Monastero et al., 2005; Unruh et al., 2008). Despite some well-designed experiments that have been conducted in this region, the depth to the heat source (magmatic material) has remained controversial. Gravity and seismic studies by Plouff and Isherwood (1980), Lees (2002), Wilson et al. (2003), and Yang et al. (2011), showed that partially molten rocks may occur at 5 km depth beneath the geothermal reservoir while seismic studies by Hauksson and Unruh (2007) and Unruh et al. (2008) show the magma chamber may occur at depths greater than 10km. The three dimensional magnetotelluric (MT) analyses by Newman et al. (2008) mapped the extent of the geothermal reservoir and fractures but could not image a magma chamber because the model used frequencies that focused on the upper 4 to 5 km in the reservoir region. The above studies show that interpretations geophysical data are non-unique. In this paper, we review the existing geophysical data and reinterpret the gravity data using 3D inversion methods and the MT data using all available frequencies to determine whether we can reduce the uncertainties in the interpretation based on new knowledge we have gained by studying geothermal systems in Kenya with similar techniques and access to drilling results.

In our studies of the Kenya geothermal systems we used gravity, seismic, and magnetotelluric data from active volcanoes to image magma in the subsurface, map fractures and constrain the lithology (Wamalwa et al in review). The integration of the geophysical data sets and an ongoing drilling program based on these studies gives us additional information on where our interpretations have been particularly accurate in the shallow subsurface and where we need to revise our interpretations. Based on this experience, we are re-examining gravity and MT (Wannamaker et al., 2004, 2005; Newman et al., 2008) data collected within the Coso geothermal field to resolve some of the differences in the various interpretations by conducting an integrated study of the gravity, magnetotelluric and seismic data similar to that done for the Kenya geothermal fields (e.g. Wamalwa et al., in review).

2.3 Coso Geothermal Field

The Coso geothermal field lies in a Pliocene-Pleistocene volcanic field located in south-eastern California (Figure 1) east of the Sierra Nevada Range in the Basin and Range province (Roquemore, 1980) of the western United States. The volcanic field is the source of one of the largest geothermal fields generating electricity in the Basin and Range region (Wilson et al 2003). It covers an area of approximately 400 km^2 and is located in a releasing bend of a dextral strike-slip fault system (Figure 1) along the eastern margin of the Sierra Nevada Range (Adams et al., 2000). The stresses that control the faulting within the Coso Geothermal region are related to its location in the transition zone between the Basin and Range to the east and the San Andreas Fault transform plate boundary to the west (Roquemore, 1980). Faults and fractures caused by interactions between these tectonic boundaries host and allow fluid flow, particularly in the upper 3-4 km of the crust as marked by the level of seismicity (Wu and Lees, 1999). The faults and fractures have been targeted for high yield hydrothermal production wells at Coso (Adams et al., 2000; Sheridan et al.,

2003; Newman, et al., 2008) similar to geothermal systems around the world like the Iceland, Kenya and USA (e.g. Simiyu and Keller, 2000; Malin et al., 2005; Onacha, 2006). The rocks in and surrounding the Coso geothermal field are comprised of a highly fractured basement complex of the Coso Range consisting of Mesozoic plutonic and metamorphic rocks that have been intruded by mafic and felsic dikes.

Pleistocene volcanic rocks that range from basalts to dacite to rhyolite cover the regions from Volcano Butte, through Silver Spring, and the Coso Peak (Figure 1). Quaternary sedimentary rocks (the Coso formation) that comprises of alluvium, sandy arkosic beds, fine grained tuffacious and lacustrine materials (Duffield et al., 1980) cover the west region in the Rose Valley area and the southeast region in the Coso Basin area. Additionally, rhyolitic domes were formed along faults marked with fumarole emissions seeping through the faults (Duffield et al., 1980; Manley and Bacon, 2000; McQuarie and Oskin, 2010). Bimodal basaltic-rhyolitic volcanism coincided with extensional tectonics that began around 3 to 4 Ma that occurs has interbedded material (tuffs, rhyolitic and basaltic flows) (Duffield et al., 1980). The geothermal system could be underlain by a magma chamber that is proposed to have been in existence for at least 1 Ma during which time it has risen from a depth of 10 km to a depth of 5 km and has become hotter by at least 30^0C (Manley and Bacon, 2000).

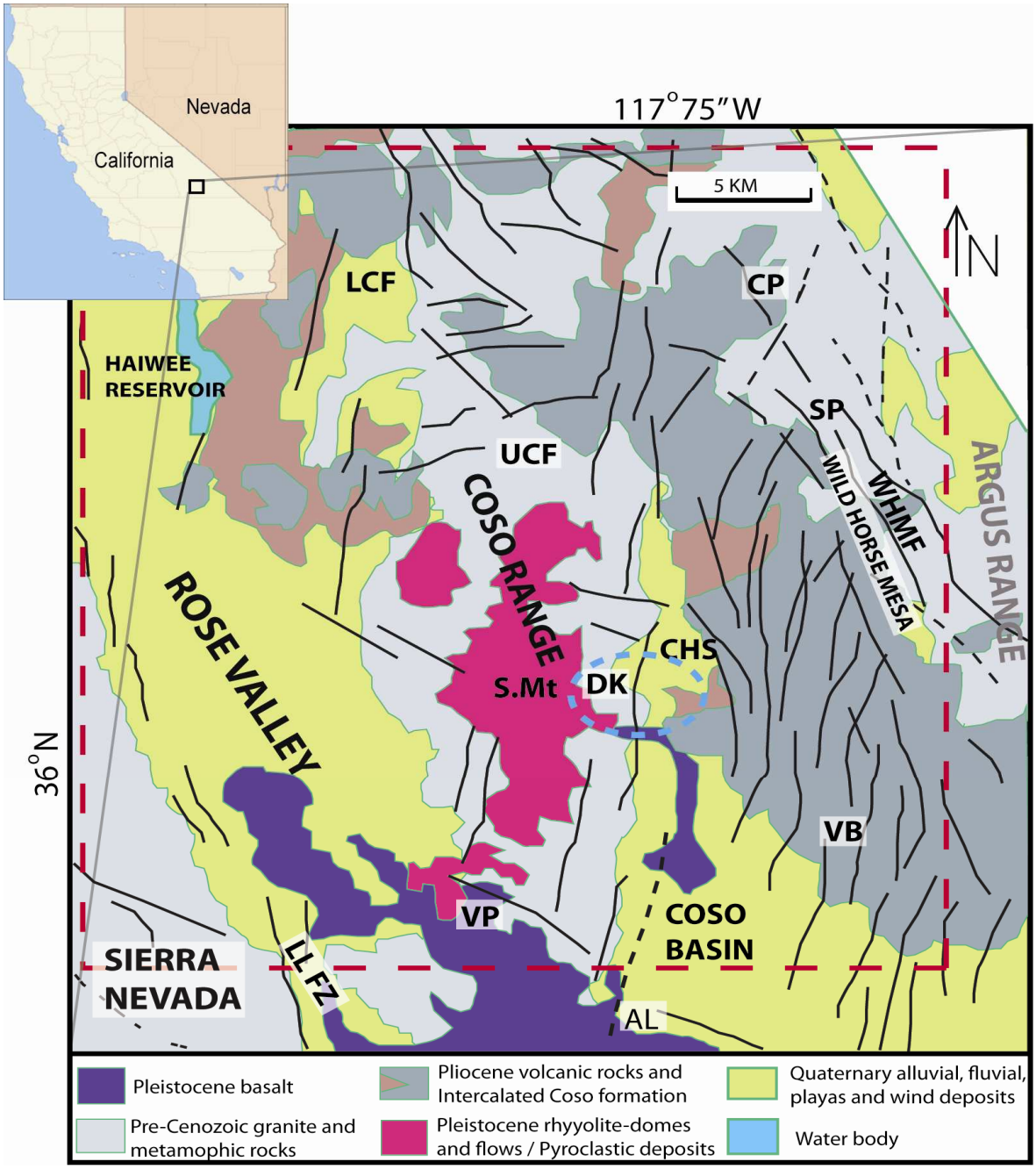

Figure 4: Location and geology of the Coso Range in southeastern California modified from Duffield et al (1980). Shown are the faults (black solid (mapped) and dashed (inferred) lines).The blue dashed ellipse is the geothermal region, S. Mt the Sugarloaf Mountains, VP is Volcanic Peak, AL is Airport Lake, LLFZ is Little Lake Fault Zone, DK is Devils Kitchen, CHS is Coso Hot Springs, VB is Volcanic Butte, CP is Coso Peak, SP is Silver Peak, UCF is Upper Cactus Flat, LCF is Lower Cactus Flat, WHMF the Wild Horse Mesa Faults. The rectangle marked by bold red dashed line, is the area covered by gravity data: Figure 2 and 5.

The Coso Range region is cut by a set of faults which probably have been active since the early Cenozoic (Figure 1). These can be grouped into two sets of major normal faults that strike west-northwest, and strike north-northeast, and minor faults that strike from east-northeast to east-southeast that mostly intersect the major faults at acute angles. The minor faults are probably related to local doming or uplift (Duffield and Bacon, 1979; Duffield et al., 1980). Young fault scarps observed in the Quaternary alluvium and Pleistocene sediments show that this region is still active (Bacon et al., 1980; Duffield et al 1980). In regions around Coso Hot Springs and the Devils Kitchen (the geothermal area) fumaroles, hot water and hydrothermally altered grounds are located along faults (Bacon et al., 1980).

2.4 Previous geophysical studies

2.4.1 Seismic

The region in and surrounding the Coso Geothermal field is characterized by a high level of local seismicity (swarms) with event magnitudes less than three and occur in the upper 5 km of the crust in the geothermal reservoir areas, such as the Devils Kitchen, Nicol Prospect and Coso Hot springs, and few deeper events (up to 12 km) in the surrounding regions (Feng and Lees, 1998; Lee and Wu, 2000; Lees, 2000; Vlahovic et al., 2002; Lees, 2002 Julian et al., 2009). Micro-earthquake event locations are used to determine which faults are active and the location of the base of the brittle/ductile transition above the heat source. Shear wave polarization data shows there is preferential fracture orientation ranging between N10W to N20E (Walter and Weaver, 1980; Vlahovic et al., 2002; Wilson et al., 2003). A low P-wave velocity zone has been observed in the Coso Geothermal Field, however, the velocity delays here are small (~0.2 sec) compared to other geothermal systems (Steeples and Iyer, 1976).

Around the geothermal reservoir, e.g. in the Devils Kitchen area, low P-wave velocities have been identified between depths of 5 to 20 km (Reasenberg et al., 1980; Young and Ward,

1980; Haukson and Unruh, 2007). Seismic wave attenuation of teleseismic data was observed by Young and Ward (1980) in the shallow crust below 5 km around the geothermal reservoir which they implied represented the presence of a magma chamber. A seismogenic boundary is inferred to be at a depth of about 5 km because most micro-earthquake events are concentrated above this depth in the geothermal reservoir region (Young and Ward, 1980, Wu and Lees, 1996, 1999; Lees, 2002; Wilson et al., 2003; Unruh et al., 2008). Similarly, Wilson et al. (2003) imaged a strong seismic wave reflector at about 5 km depth that they interpreted to be the top of the magma chamber. Their results showed no evidence of deeper reflector at greater depths and suggested that molten material is found in the 5-10 km depth range. This interpretation supported by a petrological analysis of Fe-Ti oxides, feldspars, hornblende and plagioclase phase assemblages, and Al-in-hornblende and other mineral barometry to estimate the age of the magma in the Coso geothermal field by Manley and Bacon (2000). Recent studies of ambient noise tomography by Yang et al. (2011) observed a low velocity zone in the 6-12 depth range which they suggested to be a zone of magmatic material.

In contrast, teleseismic data analysis by Haukson and Unruh (2007) showed that, like other seismic studies, a low velocity zone is present in the depth range 5-10 km below the surface, but this zone did not show any change in Vp/Vs ratios. They suggested that the low velocity zone is due to the presence of brine or other fluids rather than molten rocks. At depths below 10 km they observed low P-wave velocity and higher Vp/Vs which they related to the presence of a small volume (less than 1 km^2) of magma.

2.4.2 Gravity

Although a rich gravity database for the Coso geothermal field area and the regions around is available, the majority of the data have not been interpreted or published. The complex

volcanic and tectonic setting of this region makes it difficult to interpret the gravity data for upper crustal geology. This is probably due to the fact short wavelength anomalies of the upper crustal features are suppressed by medium to long wavelength lower crust and upper mantle features. Nevertheless, high amplitude gravity gradients (Figure 2) observed from Bouguer gravity anomaly maps have been used to imply the presence of numerous faults within the region (Plouff and Isherwood, 1980; Feighner and Goldstein, 1990). Previous gravity studies (Plouff and Isherwood, 1980) mapped a high gradient between -150 and -145 mGal that forms a crude horseshoe shape that encloses most of the Pleistocene rocks of the Coso Range (Figure 2). A 5 to 50 mGal, 20 km diameter gravity high around the Sugarloaf Mountains area (Figure 2 and 5) is interpreted as an underlying pluton or mantle derived, partially molten mafic rocks that are remnants of fractional crystallization rocks approximately 10 km deep (Feighner and Goldstein, 1990; Monasteto et al., 2005). These authors modelled the complete Bouguer gravity data that comprises all the frequencies from deeper mantle to shallow crustal features. In this study we focus our analysis on the shallow crustal features. Unlike the previous studies we separate the residual from the complete Bouguer data to enhance shallow or crustal features. The residual data were then inverted to obtain a 3-D density distribution of the shallow crust to determine the source of the anomalies in the residual data.

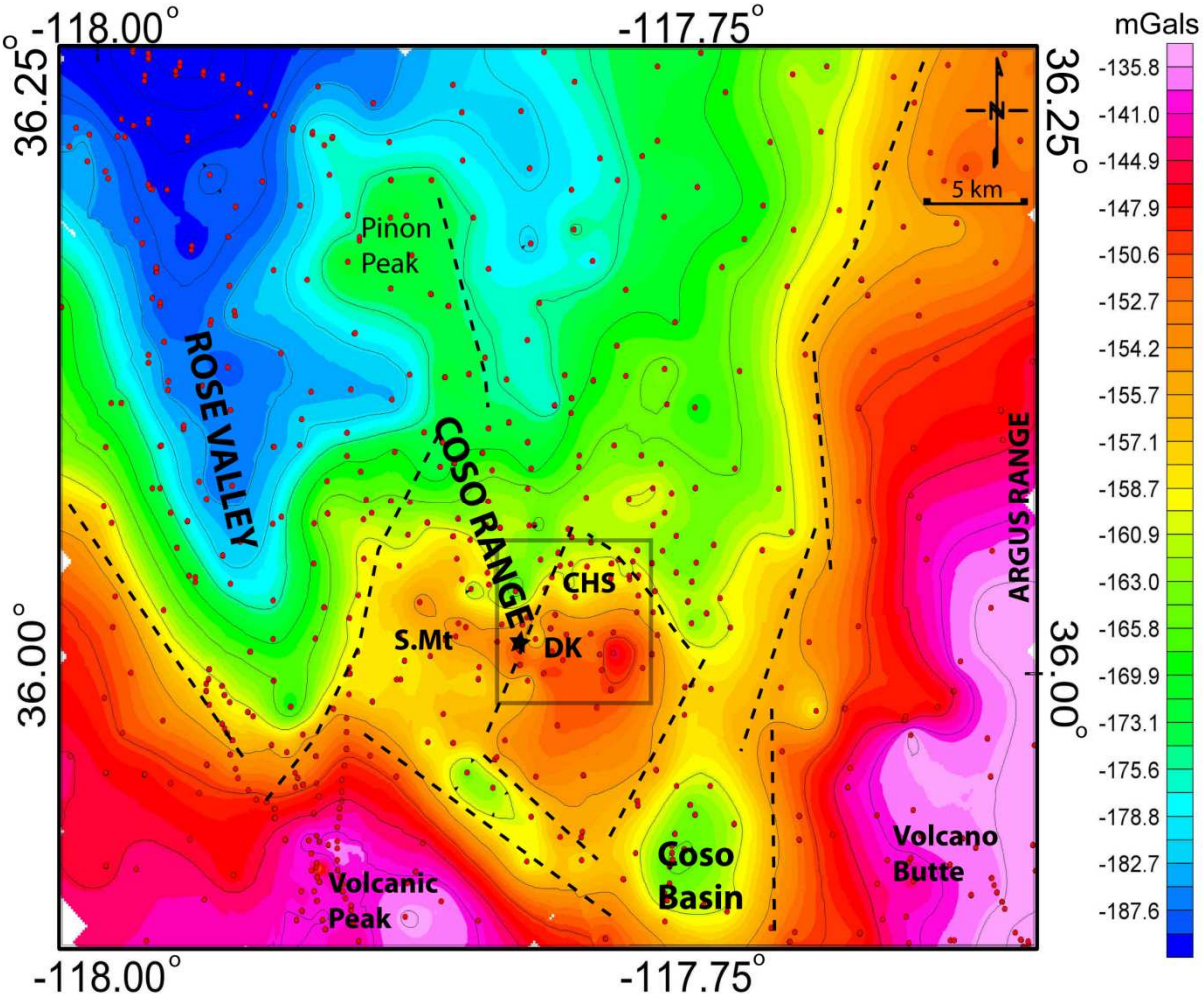

Figure 5: Complete Bouguer gravity anomaly map of the Coso geothermal field and the surrounding region contoured at a 5mGal interval. The dashed lines are inferred faults from gravity gradients. The red points are locations of the gravity stations. The location of the geothermal resource is around the Devils Kitchen (DK) and the Coso Hot Spring (CHS) areas. The rectangle box enclosing DK and CHS is the area covered MT soundings shown in Figure 3.

2.4.3 Resistivity

Resistivity methods are effective in imaging electrically conductive subsurface features such as fluid filled fractures, hydrothermal minerals, metallic minerals, high temperature regions or clays commonly formed within high temperature geothermal fields (Wannamaker, et al, 2004, 2005; Newman et al., 2008). Initial resistivity studies in the Coso geothermal field included Schlumberger, audio-magnetotelluric and telluric mapping (Jackson et al., 1977;

Jackson and O'Donnel, 1980).The main finding of these studies were that major low resistivity were associated with Rose Valley and Coso Basin/Wash, regions of valley fills or alluvium, and also areas around Coso Hot springs and Devils Kitchen regions associated with rocks hydrothermally altered by hot and saline water (Jackson and O'Donnel, 1980). Most of these early studies could only investigate to very shallow depths (less than 1 km) in the subsurface. In order to characterize and monitor the geothermal reservoir, magnetotelluric (MT) data were recently collected around the Coso geothermal field and also east of the main geothermal field (Wannamaker et al., 2004; 2005), part of which were available and used in our analysis (Figure 3a). The region east of the main Coso geothermal field was included in the MT survey because it has high temperatures (about 300^0C at about 2.7 km) and appears to be a favourable region for geothermal resources. However, preliminary analysis of the MT data indicates that the rocks appear to have low permeability (Wannamaker et al., 2004; 2005) and this factor limits drilling and exploitation of the heat source. The MT data were interpreted by Newman et al. (2008) who performed a 3D inversion and generated a detailed image of the upper 5 km of the crust. However, they could not identify a magma chamber or any indication of molten rocks as the source of heat mainly because of the depth limit of their models.

2.5 Magnetotelluric method and data analysis

Naturally-occurring electromagnetic fields (2 horizontal electric fields and 3 components (2 horizontal and vertical) of the magnetic field) are recorded at an MT station as time series. The horizontal electric and magnetic fields are used to derive period dependent impedance tensors which then are converted to apparent resistivities and phases (Vozoff, 1972; 1991). The variations of resistivity with depth can be estimated from derived apparent resistivities as shown by Park and Wernicke (2003). In this study, we will use the MT data to determine the

electrical conductivity structure of the Coso geothermal field region and to investigate the presence of inferred magmatic material in the 5-10 km depth range.

MT measurements are usually vulnerable to near surface resistivity inhomogeneities that give rise to a frequency independent galvanic response (static shift) on the MT apparent resistivity curves (Berdichevsky and Dmitriev, 1976; Pellerin and Hohmann, 1990). This shift may result in significant errors either by over estimating (if the shift is upward) or underestimating (shift is downward) the true apparent resistivity values and must be removed before performing any type of interpretation.

The details of the MT data acquisition used in this study are given by Wannamaker et al. (2004; 2005) and Newman et al. (2008). The data collection was conducted in a noisy environment where the existing geothermal power plant was the main source of noise (Wannamaker et al, 2004). Various efforts were made to filter out the noise by applying remote referencing methods using data simultaneously collected at a distant station (Wannamaker et al., 2004, 2005). The electromagnetic time series data collected were corrected for noise and processed using robust methods (e.g., Egbert, 1997) to their apparent resistivities and phases and stored in standard electronic files (EDI). The data covers a frequency range between 250-0.01 Hz and based on simple skin depth calculations, the data can be used to estimate resistivity variations to at least 10 km.

Before the data were interpreted, the data were analyzed for noisy data by removing data with large errors. The remaining data were smoothed using various polynomial orders (3 to 5). The smoothed apparent resistivity and phase data were used in the modeling procedure. In addition, a dimensionality analysis was performed to determine the strike of regional electric structures (e.g., Ledo et al., 2011). The determined electric strikes were used to rotate the impedance tensors to directions parallel and perpendicular to electric strike.

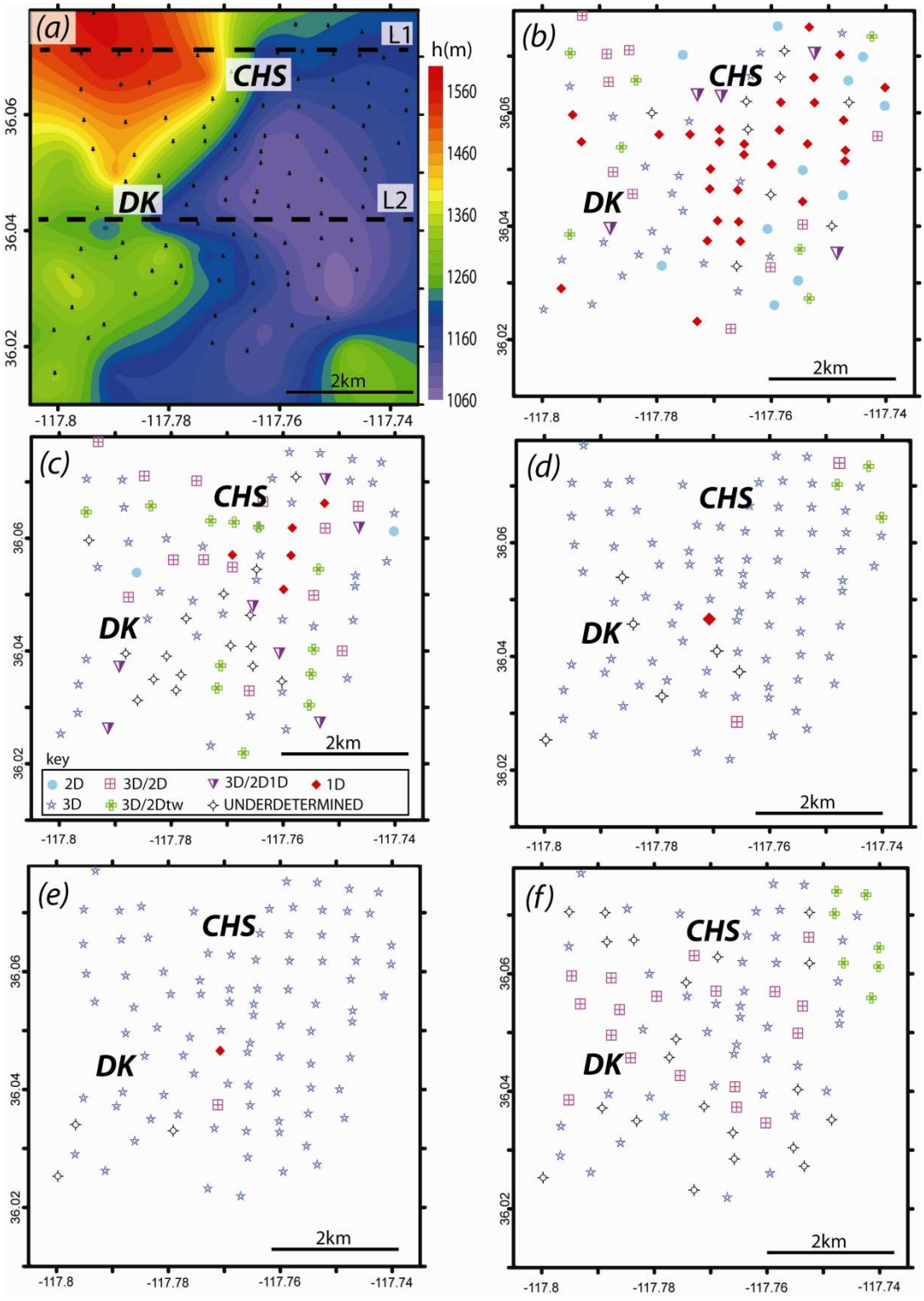

Figure 6: Dimensionality analysis (1D, 2D, 3D or underdetermined) for each MT sounding grouped in five period bands using the method of Marti et al. (2004; 2009): (a) Elevation data (colour) with MT stations (black dots). The black dashed lines are the profile lines where 2-D inverse modelling was conducted as shown in Figure 4. (b) band 1, T=0.01-0.1 sec; c) band 2, T=0.1-1sec; d) band 3, T=1-10 sec; e) band 4, T=10-100 sec; and f) band 5, T>100 sec.

The smoothed, rotated data were used in the modelling process. There are a number of methods for determining the dimensionality of MT data (e.g., Groom and Bailey, 1989; Bahr, 1991; Weaver et al., 2000; McNeice and Jones, 2001; Marti et al., 2004, 2009) and each has different limitations (see Marti et al., 2009). Here we use the WAL rotational invariant methods of Marti et al. (2004; 2009) to estimate the dimensionality of the data and the results are shown in Figure 3.

The dimensionality results indicate that the Coso geothermal field indicate a fairly 1-D to 2D for periods less than one second (T<1 sec) and above one hundred seconds (T>100 sec).Some 3D features as also included in this periods. The 2-D feature at shorter periods (less the 1sec) with the strike direction being dominantly northwest with some east strike direction (Figures 3b and c), and dominantly 3-D for periods 1 to 100 seconds (Figure 3d and e), and Despite there being a 3D electrical environment for part of the data, there is a sufficient 2-D environment to allow us to implement 2-D inversions. We believe that our results may include errors based on this assumption but recent studies have shown that 2-D inversions can give a reasonable result when applied in a 3-D environment (Wannamaker, 1999; Park and Mackie, 2000).

The choice for the MT profile line (east-west profile lines) was based on the local geology and mapped faults (Adams et al., 2000); electrical strike directions from the dimensionality analysis (Figure 3) and the residual gravity anomaly map (Figure 5). The profiles were drawn to cross structures and target the geothermal reservoir areas (i.e. the Devils Kitchen and Coso Hot Springs areas). In contrast to the previous studies which focused on the upper 5 km (Newman et al., 2008), our models were extended to 10 km in depth.

The models shown in Figure 4 were obtained after 60 iterations inversion runs. Different half space models were used with uniform resistivity of 20, 40 and 60 ohm-m and final results

showed minimal/insignificant variations and displayed the major resistivity zones shown in Figure 4. Our model convergence was fairly good with low RMS error that ranging 4% to 7%. Our results (Figure 4) are comparable to those obtained from the 3D inversion of Newman et al (2008) and the 2-D transverse magnetic model of Newman et al. (2008) and Wannamaker et al. (2004).

The 2-D inversion algorithm by Rodi and Makie (2001) was used to construct final MT models along profiles (a) and (b) (Figure 3). Before the inversion process the data were rotated to their principal axis and smoothed to minimize errors due random data scattering. The smoothed data were used for the 2-D modelling. **E**x, **H**x **E**y and **H**y data for frequency ranging from 0.01 Hz to 250 Hz were included for modelling. No other data were available to correct for static shift and hence the models presented here are not corrected for static shift. The transverse electric (electric field parallel to the strike) and transverse magnetic (magnetic field parallel to the strike) mode smoothed apparent resistivities and phases were used in the inversion process.

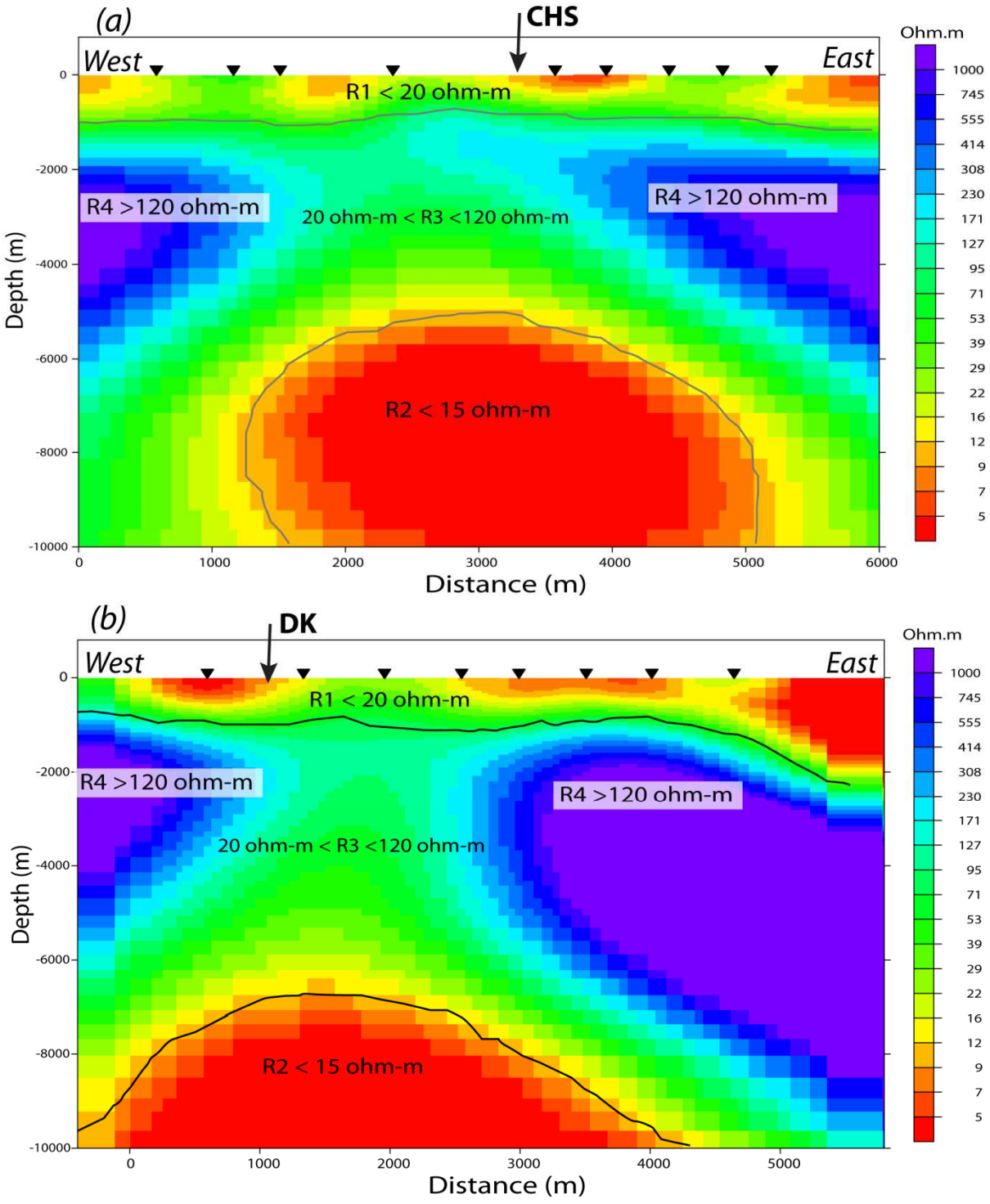

Figure 7: Two-dimensional magnetotelluric models that across the Coso Hot Spring (a) and the Devils Kitchen (b) areas constructed by inverting the TE and TM mode apparent resistivities and phases. The inverted triangles are the MT stations. The lines drawn on the models mark the major resistivity boundaries. The regions marked R1, R2, R3, and R4 are the major resistivity zones. CSH is Coso Hot Springs and DK is Devils Kitchen.

The upper 5 km sections of the 2-D models show a shallow low resistivity zone marked R1. This layer spreads laterally across the length of both models (Figures 4a, b). This layer represents mainly illite and smectite clays as shown in drill hole data in the Devils Kitchen area (Lutz et al., 1996). Two high resistivity zones (R3 and R4) and a low resistivity zone (R2) are located below the low resistivity zone R1. Zone R3 connects the shallow low resistivity R1 and the deeper low resistivity (R2) zone. R2 is less resistive than zone R4 which extends to the east and west of our models. Zone R3 is interpreted as faults correlating with a region marked by high seismicity (Lees, 2002; Hauksson and Unruh, 2007) and, in the Devils Kitchen area, this zone has been targeted for production wells. These fracture systems are favourable for the flow of fluids within the geothermal reservoir whose resistivity is believed to be controlled by illite, chlorite, epidote and wairakite minerals (Lutz et al., 1996; Newman et al., 2008) within a fluid environment. The high resistivity zone R4 is interpreted to be caused by unfractured, low saturation rocks which could imply that this is a zone with minimal porosity or no permeability. The most important discovery of both models is the position of the low resistivity zone (R2). The top of the R2 low resistivity zone is about 6 km deep. We interpret this zone to define the location of a cooling magma body that is the source of heat for the geothermal system. Previous resistivity studies did not image this zone due to the depth limitation of their methods, although a brittle-ductile transition zone was inferred at about 5km depth near the Devils Kitchen area (Newman et al., 2008).

2.6 Gravity data analysis

The main focus of this study is on the shallow crust but the complete Bouguer anomaly map shown on Figure 2 contains anomalies that appear to be from geological features that are both local/shallow and regional/deeper and, in particular, small-scale or local geology appears to

be supressed by large/regional geology due to the mismatch between the Complete Bouguer map (Figure 2) with the geologic map (Figure 1). The Bouguer map (Figure 2) shows prominent minima that are associated with the Rose Valley and the Coso Basin and probably the Pleistocene rhyolite field. The gravity gradient could indicate major fault zones that bound the sedimentary basins. The long wavelength gravity maxima in the southwest and east regions of the map coincide with regions of basalts and metamorphic rocks. It is likely that the high gravity anomaly represents a deeper mafic intrusion. To interpret anomalies caused by shallow or crustal density variations that could also be related to the geology shown in Figure 1, we separate these anomalies by removing them from longer wavelength regional density variations. There are a variety of methods to attempt the so-called regional-residual anomaly separation, including upward and downward continuation, wavelength filtering, and polynomial trend-surfaces. Although none of these methods is superior over the other, we used a fourth-order polynomial surface to fit regional gravity anomaly and subtracted it from the Bouguer gravity anomalies to produce a residual gravity anomaly map (Figure 5). A quick comparison of the residual gravity anomaly map (Figure 5) to the geology map shows more correlations than the comparison of Figure 1 to Figure 2. The residual gravity map shows high amplitude maxima in the Volcanic Peak, Volcanic Butte, Coso Peak, Silver Peak, Pinon Peak, Cactus Peak and the Sugarloaf Mountain-Coso Hot Spring regions. The anomalies are interpreted to result from dense mafic flows or dikes in the crust. Gravity minima are observed within the Rose Valley to the rest of the Coso Range, the Coso Basin to the south of Coso Range, and the areas between the Sugarloaf Mountains and Pinon Peak, Silver Peak and Volcanic Butte. These gravity low anomalies are related to sedimentary rocks (Coso formation) and rhyolite domes as also observed from the geology of the region (Figure 1). The boundaries between the high and low gravity anomalies are inferred to be faults (Figure 5) which agrees with mapped faults from previous geological studies (Duffield et al., 1980).

Thus we believe that the gravity anomalies shown in Figure 5 represent local geologic features or crustal features.

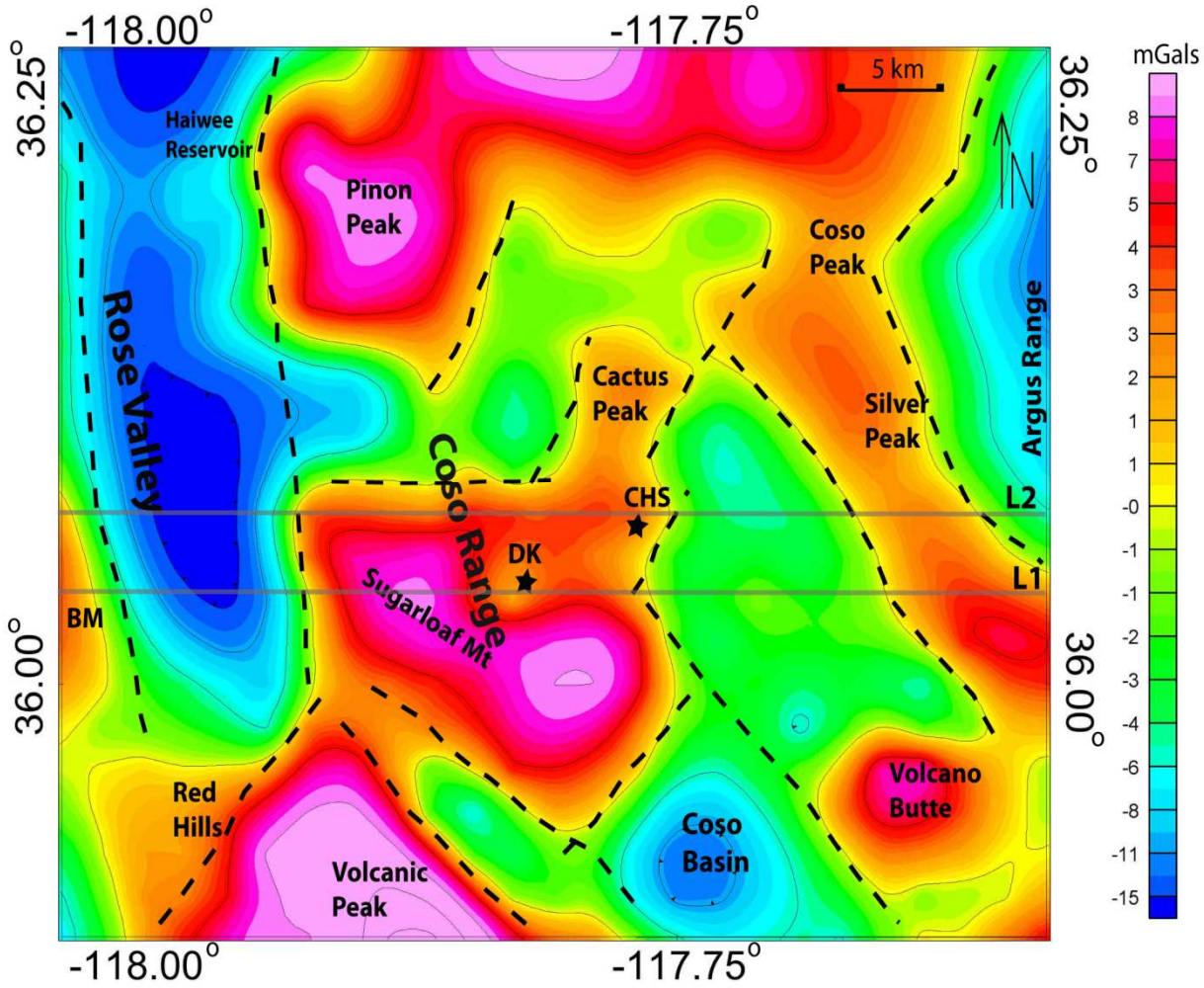

Figure 8: Residual gravity anomaly map derived from removing a fourth-order polynomial surface from the Bouguer gravity anomalies of the Coso region (Figure 3). The dashed lines are inferred faults. The two solid east-west lines L1 and L2 are the locations of cross-sections used to display the 3-D density model. The geothermal resource is found around the Devils Kitchen (DK) area and Coso Hot Spring (CHS) area. Contour interval is 5 mGal.

To estimate the depth and geometry of the sources of the residual gravity anomalies (Figure 5), a 3-D inversion (Li and Oldenburg, 1998) of the residual gravity anomaly data was performed. Different inversion parameters (e.g., weighting of the data, data errors, choice of

objective function, starting model and size of model mesh) were considered and varied in some cases to test the consistency of our models with geology. Poor choices for these parameters could lead to results that have no relationship to the actual geology despite a low RMS error (Li and Oldenburg, 1998). The inversion helps estimate the densities of the subsurface from the residual gravity anomalies and they represent a density contrast model rather than actual densities. The mean density used in this model was 2.7 g/cm^3. The inversion space domain was made of a block of 21000 m (EW) by 19750 m (NS) by 32500 m (depth) that was then divided into cubes of different sizes, with 391524 small cubes of 250 m length on the top, and 33180 medium size cubes of 500 m length in the middle, and119 large size cubes of 2500 m length in the below (bottom). The data was assigned a 5% Gaussian error. The densities were allowed to vary from 3 g/cc for basalt to 2.4 g/cc for sediments or rhyolites. Several inversions were performed to observe the effect of the different weighting and objective function on the final results. The results show in Figure 6 was obtained after 70 iterations and had a RMS error of 0.9 mGal that is consider low than acceptable.

Comparisons of the residual gravity anomaly map and the 3-D model with the surface geology of the area show a good match. The modelled densities could be related to the Mesozoic granite and metamorphic rocks, mafic rocks like gabbro, Quaternary rhyolites, Tertiary-Quaternary sediments and volcanic deposits (Adams et al., 2002). For example, the high gravity/density zones correlate with volcanic peaks or mountains like Coso Peak, Silver Peak, Sugarloaf Mountain, and Ball Mountain, while the low density regions correlate with basin fill/ alluvium, rhyolitic domes, molten rocks, or faults and fractures.

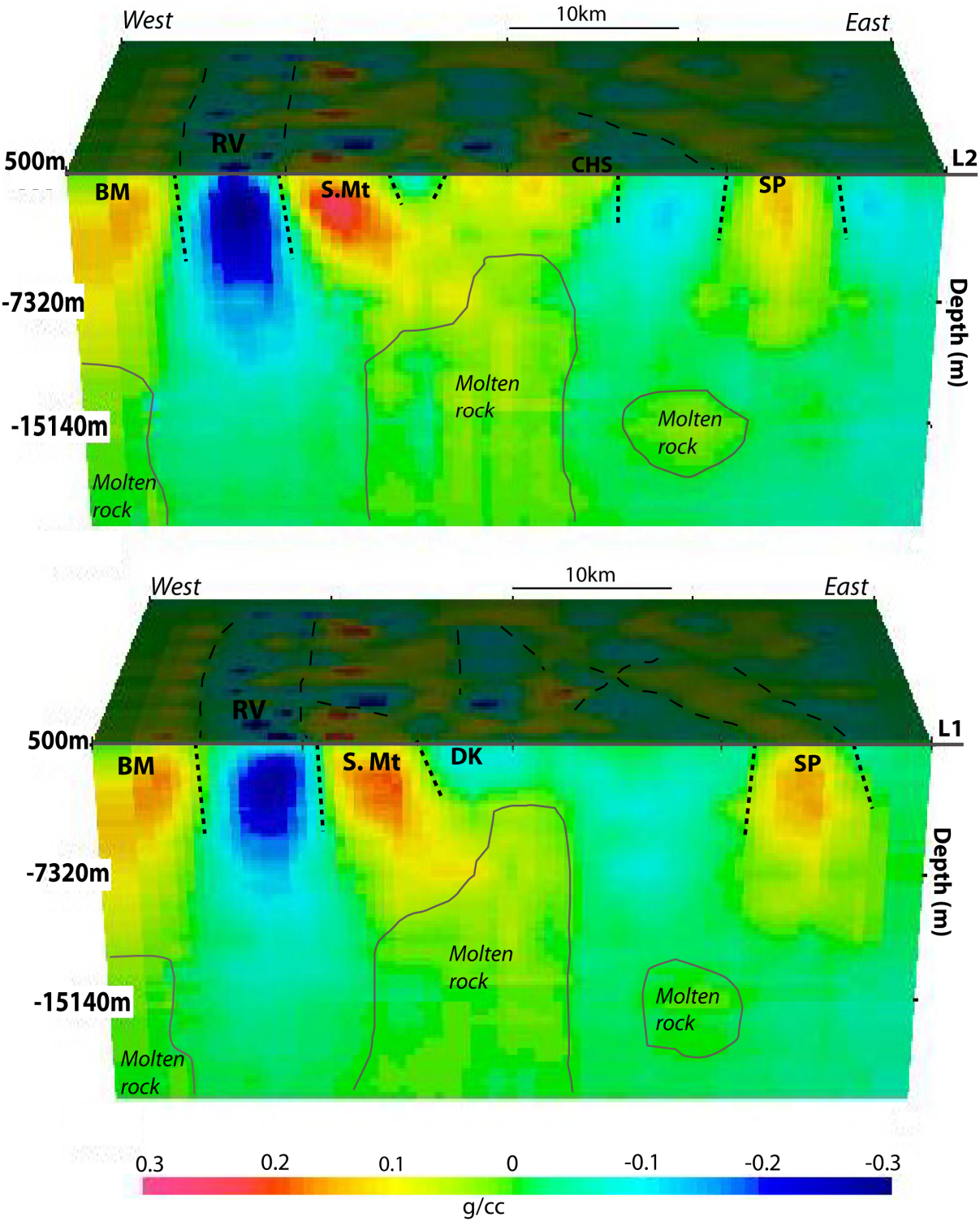

Figure 9: Three-dimensional density distribution of the Coso geothermal field and the surrounding regions determined by the inversion of the residual gravity anomalies. The dashed lines are inferred faults or contacts based on density contrasts. The mean density used here is 2.7g/cc (marked zero). The area marked BM is the Ball Mountains, S. Mt Sugarloaf Mountain, RV Rose Valley, DK Devils Kitchen, and SP is Silver Peak.

To simplify our interpretation, we divided the model densities into two groups: low density zones ranging between 2.4 g/cm^3 and 2.7 g/cm^3 to represent the felsic rocks, volcaniclastics and sediments/sedimentary rocks, low density rhyolites, or fractured rocks such as those within the geothermal reservoir, and the high density zones between 2.7 g/cm^3 and 3.0 g/cm^3 that represent the mafic lithology e.g., gabbro and basalts and the mixture of mafic (gabbro) and felsic (lucogranite) rocks that have been identified in this region whose density vary between 2.75 g/cm^3 and 2.95 g/cm^3 depending on the compositional mixture (Whitmarsh, 1998). The high density regions associated with volcanic peaks or mountains such as Sugarloaf Mountain and Ball Mountain extend from the surface to a depth of 7.3 km and are underlain by low density rocks. The high density zones are associated with high seismic velocities (Hauksson and Unruh, 2007; Yang et al., 2011) and are interpreted to be unfractured, dense rocks or cold plutons. The underlying low density zones are interpreted as partially molten rocks. We believe that from the Tertiary and through the Quaternary (Adams et al., 2002; Manley and Bacon, 2000) volumes of molten rocks/magma were forced into the shallow crust and some were extruded to the surface while others remained within the crust. With time, the top and outer part cooled to form denser rocks near the surface but hot rocks still exist beneath those cooled rocks (Figure 6).

Previous studies have suggested that there are two magma chambers in the region, a shallow and a deeper chamber (Manley and Bacon, 2000). However, other geophysical studies have indicated the existence of a single chamber system instead (Wilson et al., 2003). Our analysis also indicates a single magma chamber whose top is about 6 km deep. Its lower limit could not be resolved using the gravity or MT data. Gravity lows are observed in places where extension tectonic processes formed basins that are now filled with sediments and loose volcanic deposits like Rose Valley and Haiwee Ridge. In other places, rising magma has forced the rocks above to fracture and those fractures are now the host and channel for

hydrothermal fluids like in the Devils Kitchen area (Figure 5 and 6). A similar scenario, where magma upwelling has caused intense fracturing and high density dikes above a low density magmatic material, was observed at the Menengai geothermal field in Kenya (Wamalwa et al., 2012)

2.7 Conclusions

Geophysical methods can help understand the nature of the subsurface, but overdependence on a single method can be misleading, and hence the contribution of several techniques over a particular target is preferable. In the present study, we used a gravity and MT data analysis to show that a correlated low resistivity and low density zone may be partially melted material that provides the heat for the Coso geothermal field. The low density/resistivity region lies below a seismogenic boundary (Haukson and Unruh, 2007) and corresponds to a region of little to no seismicity which is inferred to be a result of the presence of ductile rocks. The upper region of high seismicity is characterised by earthquake swarms that may indicate on-going fracturing or thermal expansion and/or contraction related to an underlying inferred magmatic material. From our analysis and the previous studies it is evident that a major thermal boundary exists at 5-6 km depth. This is a temperature boundary that marks the brittle-ductile transition zone that could be estimated to be about 300 to 400^0C. The main question lies on what underlies this boundary. We suggest a magmatic material based on the other MT studies around the world and our Menengai study that shows a zone of restricted seismicity. This however cannot rule out the possibility of a high pressure zone containing brine as it will still give a low resistivity signature.

The 2D inversion of MT data and 3D inversion of residual gravity data is interpreted to as a zone of partially molten rocks in the Coso region based on a low resistivity and low density

zone below 6 km in depth. The presence of fracture systems that probably host the geothermal resources in this region correlate well with the locations of the micro-earthquake events like those observed in similar studies in Kenya (Wamalwa et al., in review). Unfractured rocks are marked by intermediate to high density zones and high resistivities.

Geothermal exploration is usually focused on the identification of the source of heat (magma chamber), fractures that can allow circulation of fluids, and convective heat transfer to the near surface where it can be tapped by wells and fluids. We believe our work presents an improved and more complete picture of the Coso geothermal fields by identifying all the features related to the geothermal system,

2.8 Acknowledgements

We would like to thank Mr. Andre Sabine, and Wei-Chuang Huang of the United States Navy Geothermal Program-Coso for availing the MT data used for our study. We are also grateful for Mr. James Wambugu, of Geothermal Development Company of kenya for availing the software used for MT data interpretation. This study was partly finances by NSF award No 0749382.

2.9 References

Adams, M. C., Moore, J. N., Bjounstad, S., Norman, D. I., 2000. Geologic history of the Coso geothermal system. Geothermal Resource Council Transactions 24, 205-209.

Bahr, K., 1991. Geological noise in magnetotelluric data: a classification of distortion types. Phys. Earth Planet. Inter. 66, 24-38.

Berdichevsky, M. N., Dmitriev, V. I., 1976a. Distortion of magnetic and electric field by near surface lateral inhomogeneities. Acta Geod., Geophys. Montanist. Acad. Sci. Hung. 11, 447-483.

Berdichevsky, M. N., Dmitriev, V. I., 1976b. Basic principles of interpretation of magnetotelluric sounding curves, In Geoelectric and Geothermal studies, KAPG Geophysical Monograph., Akademiai Kiado, Budapest, pp 165-221.

Duffiels, W. A., Bacon, C. R., Dalrymple, G. B., 1980. Late Cenozoic volcanism, geochronology and structure of the Coso Range, Inyo County, California. Journal of Geophysical Research, 85,2381-2404.

Feighner, M. A., Goldsten, N. E., 1999. A gravity model of the Coso geothermal area. DOE report.

Feng, R., Lees, J. M., 1998. Microseismicity, stress, and fracture in the Coso geothermal field, California. Tectonophysics, 289, 221-238.

Groom, R., Bailey, R., 1991. Analytic investigations of the effect of near-surface three dimensional galvanic scatterers on MT tensor decomposition. Geophysics 56, 496-518.

Hauksson, E., Unruh, J., 2007. Regional tectonics of the Coso geothermal area along the intra-continental plate boundary in central-eastern California: Three-dimensional Vp and Vp/Vs models, spatial-temporal seismicity pattern and seismogenic strain deformation: Journal of Geophysical Research, v. 112. [doi:10.1029/2006JB0044721]

Jackson, D. B., O'Donnell, J. E., 1980. Reconnaissance electrical surveys in the Coso Range, California. Journal of Geophysical Research. 85, 2502-2516.

Julian, B. R., Foulger, G. R., Monastero, F. C., Bjounstad, S., 2010. Imaging hydraulic fractures in a geothermal reservoir. Geophysical Research letters, 37. doi:10.1029/2009GL040933.

Lees, J. M., 2002. Three-dimensional anatomy of a geothermal field, Coso, southeast-central California. Mem. Geological Society of America, 195, 259-276.

Lees, J. M., Wu, H., 2000. Poisson's ratio and porosity at Coso geothermal area, California. Journal of Volcanology and Geothermal Research 95, 157-173.

Li, Y., Oldenburg, D. W., 1998. 3D inversion of gravity data. Geophysics 63,109-119.

Lutz, S. J., Moore, J. N., Copp, J. F., 1996. Integrated mineralogical and fluid inclusion study of the Coso geothermal systems, California. In: Proceedings of the Twenty-First Workshop on Geothermal Reservoir Engineering, Stanford University, pp. 187-194.

Malin, P., Onacha, S., Elyon, S., 2005. Deminstrating a microearthquake and magnetotelluric production and injection well targeting technology: Rhyolite plateau exploration area in the Long Vally Caldera, California. CEC Report.

Manley, C. R., Bacon, C. R., 2000. Rhyolite thermobarometry and the shallowing of the magma reservoir, Coso volcanic field. Journal of Petrology 41, 149-174.

Marti, A., Queralt, P., Ledo, J., 2009. WALDIM: A code for the dimensionality analysis of magnetotelluric data using the rotation invariants of the magnetotelluric tensor. Comp. Geosc. 35, 2295-2303.

Marti, A., Queralt, P., Roca, E., 2004. Geoelectric dimensionality in complex geological areas: application to the Spanish Betic Chain. Geophys. J. Int. 157, 961-974.

McNeice, G., Jones, A., 2001. Multisite, multi-frequency tensor decomposition of magnetotelluric data. Geophysics 66, 158-173.

McQuarrie, N., Oskin, M., 2010. Palinsplastic restoration of NAVDat and implications for the origin of magmatism in southwestern North America, Journal of Geophysical Research 115, B10401, doi:10,1029/2009JB006435.

Monastero, F. C., Katzenstein, A., Miller, J., Unruh, J. R., Adams, M., Richards-Dinger, K., 2005. The Coso geothermal field: A nascent metamorphic core complex, Geological Society of America Bulletin 117(11), 1534-1553, doi:10.1130/B25600.1.

Newman, G. A., Hoversten, M.,Gasperikova, E., Wannamaker, P. E., 2008. Three-dimensional magnetotelluric characterization of the Coso geothermal field Geothermics 37, 369-399.

Onacha, S.A., 2006. Hydrothermal fault zone mapping using seismic and electric measurements. PHD thesis, Duke University, pp. 249

Park, S. K., Mackie, R. L., 2000. Resistivity (dry?) lower crust in an active orogen, Nanga Parbat, northern Pakistan. Tectonophysics 66, 158-173.

Park, S. K., Wernicke, B., 2003. Electrical Conductivity of Quaternary faults and Tertiary detachments in the California Basin and Range. Tectonics 22, 1030.

Pellerin, L., Hohmann, G. W., 1990. Transient electromagnetic inversion: a remedy for magnetotelluric static shift. Geophysics 55, 1241-1250.

Plouff, D., Isherwood, W. F., Bacon, C. R., Duffield, W. A., VanBuren, H. M., 1980. Bulk density and magnetization measurements near the Coso Range, California, Open File Report 80-61, U.S.G.S Denver, Colo.

Rodi, W., Mackie, R., 2001. Nonlinear conjugate gradient algorithm for 2-D magnetotelluric inversion. Geophysics. 66, 174-187.

Roquemore, G., 1980. Structure, tectonics, and stress field of the Coso Range, Inyo County, California. Journal of Geophysical Research 85, 2471-2483.

Sheridan, J., Kovac, K., Rose, P., Barton, C., McCilloch, J., Berard, B., Moore, J., Petty, S., Spielman, P., 2003. In situ stress, fracture and fluid flow analysis-east flank of the Coso geothermal system. In: Proceedings of the Twenty-Eight Workshop on Geothermal Reservoir Engineering, Stanford University, pp 34-49.

Steeples, D. W., Iyer, H. M., 1976. Teleseismic P-wave delays in geothermal exploration: In, Proceeding of the Second Unites Nations Symposium on the Development and Use of Geothermal Resources. v.2, pp. 1199-1206, United Nation, New York, 1976.

Unruh, J. R., Monastero, F. C., Pullammanappallil, S. K., 2008. The nascent Coso metamorphic core complex, east-central California: Brittle upper plate structure revealed by reflection seismic data. International Geological Review, 50, 245-269. Doi:10.2747/0020-6814.50.3.245.

Vlahovic, G., Elkibbi, M., Rial, J.A. 2002. Shear wave splitting and reservoir crack characterization: Coso geothermal field, J Volcanol. Geothermal Res., 120, 123-140.

Vozoff, K., 1972. The magnetotelluric method in the exploration of sedimentary basins. Geophysics 37, 977-991.

Vozoff, K., 1991. The magnetotelluric method, , In: M.M Nabighian (Ed.), Electromagnetic method in Applied Geophysics, p. 641-711, Soc. Explor. Geophys., Tulsa, Ok.

Walter, A. W., Weaver, C. S., 1980. Seismicity of the Coso Range, California, Journal of Geophysical Research 85, 2441-2458.

Wamalwa, A. M., Mickus, K., Serpa, L. F., (in review). Geophysical characterization of the Menengai volcano, Central Kenya Rift from the analysis of magnetotelluric and gravity data.

Wannamaker, P. E. 1999. Affordable magnetotellurics; interpretation in natural environments. In; Orastaglio, M., Spies, B. (Eds.), Three-Dimension Electromagnetic. Geophysical Development Series, V. 7., p. 349-374, Soc. Explor. Geophys., Tulsa, OK.

Wannamaker, P. E., Rose, P. E., Doerner, W. M., McCulloch, J., Nurse, K., 2005. Magnetotelluric surveying and monitoring at the Coso geothermal area, California, in support of the enhanced geothermal systems concept: survey parameters and initial results. In: Proceedings World geothermal Congress, Antalya, Turkey.

Wannamaker, P. E., Rose, P., Doerner, W., Berard, B., McCulloch, J., Nurse, K., 2004. Magnetotelluric surveying and monitoring at the Coso geothermal area, California, in support of the enhanced geothermal systems concept: survey parameters and initial results. In: Proceedings of the Twenty-Ninth Workshop on geothermal Reservoir and Engineering, Stanford University, pp. 287-294.

Weaver, J., Agarwal, A., Lilley, F. 2000. Characterisation of the magnetotelluric tensor in terms of its invariants. Geophys. J. Int. 141, 321-336.

Whitmarsh, R. S., 1998. Structural development of the Coso Range and adjacent areas of east-central California, Ph.D. thesis, University of Kansas, Lawerence.

Wilson, C. K., Jones, C. H., Gilbert, H. J., 2003. Single-chamber silic magma system inferred from shear wave discontinuities of the crust and uppermost mantle, Coso geothermal area, California. Journal of Geophysical Research, v. 108[doi:10.1029/2003].

Wu, H., Lees, J. M., 1999. Three-dimensional P and S velocity structure of the Coso geothermal area, California from micro seismic travel time data. Journal of Geophysical research. 104,13,217-13,223,doi:10.1029/1998JB900101.

Yang, Y., Ritzwoller, M. H., Jones, C. H., 2011. Crustal structure determined from ambient noise tomography near the magmatic centre of the Coso region, southeaster California. Geochem. Geophys. Geosyst, 12, Q02009, doi:10.1029/2010GC003362.

SECTION 3

Geophysical Characterization of the Menengai Volcano, Central Kenya Rift from the Analysis of Magnetotelluric and Gravity Data

(Paper Submitted to Journal)

WAMALWA, Antony M.[1,3], MICKUS, Kevin L.[2], and SERPA, Laura F.[1]
1. Department of Geological Sciences, University of Texas at El Paso, 500 W. University, El Paso, TX 79968,
2. Geosciences, Missouri State University, 901 S National Ave, Springfield, MO 65804-0087
3. Geothermal Development Company, P.O. Box 100746, 00101, Nairobi, Kenya

3.1 Abstract

In this study, we qualitatively analyze detailed gravity and broadband magnetotelluric data in and surrounding the Menengai Volcano region of the East African rift in Kenya in order to assess geothermal potential of the region. Three-dimensional density models obtained by inverting residual gravity anomalies and 2D resistivity models obtained by inverting the TE and TM magnetotelluric modes show several common features. At shallow depths, 0.5 km to 1.5 km below a caldera at the summit of the Menengai volcano, a low resistivity and low density region is interpreted as a highly fractured zone that consists of clay minerals resulting from hydrothermal alteration. A higher resistivity zone is imaged just beneath the shallow low resistivity layer at a depth range of 1.5 to 4 km below the surface interpreted a high temperature reservoir zone. The increase in resistivity with depth within the caldera region in particular suggests a change in mineralization as a result of increasing temperature. At greater depths approximately 6-7 km another low resistivity (> 25 ohm-m) low density zone was identified within caldera and interpreted as molten material that is the source of heat for the geothermal system. The low resistivity regions that correlated with the low density region within the caldera are bounded by high resistivity, high density volcanic units implying that the dense and electrically resistive volcanic material is relatively cool and lacks significant fluid content. This result agrees well with the results from previous seismic studies.

3.2 Introduction

The Menengai volcano is located within the Kenya portion of the East African Rift, referred to here as the Kenya Rift (Figure 1). Since the Miocene, extensional tectonics accompanied by faulting, uplift, lava flows, and volcanism has formed the Kenya Rift. In the Quaternary, several volcanoes were emplaced within the rift axis (Simiyu and Keller, 1997, 2001; Omenda, 1997, 1998; Mariita, 2003,). Previous geophysical studies indicate that the various volcanic centres within the rift grabens correlate with a 50 km wide and 20 mGal positive gravity anomaly embedded within a broad gravity low. This gravity high, combined with high seismic velocities within the crust, has been interpreted to be caused by magmatic intrusions into the shallow crust (Simiyu and Keller, 1997, 2000, 2001; Mariita and Keller, 2007).

A recent study by Simiyu and Keller (2001) showed that a shallow, high velocity, dense body is located about 4 km beneath the Menengai volcano. Microseismc studies (Simiyu, 2009) imaged a body that attenuated seismic waves and was interpreted as an indication of partially molten material at about 6-7 km depth. In this region, faults that facilitated magma flow out of the original chamber may now control ground water and hydrothermal fluid movement (Leat, 1984).

Geophysical methods (e.g., Becktold, 1983; Bibby et al., 1995; Arnason et al., 2010) have been used extensively in resource exploration to image the geology and map subsurface structures. The results from any geophysical data modelling process are non-unique (e.g., Arnason et al., 2010; Serpa and Cook, 1984) and hence the interpretation of the data in terms of subsurface geology is not straightforward. However, integrated interpretation of models derived from different types of geophysical data may yield a more realistic geological model

of the subsurface. In this study, we focus our efforts on the Menengai volcano with a detailed qualitative analysis of gravity and broadband magnetotelluric (MT) data. We compliment the previous geophysical studies (e.g. Simiyu and Keller, 2001; Simiyu, 2009) with new 3D density and 2D resistivity models which will be analysed for anomalies that appear in each of the data sets and for features that are common to the individual models. In doing this, we intend to obtain a detailed image of the underlying magmatic body and the associated geothermal reservoir. Our collective interpretation of these individual models is intended to mitigate the errors and non-uniqueness in each of the methods leading to reasonable and reliable conclusions about the source of the observed gravity maxima and an aseismic zone.

3.3 Previous geophysical studies in the Kenya Rift

Several geophysical and geological studies (e.g. Karson and Curtis, 1989; Swain, 1992; Simiyu and Keller, 1997, 2001; Mariita and Keller 2007; Meju and Sakkas, 2007) have been conducted within the Kenya Rift that have focused on the geology at both lithospheric and crustal scales. The results from the Kenya Rift International Seismic Experiment (KRISP) are probably the most important geophysical studies because they revealed major features of the rift which provides a model for rift structures today. Keller et al. (1994a) and Prodehl et al. (1994) discussed the KRISP data in terms of the processes that formed the rift which lead to the complex lithospheric structure associated with rift formation. They showed that the crust is approximately 35km thick in the central section of the rift around the Menengai volcano and thins northwards towards Lake Turkana. In addition, Keller et al. (1994a) observed that the P-wave velocity of the upper mantle was about 7.8 km/s with a density of 3.12 g/cm^{3}near the Menengai region but it decrease to 7.5 km/s with an increase in density to 3.26 g/cm^3, to the north near Lake Turkana (Henry et al., 1990; Keller et al., 1994; Mechei et al., 1997

Simiyu and Keller 1997). Henry et al. (1990) also showed that high velocity material underlies the Menengai region.

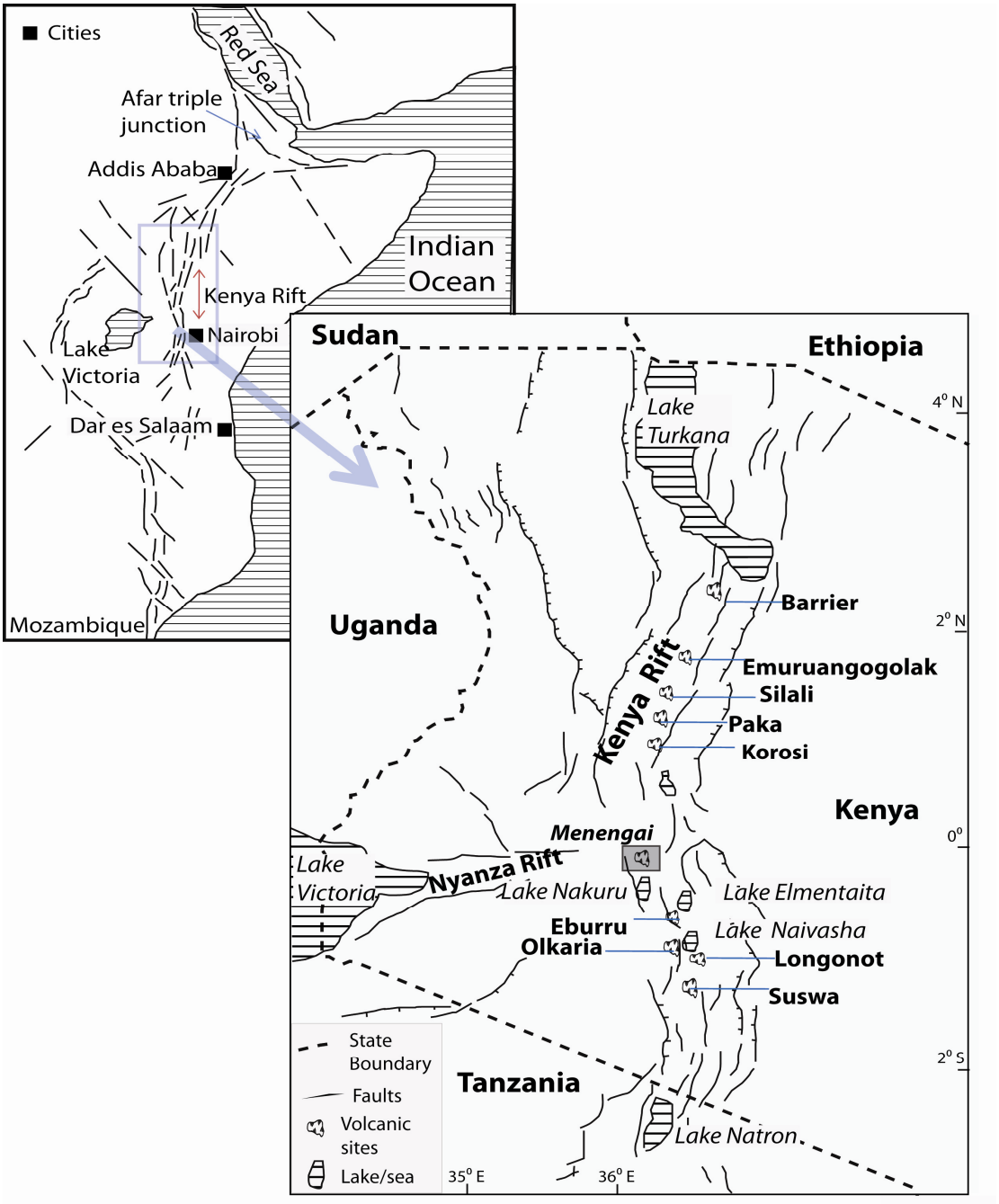

Figure 1: Map of the Kenya Rift showing the location of lakes and volcanic sites. The Menengai geothermal prospect that is located around the Menengai volcano is indicated by a rectangular box.

By integrating seismic and gravity data, Simiyu and Keller (2001) developed a detailed picture of the southern section of the Kenya rift and modelled the gravity data in and surrounding the Menengai, Suswa, and Olkaria volcanic fields (Figure 2). Their analysis formed the basis of a further investigation of the source of the gravity anomalies within the Menengai region (Simiyu and Keller, 2001). They modelled a dense magmatic body (20 km wide and 6 km deep) in this region which they interpreted as a cooling magmatic body. An earthquake survey within the Menengai region showed a micro-earthquake events happened mainly in the upper 5 km within the caldera and deeper to about 7 km outside the caldera (Simiyu, 2009). Within the Menengai caldera, seismic wave attenuation zones were identified and interpreted as regions containing molten rocks (Simiyu, 2009).

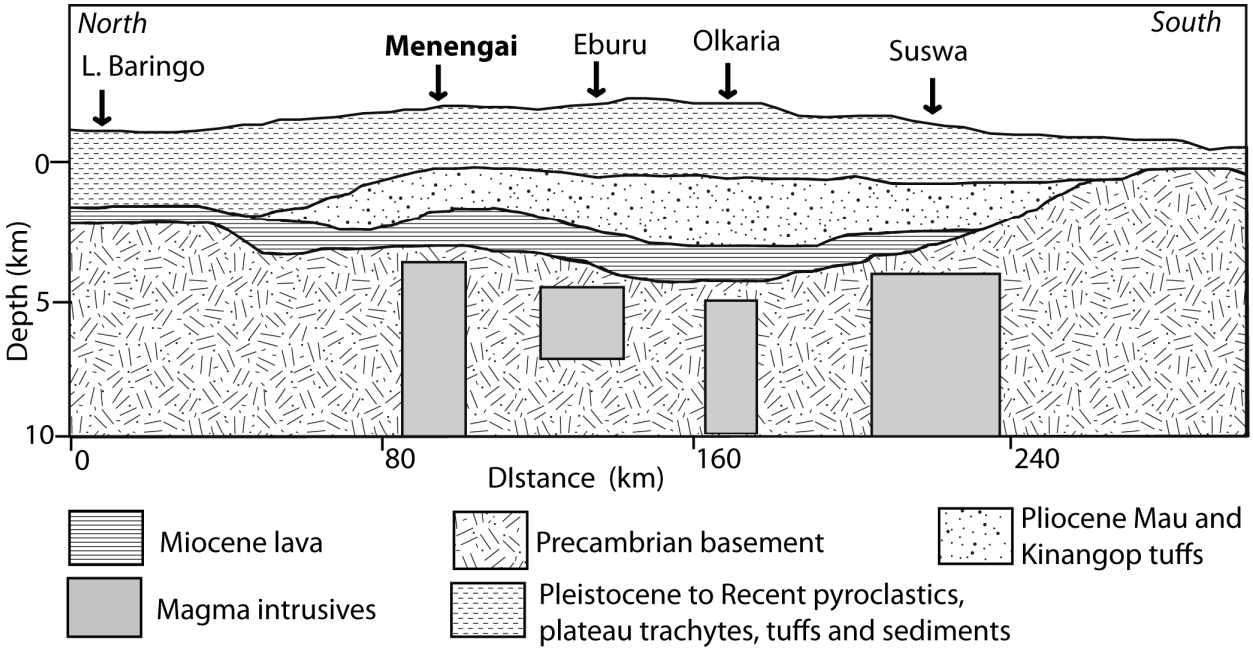

Figure 2: An interpreted geological cross-section along the rift axis from Lake Baringo to Lake Magadi from seismic refraction and gravity models (modified from Simiyu and Keller, 2001).

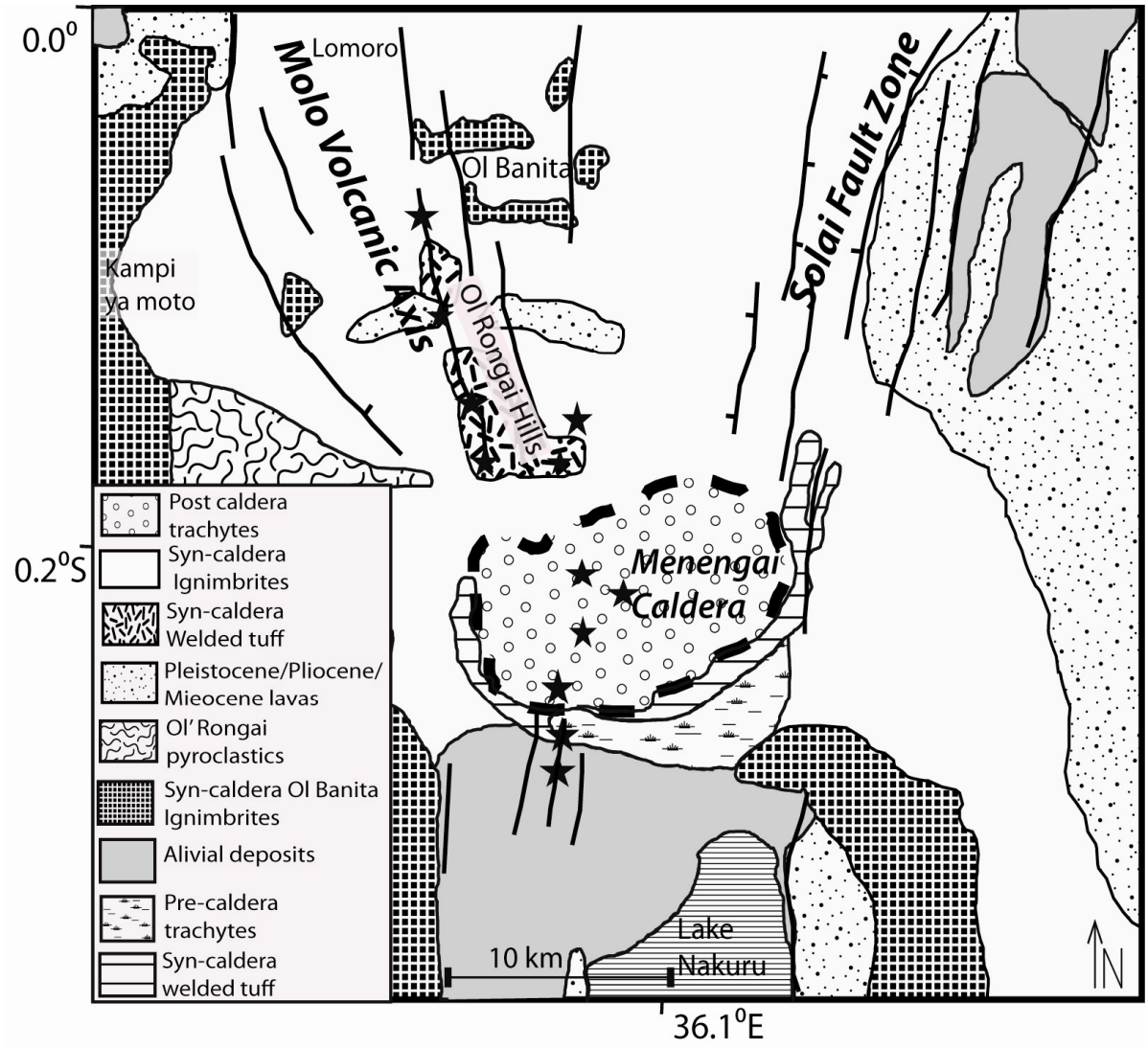

Figure 3: A simplified geologic map of the Menengai region. The bold dashed lines are the bounds of the Menengai caldera, the other lines are faults, and the dark stars are the eruption centres (Modified from Leat, 1984 and Mungania, 1999).

3.3.1 Menengai Volcano

The Menengai volcano is predominantly trachytic and is located at the intersection of the Nyanza Rift system and the main Kenya Rift (Figure 1) and a point where the Molo and the Solai tectonic axes converge (Figure 3). The volcano formed about 180 ka as a trachyte lava shield volcano which collapsed at about 29ka to form a caldera after a large volume of magma was extruded from an underlying magma chamber (Leat, 1984; Mungania, 1999). The caldera is within the apex of the Kenya Dome with an elevation about 2 km above sea

level. The caldera has an elliptical shape with major and minor axes of 12 km and 8 km, respectively. Its floor covers an area of about 88 km^2 and is made up of young lavas emplaced 14,000 yrs ago (Leat, 1984).

The volcanic rocks found in this region (Figure 3) range from phonolite to trachyphonolites to trachyte and minor tuffs that were emplaced in the region before the caldera formed and post-caldera ignimbrites with some trachyte lava flows and minor pyroclastic material. The older rocks are exposed on the caldera walls while the younger rocks make up the exposed caldera floor (Mungania, 1999). The faults in this region appear to have facilitated the eruptions of an ash-flow tuff that led to the emptying of the magma chamber beneath Menengai (Leat et al., 1984; Macdonald et al. 1994; Omenda et al., 2000; Simiyu and Keller, 2001; Macdonald and Scaillet, 2006; Simiyu, 2009). Most of these faults strike north, northwest or northeast and may control the hydrology and hydrothermal system in this region.

3.4 Geophysical data analysis

3.4.1 Gravity

The Kenya Rift system has been extensively studied using gravity and seismic data (e.g., Searle, 1970; Baker and Wohlenberg, 1971; Khan and Swain, 1978; Swain et al., 1981, 1994; Swain, 1992; Simiyu and Keller, 1997, 2001). The most important finding from these studies is that the majority of the Kenya Rift is characterized by a negative Bouguer gravity anomaly that is about 350km wide. A local positive gravity anomaly, 40-60 km wide, is superimposed on the negative anomaly (Figure 4a). The positive anomalies are more obvious on a residual gravity anomaly map created by bandpass filtering (Figure 4b). These anomalies have been interpreted as low density material in the upper mantle providing the source of the negative gravity anomaly (Fairhead, 1976; Banks and swain, 1978; Simiyu and Keller, 1997) while the

gravity high is caused by an intrusion of mantle derived material into the shallow crust (Swain et al., 1981; Simiyu and Keller, 2001). The gravity data along the rift indicate that the major volcanic centres, such as Menengai, Eburru, Olkaria, and Suswa are associated with the positive anomaly (Figure 2).

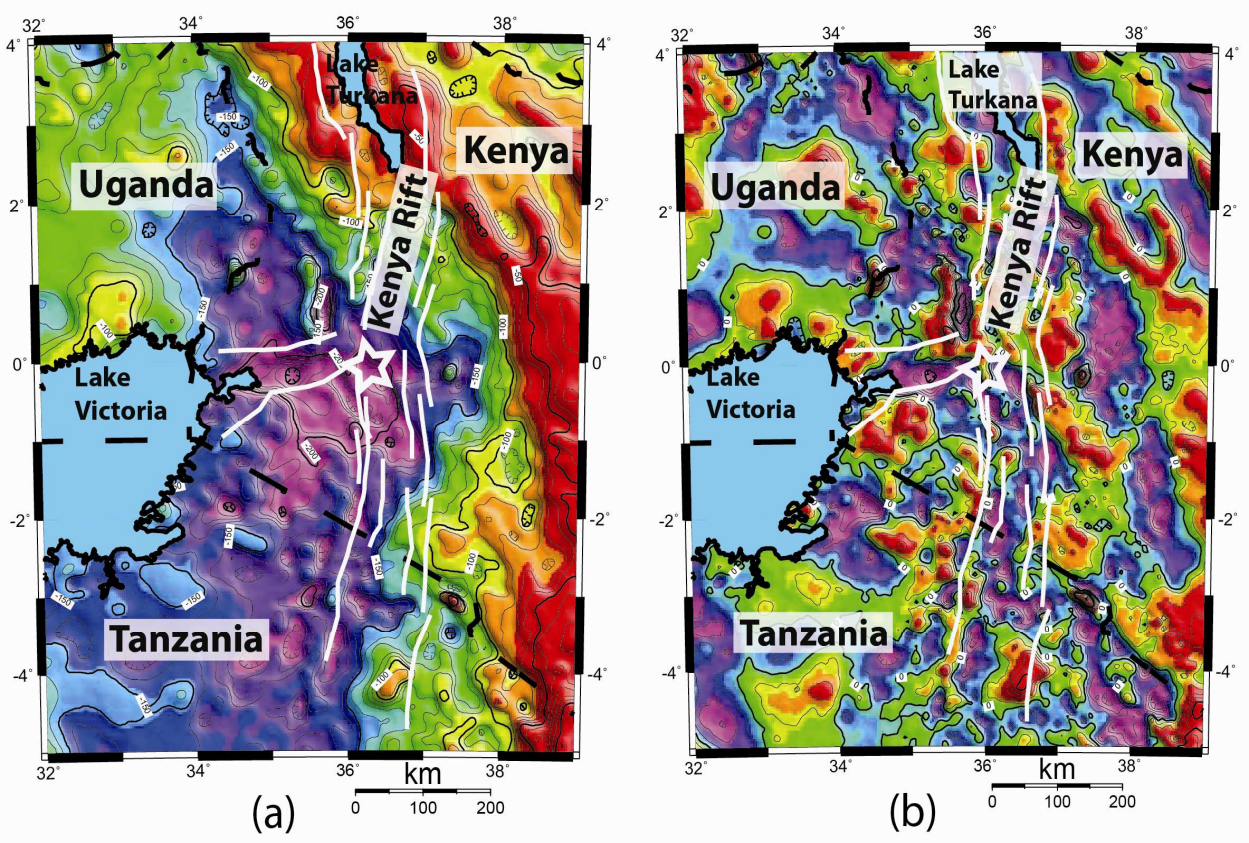

Figure 4: Bouguer gravity anomaly map of the Kenya rift (a) and (b) Band-pass (5-250 km) filtered map of the Bouguer gravity anomaly map. White lines show the fault boundaries of the rift and the star is the location of the Menengai volcano. The red colours are relative positive gravity anomalies.

For this study, the gravity data from the Menengai volcano and the surrounding area from the gravity database of Simiyu and Keller (2001) and Mariita and Keller, (2007) are analysed. Simiyu and Keller, (2001) merged all previous data with new data collected by the KRISP investigations and the Kenya Electricity Generating Company. These data were processed to obtain complete Bouguer gravity anomalies using sea level as a datum and 2.67 gm/cc as a

reduction density. The resultant data were gridded and contoured to produce a complete Bouguer gravity anomaly map of the Menengai region (Figure 4a).

The data indicate a gravity low that is associated with faults and fractures or low density volcanic material within the Menengai volcano. This gravity low occurs between two gravity maxima north of the caldera in the Ol'rongai Hills area and south of the caldera that can be associated with dikes and intrusions as modelled by Simiyu and Keller (2001). Another gravity low is located west of the caldera in the Menengai Farms and the east of the caldera towards the Bahati region. These gravity lows to the east and west of the caldera are part of the broad low anomaly associated with the rift as shown in Figures 4a, b.

By just analysing the complete Bouguer gravity anomaly map, one cannot interpret the depth and geometry of the sources of the various anomalies. To better interpret the sources of the anomalies, 2 or 3D modelling must be undertaken and, given the 3D nature of the anomalies on Figure5a, we chose to perform a 3D inversion in order to estimate the density distribution that causes the observed anomalies. Because we are interested in the upper crustal features that are related to the formation of the Menengai volcano and those related to geothermal resources, a residual anomaly map was constructed (Figure 5b).

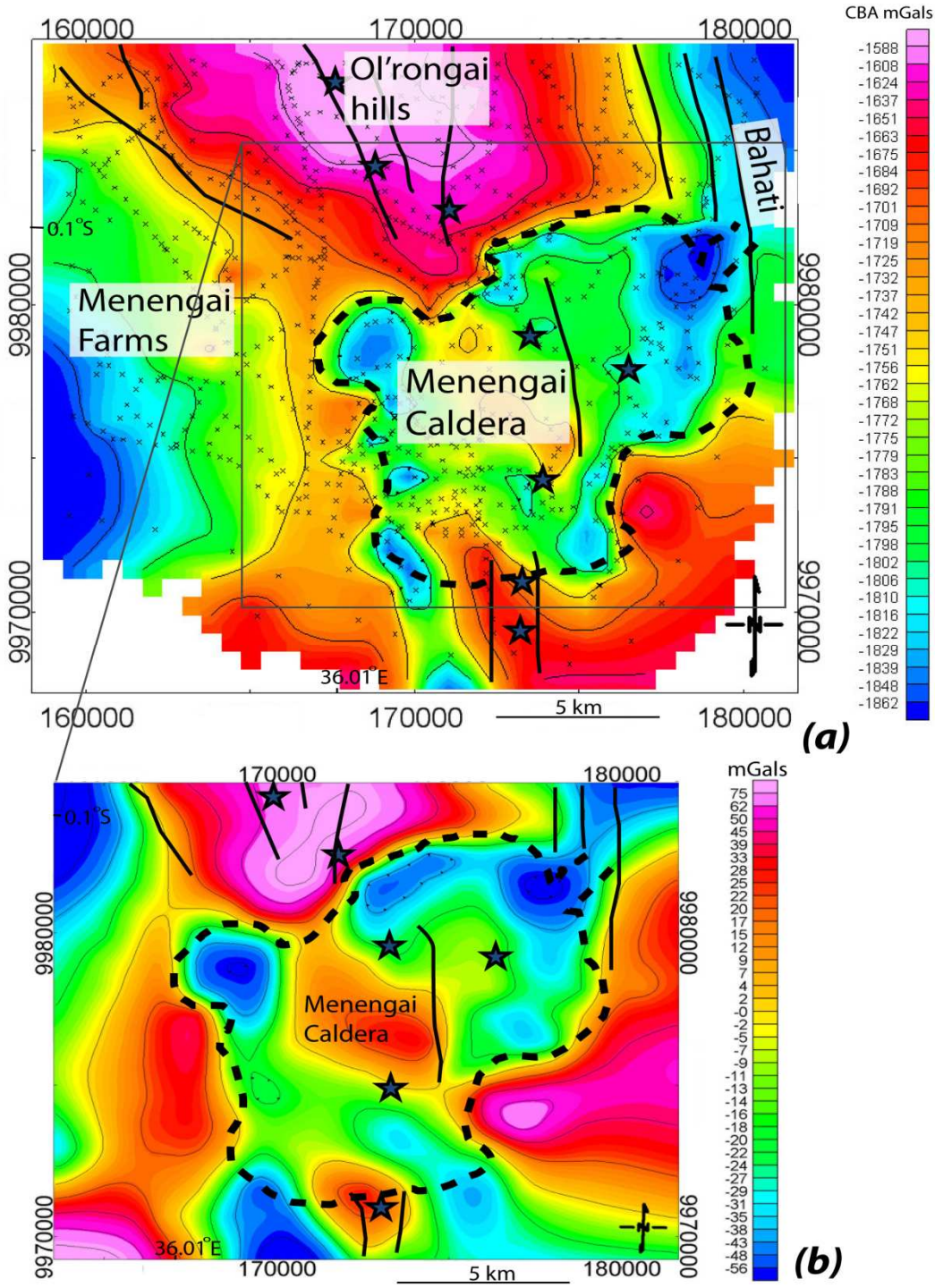

Figure 5: (a) Bouguer gravity anomaly map of the Menengai volcanic centre and surrounding region and (b) residual gravity anomaly map derived from a fourth-order polynomial surface removed from the Bouguer gravity anomalies. The dashed lines are the faults bounding of the caldera while the continuous lines are faults associated with rifting. The stars show the eruption centres. The crosses in (a) represent the gravity stations.

There are numerous methods (e.g. wavelength filtering, upward continuation and polynomial trend-surfaces) that can be used to construct the residual anomaly map. We tried the above methods and found that they all produced similar results. Our final residual map (Figure 5b) was based on a fourth-order polynomial surface that was removed from the Bouguer gravity anomaly data (Figure 5a).

The gravity anomalies show low "negative" gravity values within the caldera that are associated with fractured zones or low density volcanic material. High "positive" gravity anomalies appearing at the centre of the caldera are associated with post caldera lava flows that cover most of the inside of the caldera. The caldera is bounded by positive gravity anomalies which we relate to cold magmatic material or dikes, while the negative anomalies outside the caldera may be related to either faults or low density volcanic material that covers most of the region around the Menengai volcano (Mungania 1999).

To determine the upper crustal density structure of the Menengai region we used a 3D inversion routine (Li and Oldenburg, 1998) where the calculated gravity anomalies are determined using the gravity station elevations. Because the inversion problem for density using gravity data is non-unique, various inversion parameters (e.g., weighting of the data, data errors, choice of objective function, starting model and size of model mesh) were considered and in some cases varied.

The modeling space domain was designed to cover the region shown on the residual gravity data and measured 12750 m (NS), 10750 m (EW) and 26500 m (depth). This space was divided in 3 horizontal layers containing cubes of different sizes. The top 8000 m thick layer was divided into 250 m length cubes, the middle 10500 m thick layer was divided into 500 m length cubes, while the third bottom 8000 m thick layer was divided into cubes of 2000 m length. Different weights and objective functions were used in different runs in order to

obtain a reasonable model that is comparable to the mapped local geology. Since there were no data we assigned a 5% Gaussian error to the data. The choice of wrong inversion parameters can lead to results that have no relationship to the actual density structure despite a low RMS misfit between the observed and calculated data (Li and Oldenburg, 1998). In order to minimize these factors, we performed numerous inversions to explore the effects of these parameters on the final model. The result presented here in Figure 6 was obtained after 36 iterations giving a reasonably low RMS error misfit of 0.73 mGals on average.

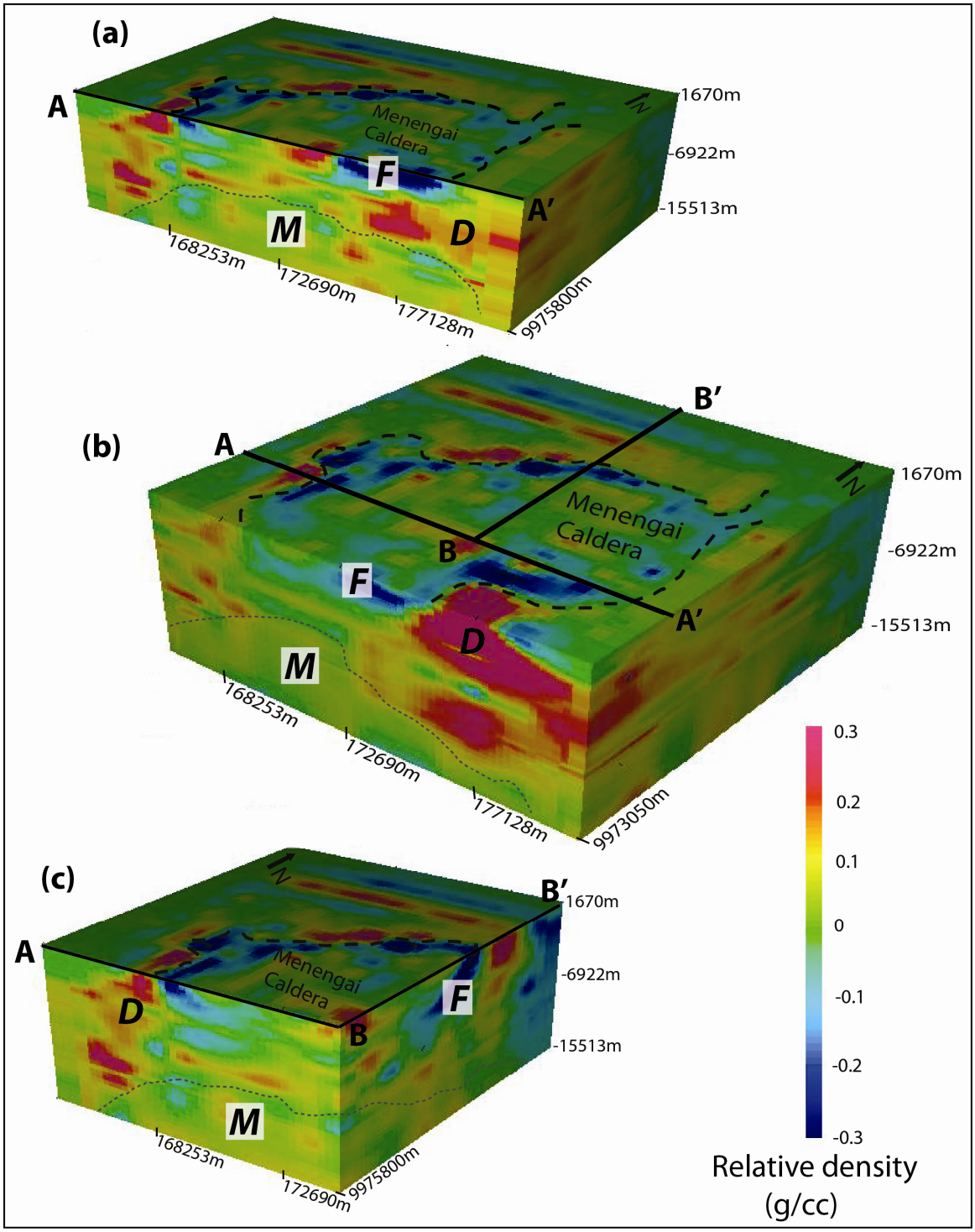

Figure 6: Three-dimensional density model of the Menengai region (b). Figure (a) is a model that shows the inside of the caldera when sliced in the east-west (AA') direction along a northing (9975800) while (c) shows a section of the caldera when sliced in north-south (BB') and east-west (AB) directions through the center of the caldera. The region D represents high density body, F a low denstity zone while M a zone of intermediate denssity. The color scale is relative to 2.7 g/cc.

3.4.2 Gravity data interpretation

The density model (Figure 6) obtained from the inversion indicates that the greatest variations, producing both high and low gravity anomalies, are focused along the caldera boundary. In particular, the gravity lows were modelled as low density zones (zones F on Figure 6) with a density range between 2.4-2.6 g/cm^3 along the boundary of the caldera and extending to a depth of about 6 km. These low densities are interpreted to be highly fractured zones that probably formed during the caldera eruption. High density zones (zones D) are also modelled around the caldera margin and have a density range of 2.9-3 g/cm^3. These high density zones also extend to a depth of about 6 km, similar to the low density boundary material. We interpret the high density zones to be cold, mafic magmatic material filling some of the fractures that formed during caldera collapse.

Away from the caldera rim, the modelled density variations and the gravity anomalies (Figure 5 and 6) around the Menengai caldera are relatively subdued compared to the low density zones (Zone F) that are related to the fracturing and magma intrusion along the caldera rim. The surface of the region is covered with recent volcanic flows and there is geologic evidence for intense fracturing in much of the area (Mungania, 1999). Because the inner rim of the caldera shows very low densities, we infer that either the rim is much more fractured and intruded than elsewhere in the area or that there are some other density variations in the subsurface that counters the shallow fracturing. Our models suggest that the caldera may be underlain by lower density molten rocks below the 6 km base of the caldera and that may contribute to the lower densities found within the caldera. The gravity model implies that there are fewer fractures and mafic intrusions within the shallow caldera, and when combined with the presence of a large low density intrusion beneath the caldera, produces the low amplitude gravity anomaly that characterizes the main part of the caldera. To further test this

idea, we examined the MT data within and surrounding the caldera to identify more fluid rich regions and fractures, and to evaluate the possible geothermal potential of the area.

3.4.3 Magnetotellurics

The MT method involves recording time-varying naturally-occurring magnetic and electric fields on the Earth's surface. These time-varying fields are used to infer the lateral and vertical electrical resistivity structure of the Earth's interior. These electromagnetic fields are recorded as time series and then a period dependent impedance tensor between the source magnetic field and induced electric field is constructed (Vozoff, 1972, 1991). These tensors are then decomposed into two principal orthogonal directions namely: the transverse electric (TE) where the electric fields are oriented parallel to the electric strike and the transverse magnetic (TM) where the field is oriented perpendicular to the electric strike for an assumed 2D subsurface (Vozoff, 1991). The decomposition of the tensor into a TM and TE mode is only strictly valid for 2-D electrical structures and the validity of using 2-D modelling routines will be discussed below. To interpret MT data, the magnitude and phase of principal impedance modes are converted to apparent resistivities which vary according to period. The conversion of the apparent resistivities to depth is not simple (Park and Wernicke, 2003) and usually involves some type of inversion process. However unlike the gravity and magnetic fields, MT has the ability to resolve depth information based on the variation of depth of penetration with signal frequency (Jones et al., 2003). In this study, we will use the MT data to determine the electrical conductivity structure of the Menengai volcano region will specifically aid in determining the depth and geometry of the geothermal reservoir and the magma chamber.

Local near surface inhomogeneities may cause a pronounced galvanic response on MT apparent resistivity curves independent of frequency. This is commonly known as static shift

due to the fact that an electric field is generated from boundary charges from a near surface resistivity body that will persist through the entire MT recording range (Berdichevsky and Dmitriev, 1976; Pellerin and Hohmann, 1990). This so-called static shift causes the apparent resistivity curve to be shifted up or down parallel to the actual resistivity. There are several techniques proposed for correcting static shift on MT data but no single technique is unique (Beamish and Travassos, 1992). In this study we used time domain electromagnetic (TDM) and transient electromagnetic (TEM) data collected at or near a MT sounding location to determine the near surface resistivity values in order to correct any static shifts in MT data.

3.4.4 Data collection and processing

Broadband (0.0025-400 seconds) MT measurements were made using a Phoenix Geophysics MTU-5A bit data acquisition unit. The electric fields were obtained using 100 m long orthogonal dipoles (oriented north-south and east-west) while the magnetic field was measured using solenoids (coils) buried in the ground for thermal and mechanical stability. A total of 98 stations were randomly collected around the Menengai volcano by the Kenya Electricity Generating Company (KenGen) and the Geothermal Development Company (GDC) as shown in Figure 7. Each station recorded for approximately 20 hours. One station was held fixed at a location 30km away from the Menengai volcano and was used for remote referencing processing. The roaming instruments and the stationary one were synchronized by a satellite Global Positioning System (GPS). The data were processed using robust processing codes that incorporated remote referencing (Egbert, 1997). The resulting principal impedance tensors which were used to estimate the apparent resistivity and the impedance phase. Although some data contained noise that minimised by smoothing, some station that were very noisy were not included in the modelling.

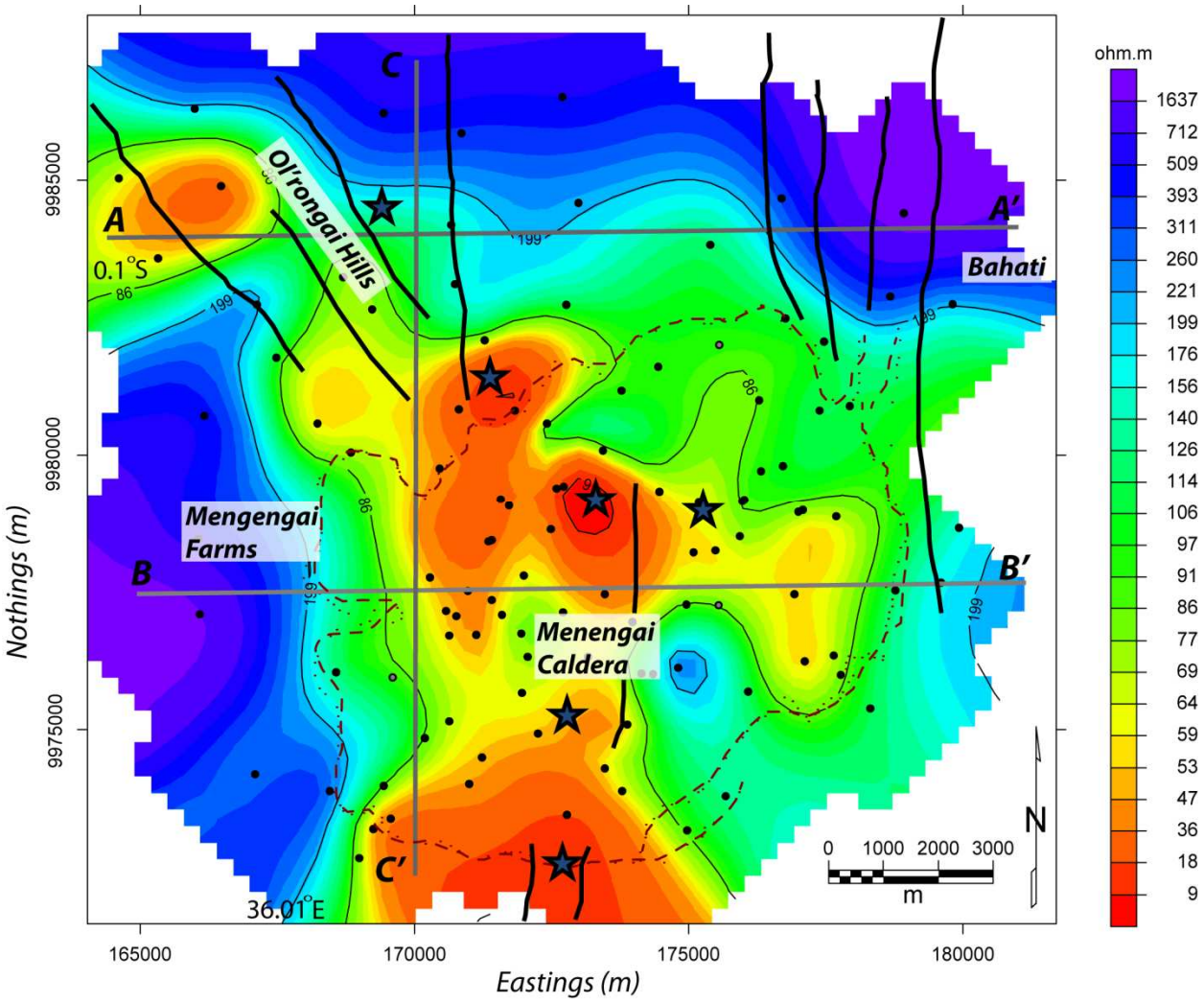

Figure 7: Electrical resistivity variations at 2000m below sea level (mbsl) as determined from a one-dimensional Occam inversion of each. The MT stations are shown as black circles. The solid lines are faults and the dashed line is the caldera boundary. Two-dimensional modelling was run along lines connecting points AA', BB', and CC' and are shown in Figure 9 and 10.

To investigate the shallow resistivity distribution of the study region, a one-dimensional (1D) inversion using Occam's method (Constable et al., 1987) for each sounding was performed and then used to generate a map of resistivity variation at a depth of 2000m below sea level (Figure 7). Such a model gives a rough idea of the resistivity variations at depths. The resistivity map indicates low resistivity regions northwest of the caldera in the Ol'rongai Hills area, within the caldera and south of the caldera. These regions correlate with faults in these

regions and along the Molo tectono-volcanic axis (see Figure 3). We infer this low resistivity zone to be related to the presence of fluids circulating along the faults and fractures or hydrothermally altered rocks. High resistivity zones cover the regions west of the Menengai volcano around Menengai Farms and to the north and northwest in the Bahati area. The high resistivity is inferred to be the result of either less fractured or faulted zones, dry sediments or volcaniclastics, or the absence of hydrothermal altered grounds.

3.4.5 Data interpretation

Before an MT model is created and interpreted, a dimensionality analysis must be performed to determine the electrical strike of regional structures and the regional impedance tensors (e.g., Ledo et al., 2011). These values will be used to determine whether the data suggest that the structures beneath a station is 1D, 2D or 3D and which modelling method can thus be used in the data interpretation. There are numerous methods for determining the dimensionality of MT data (e.g., Groom and Bailey, 1989; Bahr, 1991; Weaver et al., 2000; McNeice and Jones, 2001; Marti et al., 2004, 2009), however the majority of the methods (e.g., Groom and Bailey, 1989; Bahr, 1991; McNeice and Jones, 2001) have some sort of limitations as explained by Marti et al. (2009). To overcome the limitations of the above methods, Marti et al. (2004; 2009) modified the method of determining the rotational invariants of Weaver et al. (2000) to determine the dimensionality of the MT data. The method (called WAL rotational invariants) provides estimates of dimensionality over bands of frequencies at each station and the amount of galvanic distortion which is determine using the methods of Groom and Bailey (1989) and McNeice and Jones (2001). We will use the WAL rotational invariants in our analysis.

Traditionally, MT data analysis has used the methods of Swift (1967) in order to determine the electrical strike directions and dimensionality of the data. One value, called skew, can be

used as a quick check for dimensionality and our analysis found that the skew values were below 0.2 which indicates the data were taken over either 1D or 2D structures, particularly for the short periods, but for skew values greater than 0.2 this may imply the data are located over 2D or 3D structures for longer periods (Ranganayaki, 1984).

The results of the dimensionality analysis (Figure 8) indicate that the Menengai region is complex with dimensionalities ranging from 1-D to 2D to 3-D for the different frequency bands, in particular, the region within the caldera. However, the results show that the regional strike, particularly for at shorter periods (periods less than 10seconds), is mainly 2D with a NW direction. This strike direction is still observed for longer periods (> 10 seconds), however most of the stations indicate a three dimensional structure. The NW strike direction is consistent with the local geology, as this direction aligns with the Molo tectono-volcanic axis. Even though the dimensionality analysis indicates 3D electrical structure at depth, we believe that our interpretation for the 2D resistivity model of this region is acceptable (Wannamaker, 1999; Park and Mackie, 2000).

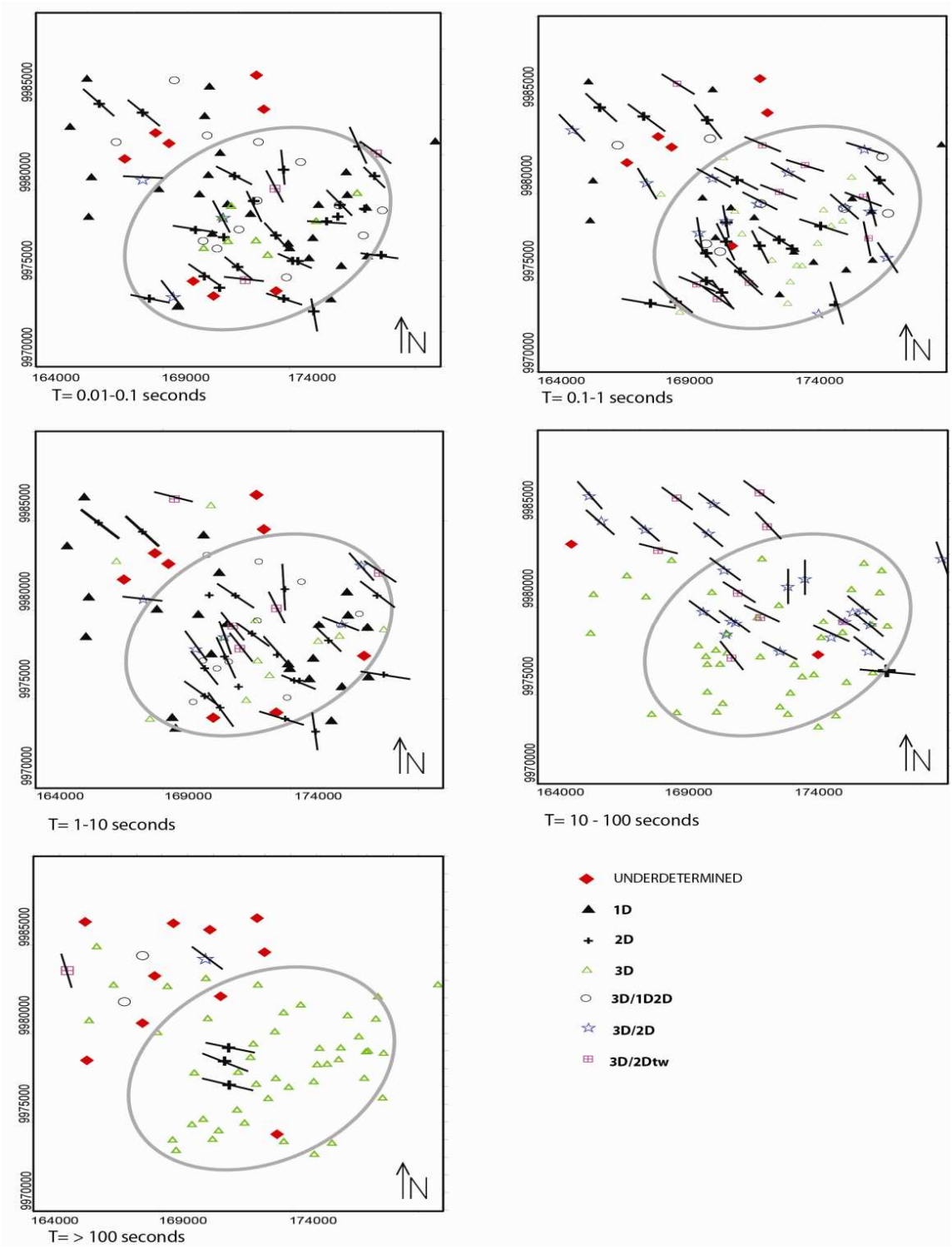

Figure 8: Dimensionality analysis for each MT sounding grouped in five period bands using the method of Mart et al. (2004, 2009): band 1, T=0.01-0.1 sec; band 2, T=0.1-1sec; band 3, T=1-10 sec; band 4, T=10-100 sec; band 5, T>100 sec. The black lines show the strike direction.

2.4.6 Two-dimensional modeling

Based on the above dimensionality analysis, both the TE and TM apparent resistivity and phase and the transfer functions of the available static shift corrected MT data were analyzed using a 2D regularized inversion algorithm (Rodi and Mackie, 2001) that jointly minimizes the data misfit. This technique tries to jointly fit the observed impedance elements and the magnetic transfer function. Although much of our data had very minimal noise levels, a few stations were noisy and were excluded from the inversion process. The data were smoothed and static shift corrected using the controlled source electromagnetic data before the 2D inversion was run. We started the inversion with a simple 10 km thick layer of 500 ohm-m resistivity. During the inversion, the data were weighted by the inverse of their variance where data with low variance were given large weights (Rodi and Mackie, 2001). Several inversions were conducted to determine which features were required by the data by varying the starting models. The final models have an overall RMS error between 2% and 5% which we consider a reasonable fit given the observed data errors.

The resistivity data were modelled along three profile lines (Figure 7)); two east-west lines and one north-south line that cross four prominent resistivity zones from the 1D analysis (Figure 7). These models (Figures 9a, b and 10) indicate two distinct low resistivity zones (less than 25ohm-m), LRZ1 (Figure 9b) and LRZ2 (Figures 9a, 10). They are separated by intermediate resistivity zones (25 ohm-m to 100 ohm-m) (IRZ). LRZ1 is shallow and spreads laterally across the study region while LRZ2 is deeper. The fourth zone is a high resistivity zone (more than 100 ohm-m) (HRZ). This zone appears on either side of the deep low resistivity zones (LRZ2) and the intermediate resistivity zones (IRZ) on all the cross-sections (Figures 8 and 9) and is inferred to be the background resistivity signature of the region while LRZ1, LRZ2, and IRZ are resistivity anomalies that reflect the changes in lithology, porosity fracture intensity, temperature or fluids relative to the background material.

Most of the shallow geology around the Menengai volcano is covered by post caldera volcanic materials, primarily ash and tuffs as discussed above. The basement rocks of the mobile belt in this region were estimated to be at about 5 km depth (Simiyu and Keller, 2001, 1997) and are overlain by post caldera Miocene lavas and by phonolite and trachyphonolite volcanic deposits, all of which are expected to have high resistivity unless altered by fluids, temperature, or fractures.

Resistivity studies over volcanic regions such as Coso in the United States (Newman et al., 2008), and Krafla and Hengill in Iceland ((Onacha, 2006; and Anarson et al., 2010) have shown that resistivity increases with temperature. These studies have also related an observed shallow low resistivity zone to hydrothermal effects based on the correlation of drill core data with resistivity. Based on these analyses, it is reasonable to assume that the shallow (about 1000m above sea level) low resistivity (LRZ1) (< 25 ohm-m) layer of our models (Figure 6 and 7) indicates a clay-rich, low temperature, mineralized zone, while the high resistivity underlying it is probably a high temperature mineralized zone with low porosity.

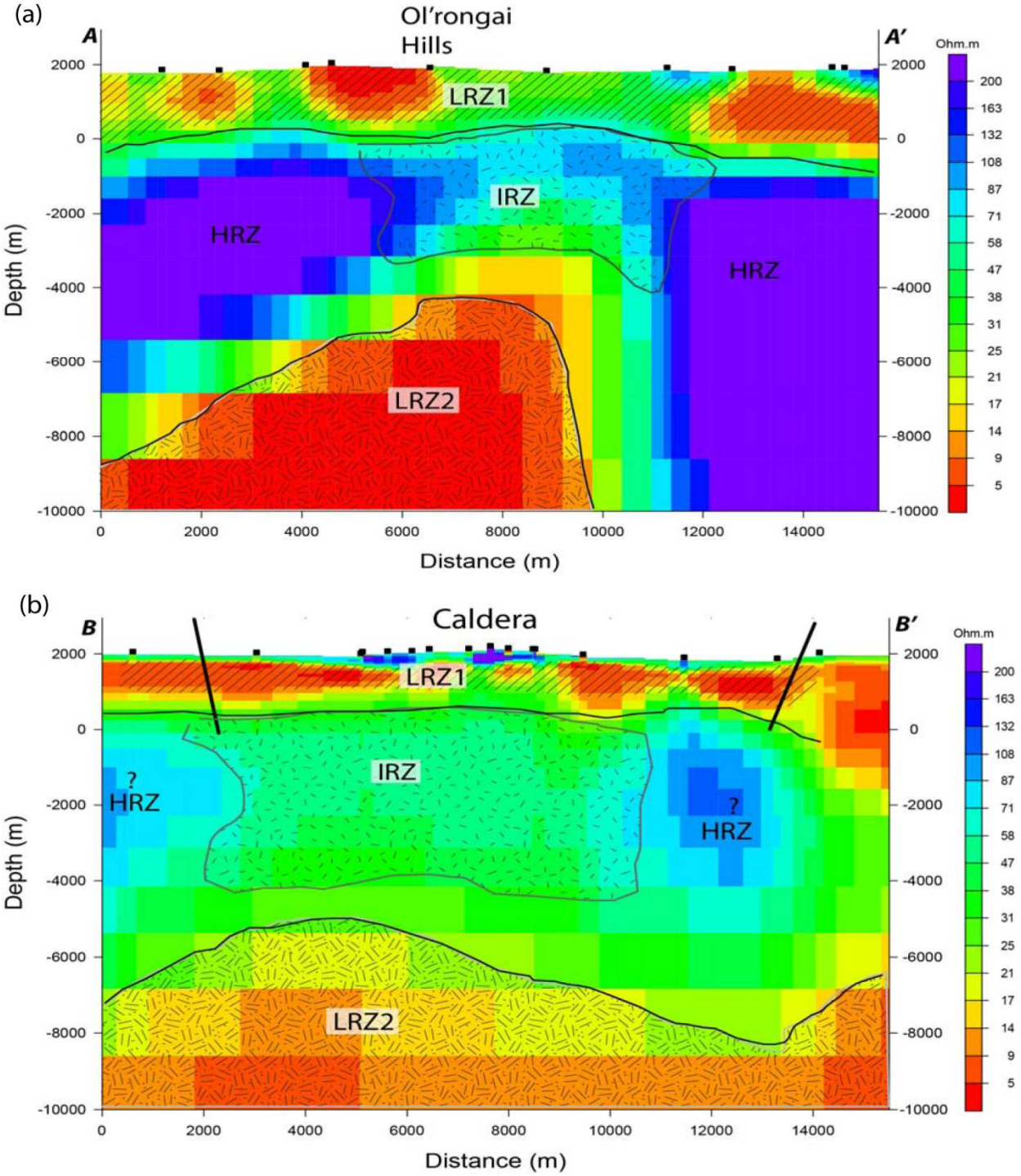

Figure 9: Two dimensional resistivity models for the east-west profiles: (a) AA' and (b) BB'. The shaded regions are the various resistivity zones representing the subsurface geology of the region. The LRZ1 is the low resistivity zone one, IRZ the intermediate resistivity zone, LRZ2 is the low resistivity zone two and HRZ the high resistivity zone, respectively. The black squares on the surface of the cross-section are the MT stations while the bold dipping lines are the caldera boundaries.

The high resistivity zones (HRZ) (>100 ohm-m) shown in both the east-west and the north-south models are interpreted to be caused by the compacted dry volcanic materials or crystalline basement rocks. The deeper low resistivity zone (LRZ2) is inferred to be magma that acts as the source of heat for the geothermal system. This interpretation is consistent with the interpretations of Simiyu and Keller (2001) and Simiyu (2009) that indicated the presence of magmatic material at about 6 km below Menengai.

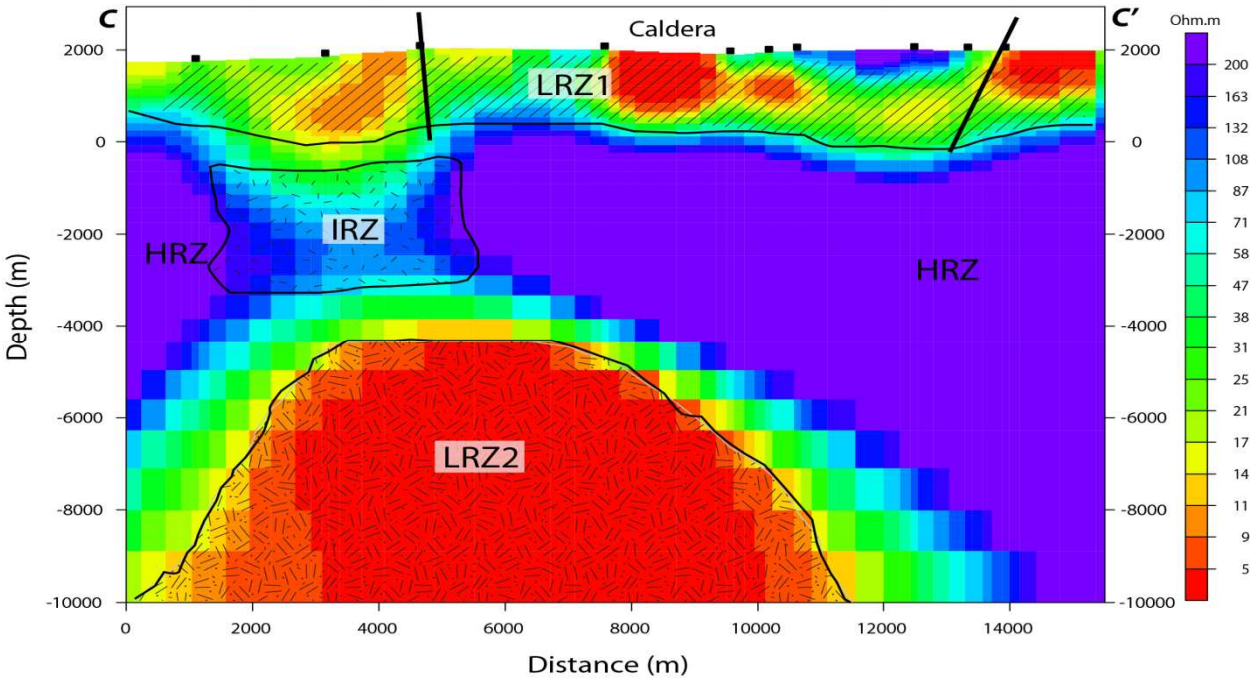

Figure 10: Two dimensional resistivity model for the north-south profile. The shaded regions are the various resistivity zones representing the subsurface geology of the region. LRZ1 is low resistivity zone one, IRZ the intermediate resistivity zone, LRZ2 is low resistivity zone. two and HRZ the high resistivity zone, respectively. The black squares on the surface of the cross-section are the MT station while the bold dipping lines are the caldera boundaries.

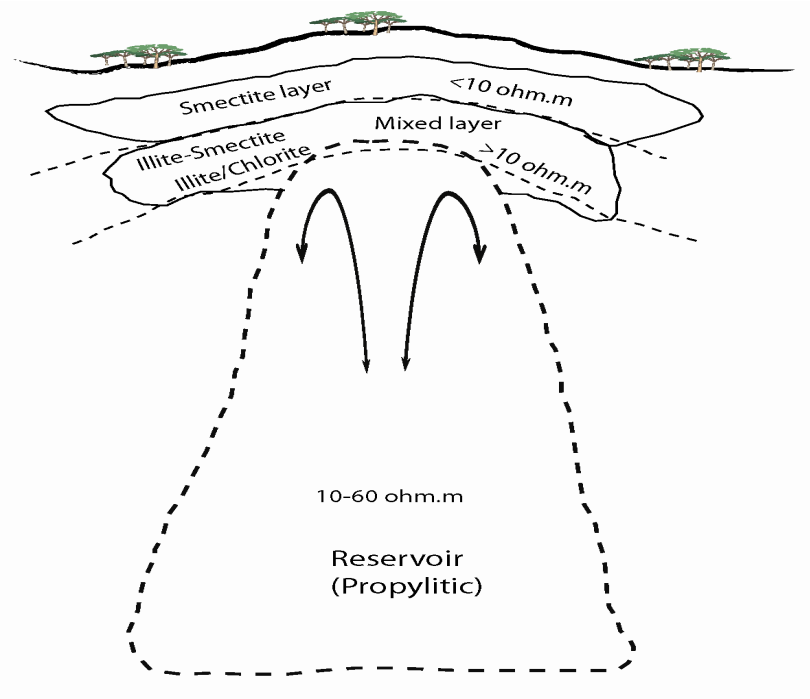

Figure 11: A conceptual resistivity model of a convective geothermal system. Modified from Oskooi et al., (2005) and Pellerin et al., (1996)

A proposed conceptual model (Figure 11) for a high temperature geothermal system indicates a temperature dependent electrical resistivity structure due to changes in mineralogy that helps guide the interpretation of resistivity models over geothermal fields (Pellerin et al., 1996; Oskooi et al., 2005; Cumming, 2009; Spichak and Manzella, 2009; Anarson et al., 2010; Cumming and Mackie, 2010). These authors have shown that shallow, low resistivity layers consist of low temperature hydrothermal alteration products distinguished by the abundance of electrically conductive smectite and zeolite minerals that form the cap rock above the reservoir (Anderson et al., 2000; Oskooi et al., 2005; Cumming, 2009). As temperature increases with increasing depth along the geothermal gradient, the smectite and zeolite concentration decreases while illite and chlorite minerals form in the reservoir region (Figure 11). Flovenz et al. (2005) have shown that the resistivity change in the reservoir is caused by the increased illite and chlorite concentrations and low cation exchange. The

deeper conductor in such fields is suggested to be molten magmatic material interpreted as the heat source for the geothermal system (Arnason et al., 2010).

3.5 Integrated analysis

The primary elements of a geothermal system are the heat source, the cap rock, the fractured reservoir, and the thermal fluids. Each of these has a geophysical signature that may be easier to recognize in either gravity or resistivity data, but not necessarily in both. We observed that there are several similar features in both our gravity and resistivity data sets, although there is no direct mathematical relationship between the two methods. For this reason, we decided to combine the interpretation of these data to determine the optimal subsurface model.

We combined the interpretation of our density and resistivity models with the previous micro-seismic studies of Simiyu (2009) as show in Figure 12. These results show features labelled as MB and R (Figure 12). The region MB appears at a depth below 6-7 km in the gravity, resistivity and micro-seismic models. This zone is defined by an intermediate density (about 2.8 g/cm^3), a low resistivity (less than 25 ohm-m), and is also a region with no seismic events as shown in Figure 12a, b and c, respectively. This zone is interpreted as molten magmatic material of mantle origin. This is an inferred remnant of the magma chamber, part of which was emptied during the collapse of the caldera.

The region above the MB zone is marked as the R zone. This zone is defined by relative low density in the gravity model, high resistivity zones below a low resistivity zone in the resistivity models and a region of high seismicity in the seismic data (Figure 12). This region is interpreted as a zone of high fracture density and hence high porosity. The correlation of high seismicity with low density zones favours the interpretation of the low density zones as highly fractured and faulted rather than being composed of low density volcaniclastics or

sediments. The change in resistivity from higher resistivity below a low resistivity zone in these inferred fractured zones resembles the proposed reservoir in the conceptual model as shown in Figure 11. Hence, we suggest that fracturing has allowed fluid circulation to transfer heat to shallow depths. We suggest that the 240^0C isotherm is located at an elevation of about 1km above sea level at the boundary between the low and high resistivity zones Because those zones are interpreted to be two distinct mineralogical zones where minerals such as smectite, quartz and carbonates occur in the upper low resistivity zone while chlorite, illite, potassium feldspar and epidote quartz appear below this isotherm (e.g. Browne, 1989; Flovenz et al., 2005; Oskooi et al., 2005; Arnason et al., 2010). We envisage that it is in this region were most of the hydrothermal resource is located.

In addition the gravity data reveal the source or part of the source of the gravity high observed around the Menengai volcano. The high density zones (about 2.9-3.0 g/cm^3) are interpreted as magmatic material that cooled along the fractures or vents through which the magma reservoir beneath was emptied. These zones are limited to a depth of 6-7km. The reduction in density below the high density bodies is interpreted to be a change from cold to hot molten rocks. This interpretation is consistent with the micro-earthquake plot that shows the lateral extent of the seismic aseismic zones in the MB zones (Figure 12)

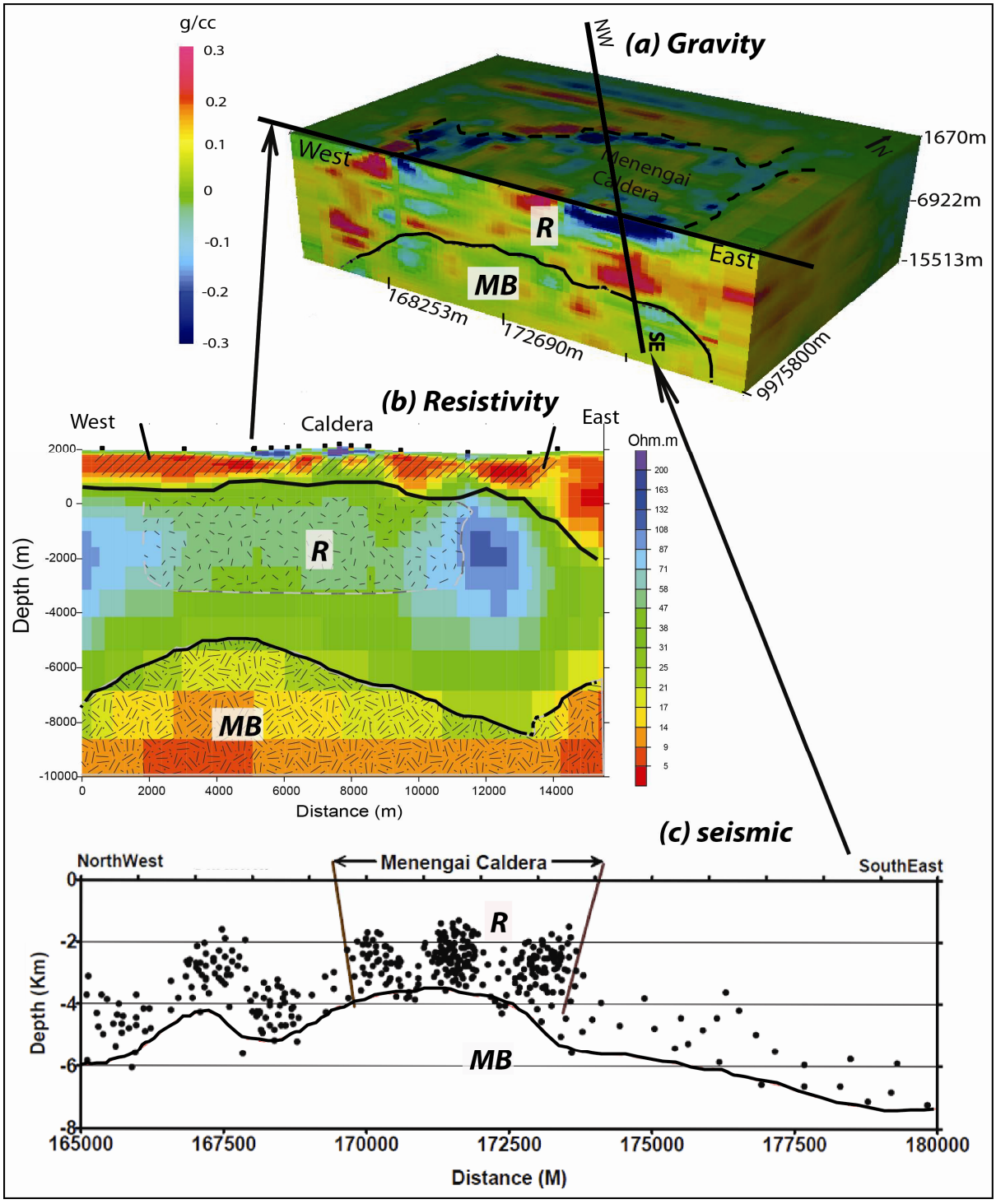

Figure 12: Geophysical models of (a) 3D density distribution (b) resistivity distribution and (c) a micro-seismicity plot from Simiyu (2009). The model show major zones revealed from the different datasets as the MB (magma body) zone and the R (reservoir) zones. The resistivity profile is along an east-west line while the seismic is along a northwest-southeast through the caldera as illustrated in (a).

3.6 Conclusions

We have demonstrated that an integrated analysis of geophysical data, in this case gravity, micro-seismicity, and MT, can give reliable subsurface information about faults and lithology, as well as the distribution of various physical parameters such as porosity, density and conductivity. Collectively the results indicate that an integrated analysis can improve the characterization of the geothermal reservoir. In this study gravity data gave vital information on the intensely fractured zones that could be a potential reservoir, while the MT data gave better resolution of the depth to the heat source and the clay cap rock. Micro-seismicity information further helped to constrain both data sets.

Our results indicate that the Menengai region is covered by volcanic rocks with high resistivity and relatively low density overlying the crystalline mobile belt basement rock that forms the rift floor. Tectonic processes and volcanism have caused fracturing that led to increased porosity and permeability and favoured fluid flow in the subsurface. Our data show that there is highly fractured zone within the caldera that is marked by low density and low resistivity. This highly fractured zone is identified as the best target for drilling for geothermal steam. The high gravity anomaly observed in this region is related to shallow, high density material interpreted as dikes or the top of an intrusion (e.g. Omenda, 1998; Simiyu, 2009) that is denser than the underlying molten material, with the change in density appearing at about 7km depth. The deep, low density material correlates with a low resistivity zone below the inferred hydrothermal reservoir. This zone appears to consist of hot, molten material and provides the heat that drives the geothermal system in the Menengai volcano region.

3.7 Acknowledgements

We would like to thank Dr. Silas Simiyu for allowing us to use his seismic model in this manuscript and the Geothermal Development Company for allowing us to use their data for this study and also providing the software for data processing. We also thank Dr. Terry Pavlis, Dr. Elizabeth Anthony, and Dr. Diane Doser for good reviews that helped improve this manuscript. This work was supported by NSF grants EAR0749382 awarded to Dr. Laura Serpa.

3.8 References

Anderson, E., Crosby, D. and Ussher, G. (2000). "Bull's Eye! — Simple resistivity imaging to reliably locate the geothermal reservoir." Proceedings World Geothermal Congress 2000. 909–914.

Arnason, K., (1989). Central loop transient electromagnetic sounding over a horizontally layered earth. (No. OS-89032/JHD-06) Reykjavik: Orkustofnun.

Arnason, K., Eysteinsson, H., Hersir, G. P., (2010). Joint 1D inversion of TEM and MT data and 3D inversion of MT data in the Hengill area, SW Iceland. Geothermics, 39, 13-34.

Bahr, K., (1991). Geological noise in magnetotelluric data: a classification of distortion types. Phys. Earth Planet. Inter. 66, 24-38.

Baker, B. H., Wohlenberg, J., (1971). Structure and evolution of the Kenya rift valley. Nature 229, 538-542.

Banks, R. J., Swain, C. J., (1978). The isostatic compensation of the East Africa. Proc. R. Soc. London A364, 331-352.

Beamish, D., and Travassos, J., (1992). A study of static shift removal from magnetotelluric data: J.Appl.Geophys. 29, 157-178.

Berdichevsky, M. N., Dmitriev, V. I., (1976a). Distortion of magnetic and electric field by near surface lateral inhomigeneities. Acta Geod., Geophys. Montanist. Acad. Sci. Hung. 11, 447-483.

Berdichevsky, M. N., Dmitriev, V. I., (1976b). Basic principles of interpretation of magnetotelluric sounding curves, In Geoelectric and Geothermal studies, KAPG Geophysical Monograph., Akademiai Kiado, Budapest, pp 165-221.

Berktold, A., (1983) Electromagnetic studies in geothermal regions. J. Geophys. Surv. 6, 173-200.

Bibby, M. H., Risk, F. G., Candwell, G. T., Heise, W., (2008). Investigation of deep resistivity structures at the Wairakei geothermal fields. Geothermics. 38, 98-107.

Bibby, H. M., Cladwell, T. G., Davey, F. J., Webb, T. H., (1995). Geophysical evidence on the structure of the Taupo Volcanic Xone and its hydrothermal circulation. J. Volc. Geother. Res. 68, 29-58.

Browne, P. R. L., (1989). Constraining alteration style of andesitic and rhyolitic rocks in geothermal fields of the Taupo Volcanic Zone. Proceedings 11th New Zealand geothermal Workshop, P. R. L. Browne and K. Nicholson, eds., University of Auckland, 111-116.

Constable, S. C., Parker, R. L., Constable, C. G., (1987). Occam's inversion: A practical algorithim for generating smooth model from electromagnetic sounding data Geophysics, 52, 289-300.

Cumming, W., (2009a), Geothermal resource conceptual models using surfece exploration data. Proceedings 34th workshop on Geothermal Reservoir Engineering, Starnford University, Starnford, CA.

Cumming, W., (2009b). A conceptual model approach to the geophysical exploration of permeable geothermal reservoirs that considers context and uncertainty. 79th Ann. Internal. Mtg., Soc. Expl. Geophys. Expanded Abstract.

Cumming, W., Mackie, R., (2010). Resistivity imaging of geothermal resource using 1D, 2D, and 3D MT inversion and TDEM static shift correction illustrated by a Glass mountain case history. Proceeding World Geothermal Congress, 2010.

Egbert, G. D., (1997). Robust multiple station magnetotelluric data processing. Geophys. J. Inter. 130, 475-496.

Fairhead, J. D., (1976). The structure of the lithosphere beneath the eastern rift, East Africa, deduced from gravity studies. Tectonophysics 30, 269-298.

Flovenz, O., Spangenberg, E., Kulenkampff, J., Anarson, K., Karlsdottir, R., Huenge, E., (2005). The role of electrical conduction in geothermal exploration. Paper presented at the World Geothermal Congress, Antalya, Turkey.

Groom, R., Bailey, R., (1989). Decomposition of magnetotelluric impedance tensors in the presence of local three-dimensional galvanic distortion. J. Geophys. Res. 94, 1913-1925.

Groom, R., Bailey, R., (1991). Analytic investigations of the effect of near-surface three dimensional galvanic scatterers on Mt tensor decomposition. Geophysics 56, 496-518.

Ingham, M., (2004). High resolution electrical imaging of fault zones. Physics Earth Planet. Int. 150, p. 93-105

Jones, A. G., Lezaeta, P., Ferguson, I. J., Chave, A. D., Evans, R. L., Garcia, X.,Spratt, J., (2003). The Electrical structure of the Slave craton. Lithos 71, 505-527.

Jones, A. K., Ingham, R. M., Bibby, M. H., (2008). The hydrothermal vent system of mount Ruapehu, New Zealand-a high frequency MT survey of the summit plateau. Doi:10.1016/j.jvolgeores.2008.05.006

Henry, W. J., Mechie, J., Maguire, P. K. H., Khan, M. A., Prodehl, C., Keller, G. R.,Patel, J., (1990). Aseismic investigation of the Kenya rift valley. Geophys. J. Inter. 100, 107-130.

Karson, J. A., Curtis, P. C., (1989) Tectonic and magmatic processes in the Eastern Branch of the East African rift and implication for magmatically active continental rift. J. African Earth Sci. 8, 431-453.

Keller, G. R., Prodehl, C., Khan, M. A., Morgan, P., Braile, L. W., Olsen, K. H., Wendlandt, R. F., Baldridge, W. S., (1994a) The East African rift system in the light of KRISP 90. In : Prodehl, C., Keller, G. R., Khan, M. A. (Eds),. Crustal and Upper mantle structure of the Kenya Rift. Tectonophysics 236, 465-483.

Keller, R. G., Mechie, J., Braile, L. W., Mooney, W. D., Prodehl, C., (1994b) Seismic structure of the Upper most mantle beneath the Kenya rift. In: Prodehl, C., Keller, G. R., Khan, M. A. (Eds),. Crustal and Upper mantle structure of the Kenya Rift. Tectonophysics 236, 201-210.

Khan, M. A., Swain, C. J., (1978). Geophysical investigation and geology of Kenya. In: Bishop, W. W. (Ed.) Geological Background of Fossil Man. Geol. Soc. London Spec. Publ. 6, 71-83.

Lagat, J., (2003). Geology and the geothermal system of the southern segment of the Kenya Rift. International geothermal conference, Reykjavik, Iceland..

Leat, P.T. (1984). Geological evolution of the trachytic caldera volcano Menengai, Kenya rift valley. J. Geol.Soc. Lond. 141 1057-1069.

Leat, P.T., Macdonald, R., Smith, R.L., 1984. Geochemical evolution of the Menengai caldera volcano, Kenya. J . Geophys. Res. 89, 8571-8592.

Ledo, J., 2006. 2-D versus 3-D magnetotelluric data interpretation, Surveys in Geophysics 27, 511-543.

Li, Y., Oldenburg, D. W., (1998). 3D inversion of gravity data. Geophysics 63,109-119.

Macdonald, R., Navarro, J.M., Upton, B., Davies, G.R., (1994). Strong composition variation in peralkaline magma: Menengai, Kenya Rift Valley. J. Volc.. Geotherm. Res. 60, 301-325.

Macdomald, R., Scallet, B., (2006).The Central Kenya peralkaline province: Insight into the evolution of peralkaline salic magma. Lithos 91, 59-73.

Mariita, N. O., Keller, G. R., (2007). An integrated geophysical study of the northern Kenya rift. J. African Earth Sci. 48, 80-94.

Marti, A., Queralt, P., Ledo, J., (2009). WALDIM: A code for the dimensionality analysis of magnetotelluric data using the rotation invariants of the magnetotelluric tensor. Comp. Geosc. 35, 2295-2303.

Marti, A., Queralt, P., Roca, E., (2004). Geoelectric dimensionality in complex geological areas: application to the Spanish Betic Chain. Geophys. J. Int. 157, 961-974.

McNeice, G., Jones, A., (2001). Multisite, multi-frequency tensor decomposition of magnetotelluric data. Geophysics 66, 158-173.

Marquis, G., Jones, A. G., Hyndman, R. D., (1995). Coincident conductive and reflective lower crust across a thermal boundary in southern British Columbia, Canada. Geophys. J. Inter. 120, 111-131.

Meju, M. A., Sakkas, V., (2007). Heterogeneous crust and upper mantle across southern Kenya and the relationship to surface deformation as inferred from magnetotelluric imaging. J.Geophys. Res. 112, B04103.

Mechie, J., Prodehl, C., Ritter, J., Keller, G. R., Khan, M. A., Jacob, B., Funchs, K., Nyambok, I. O., Obel, J. D., (1997). The KRISP 94 lithospheric investigation of the southern Kenya-the experiment and their main results. In: Funchs, K., Altherr, R., Muller, B., Prodehl, C., (Eds), Stress and Stress release in the Lithosphere. Tectonophysics 278, 121-148.

Mungania, J., (1999). Overview of the geology of Menengai volcanic complex. Kenya Electricity Generating Company. Internal report.

Newman, G. A., Hoversten, M.,Gasperikova, E., Wannamaker, P. E., (2008). Three-dimensional magnetotelluric characterization of the Coso geothermal field Geothermics 37, 369-399.

Omenda, P. A. (1997). The geochemical evolution of the Quaternary volcanism in the southern central portion of the Kenya rift. PhD Dissertation University of Texas at El Paso, pp 23.

Omenda, P. A., (1998). The geological structure of the Olkaria geothermal field. Geothermics 19, 125-130.

Omenda, P.A., Opondo, K., Lagat, J., Mungania, J., Mariita, O., Onacha, S., Wetangula, G., and Ouma, P., (2000). Ranking of geothermal prospect in the Kenya rift. Kenya Electricity Generating Company Limited, Internal report, pp 121.

Onacha, S.A., (2006). Hydrothermal fault zone mapping using seismic and electric measurements. PHD thesis, Duke University, pp. 249

Oskooi, B., Pedersen, L.B., Smirnov, M., Arnason, K., Eysteinsoon, H., and Manzella, A., (2005). The deep geothermal structure of the Mid-Atlantic Ridge deduced from MT data in SW Iceland. Physics Earth Planet. Inter. 150, 183-195.

Park, S. K., Mackie, R. L., (2000). Resistivite (dry?) lower crust in an active orogen, Nanga Parbat, northern Pakistan. Tectonophysics 66, 158-173.

Park, S. K., Wernicke, B., (2003). Electrical Conductivity of Quaternary faults and Tertiary detachments in the California Basin and Range. Tectonics 22, 1030.

Pellerin, L., Hohmann, G. W., (1990). Transient electromagnetic inversion: a remedy for magnetotelluric static shift. Geophysics 55, 1241-1250.

Pellerin, L., Johnston, J. M., Hohmann, G. W., (1996). A numerical evaluation of electromagnetic methods in geothermal exploration. Geophysics 61, 121-130.

Prodehl, C., Jacob, A. W. B. Thybo, H., Dindi, E., Stangl, R., (1994) Crustal Structure on the northeastern flank of the Kenya rift. In: Prodehl, C., Keller, G. R., Khan, M. A. (Eds), . Crustal and upper mantle structure of the Kenya Rift. Tectonophysics 236, 271-290.

Ranganayaki, R. P., (1984). An interpretive analysis of magnetotelluric data. Geophysics 49, 1730-1748.

Rodi, W., Mackie, R., (2001). Nonlinear conjugate gradients algorithm for 2-D magnetotelluricinversion. Geophysics. 66, 174-187.

Searle, R. C., (1970). Evidence from gravity for thinning of the lithosphere beneath the rift valley in Kenya. Geophys. J. Astron. Soc. 20, 13-31.

Serpa, L., and Cook, K.L., (1984). An application of simultaneous inversion modelling of gravity and aeromagnetic data to a geothermal study in Utah. Geophysics49, 1327-1338.

Simiyu, S. M., (2009). Application of micro-seismic method to geothermal exploration from the Kenya Rift. UNU. Short Course for Exploration for Geothermal Resources.

Simiyu, S. M., Keller, G. R., (1997). Integrated geophysical analysis of the East Africa Plateau from gravity anomalies and recent seismic studies. Tectonophysics 278, 291-314.

Simiyu, S. M., Keller, G. R., (2000). Microseismic monitoring within the Olkaria geothermal area, Kenya. J. Volc. Geoth. Res., 95, 197-208.

Simiyu, S. M., Keller, G. R., (2001). An integrated geophysical analysis of the upper crust of the Southern Kenya rift. Geophys. J. Int. 147, 543-561.

Simiyu, S. M., Omenda, P. A., Anthony, E. Y., Keller, G.R (1995). Geophysical and geological evidence for the occurrence of shallow magmatic intrusions in the Naivasha sub-basin of the Kenya Rift. EOS, Trans Am. Geophys. Union. 76;, 46, 257-258.

Smith, M., (1994). Stratigraphic and structure constraints on the mechanism of active rifting in the gregory rift Kenya. In: C. Prodehl, G. R. Keller and M. A. Khan (Eds), Crustal and Upper mantle structure of the Kenya rift. Tectonophysics, 236, 3-22.

Spichak, V., Manzella, A. (2009). Electromagnetic sounding of geothermal zones. J. Appl. Geophys. 68, 459-478.

Swain, C. J., (1992). The Kenya rift axial high: a re-interpretation. Tectonophysics 204, 59-70.

Swain, C. J., Khan, M. A., Wilton, T. J., Maguire, P. K. H., Griffiths, D. H., (1981). Seismic and gravity surveys in the Lake Baringo-Tungen Hills area, Kenya Rift Valley. J. Geol. Soc.London 138, 93-102.

Swain, C. J., Maguire, P. K. M., Khan, M. A., (1994). Geophysical experiments and models of the Kenya rift before 1989. Tectonophysics 236, 23-33.

Swift, C., (1967). A magnetotelluric investigation of an electrical conductivity anomaly in the Southwestern United States. Ph.D Thesis, MIT, Cambridge, MA.

Vozoff, K., (1972). The magnetotelluric method in the exploration of sedimentary basins. Geophysics 37, 977-991.

Vozoff, K., (1991). The magnetotelluric method, , In: M.M Nabighian (Ed.), Electromagnetic method in Applied Geophysics, p. 641-711, Soc. Explor. Geophys., Tulsa, Ok.

Wannamaker, P. E. (1999). Affordable magnetotellurics; interpretation in natural environments. In; Orastaglio, M., Spies, B. (Eds.), Three-Dimension Electromagnetic. Geophysical Development Series, V. 7., p. 349-374, Soc. Explor. Geophys., Tulsa, OK.

Weaver, J., Agarwal, A., Lilley, F. (2000). Characterisation of the magnetotelluric tensor in terms of its invariants. Geophys. J. Int. 141, 321-336.

SECTION 4

APPENDIX

4.1 Cover Letters

November, 12th, 2011

Dear the editor (s),

Please find the attached manuscript: "**Joint Geophysical Analysis of the Coso Geothermal Field, south-eastern California**" by Wamalwa, et al., is a case study on geothermal field characterization at the Coso geothermal field located in southeast California using magnetotelluric and gravity data. All the co-authors have seen and agree with the content of the manuscript. We verify that this is original work and is not under review at any other publication except on a PhD thesis of Antony M Wamalwa; the first author on this manuscript.

Sincerely yours
Antony Wamalwa

October, 20th, 2011

Dear the editor (s),

Please find the attached manuscript: "**Geophysical Characterization of the Menengai Volcano, Central Kenya Rift from the Analysis of Magnetotelluric and Gravity Data.**" by Wamalwa, et al., is a case study on geothermal field characterization at the Menengai geothermal field located in the central section of the Kenya Rift using magnetotelluric and gravity data. All the co-authors have seen and agree with the content of the manuscript. We verify that this is original work and is not under review at any other publication except on a PhD thesis of Antony M Wamalwa; the first author on this manuscript.

Sincerely yours
Antony Wamalwa

September, 12th, 2011

Dear the editor (s),

Please find the attached manuscript: "**Resistivity Investigation of the Geothermal Potential at the Silali Volcano, Northern Kenya Rift, Using Electromagnetic Data.**" by Wamalwa, et al., is a case study on geothermal field characterization at the Silali geothermal prospect located in the northern section of the Kenya Rift using magnetotelluric data. All the co-authors have seen and agree with the content of the manuscript. We verify that this is original work and is not under review at any other publication except on a PhD thesis of Antony M Wamalwa; the first author on this manuscript.

Sincerely yours
Antony Wamalwa

SECTION 5

VITA

Antony Munika Wamalwa was born in Lumakanda District, Kenya on 29th December, 1981. The first born son of Jared Nahando and Mary Wamalwa, he graduated from Moi University, Kenya in 2005 with a BSC (Hons) in Physics, Chemistry, and Mathematics. From May to November 2005 he worked as an intern with the Kenya Electricity Generating Company (KENGEN) geophysics section. In then enrolled in an MS program in the Physics Department of the University of Texas at El Paso (UTEP) in August 2006. In July 2008, he graduated with an MS program in Physics (geophysics emphasis) form the same university. His thesis work involved the analysis resistivity and magnetic geophysical data to investigate the grounds water flow within the Death Valley region, California. This work is published in Tectonophysics Journal, 2011. In August 2008 he joined the Department of Geological Sciences at UTEP for a Doctoral program. During his doctoral study he presented his research work in various international conferences, published conference papers on proceedings and has several papers (included in this Dissertation) submitted to different journal and are under review. After completion of his PhD program he will work as a geophysicist at the Geothermal Development Company in Kenya where he will focus in integrating different geophysical data in evaluating geothermal resources.

Permanent Address

Geothermal Development Company
P. O. Box 17700 Nakuru, Kenya. 20100
Email- munikatony@yahoo.com

This dissertation was typed by Antony Munika Wamalwa.